NASA CR-54956
DOUGLAS REPORT DAC-59256

PLANE STRESS CYCLIC FLAW GROWTH OF 2219-T87 ALUMINUM AND 5Al-2.5 Sn ELI TITANIUM ALLOYS AT ROOM AND CRYOGENIC TEMPERATURES

by
D.A. Eitman and R.A. Rawe

Prepared for
NATIONAL AERONAUTICS AND SPACE ADMINISTRATION
September 1, 1966

CONTRACT NAS 3-4192

Douglas Aircraft Company, Inc.
Missile and Space Systems Division
Santa Monica, California

NOTICE

This report was prepared as an account of Government sponsored work. Neither the United States, nor the National Aeronautics and Space Administration (NASA), nor any person acting on behalf of NASA:

A.) Makes any warranty or representation, expressed or implied, with respect to the accuracy, completeness, or usefulness of the information contained in this report or that the use of any information, apparatus, method, or process disclosed in this report may not infringe privately owned rights; or

B.) Assumes any liabilities with respect to use of, or for damages resulting from the use of any information, apparatus, method or process disclosed in this report.

As used above, "person acting on behalf of NASA" includes any employee or contractor of NASA, or employee of such contractor, to the extent that such employee or contractor of NASA, or employee of such contractor prepares, disseminates, or provides access to, any information pursuant to his employment or contract with NASA, or his employment with such contractor.

Requests for copies of this report should be referred to

National Aeronautics and Space Administration Office of
Scientific and Technical Information
Attention: AFSS-A
Washington, D. C. 20546

NASA CR-54956
DOUGLAS REPORT DAC-59256

FINAL REPORT

PLANE STRESS CYCLIC FLAW GROWTH OF 2219-T87 ALUMINUM AND 5Al-2.5 Sn ELI TITANIUM ALLOYS AT ROOM AND CRYOGENIC TEMPERATURES

by

D.A. Eitman and R.A. Rawe

Prepared for
NATIONAL AERONAUTICS AND SPACE ADMINISTRATION
September 1, 1966

CONTRACT NAS 3-4192

Technical Management
NASA Lewis Research Center
Cleveland, Ohio
Chemical Rocket Systems Division
Gordon T. Smith

Douglas Aircraft Company, Inc.
Missile and Space Systems Division
Santa Monica, California

PREFACE

This report was prepared by Douglas Aircraft Company, Inc., Missile and Space Systems Division, under NASA Contract NAS 3-4192. This investigation was initiated by Lewis Research Center of NASA to determine the plane-stress fatigue-crack propagation behavior of cryogenic tank materials under uniaxial and biaxial stresses. The program was administered under the direction of the Chemical Rocket System Division, G. T. Smith, Project Manager.

The report covers the work period 1 July 1964 through 1 May 1966. It is submitted to fulfill this contract and is catalogued by Douglas as Report No. DAC-59256.

At Douglas, B. V. Whiteson, Chief of the Metallurgy Development Section, Metals-Ceramics Branch, Materials Research and Production Methods Department, provided technical direction and program management. D. A. Eitman was principal investigator, and R. A. Rawe performed the analytical work.

ABSTRACT

Fatigue crack propagation tests of flat uniaxial panels and cylindrical (biaxial) specimens were conducted at room temperature, -320° and -423°F. A broad range of stresses and crack lengths were studied at each temperature. Parametric and fracture mechanics approaches were used in analyzing the data. A parametric method was developed which permits prediction of cyclic life of a through-cracked structure, crack-growth curves, and growth rates. A correlation of uniaxial and biaxial crack-growth behavior has been established, and a method for use of plane-stress fatigue crack propagation data in tank design is presented.

ACKNOWLEDGMENT

The authors wish to express their appreciation to G. V. Bennett, Chief of the Metals-Ceramics Branch, Materials Research and Production Methods Department, for his guidance during critical aspects of the program. In addition, the assistance of E. W. Steffan, R. T. Hartunian, R. E. Williams, and A. Ackerman is gratefully acknowledged.

CONTENTS

FIGURES

TABLES

SYMBOLS

a	One-half critical crack length
A	Distance between first strands of crack propagation gauges No. 1 and No. 2
B	Distance between first strands of crack propagation gauges No. 3 and No. 4
C	Bulge coefficient, eq. (6-1)
D	Biaxial specimen diameter
F	Parametric constant, eq. (5-6)
F_B	Parametric constant for biaxial stress
F_U	Parametric constant for uniaxial stress
g	Total length of crack propagation gauge
k	Size effect constant, eq. (7-1)
k_g	Correction factor for crack propagation gauge readings
K	Stress intensity factor
K_o	Initial stress intensity factor
K_c	Critical stress intensity factor
K_{cn}	Nominal fracture toughness
ℓ	Crack length at any time
ℓ_o	Initial crack length
ℓ_c	Critical crack length, uniaxial stress
ℓ_{cB}	Critical crack length, biaxial stress
ℓ_F	Parametric constant, eq. (5-6)
L	Longitudinal

N	Cycles
N_F	Cycles at failure
N_R	Cycles remaining to failure
r	Radius of cylinder
R	Ratio of minimum cyclic stress to maximum cyclic stress
R_p	Notch resistance factor
s	Distance between strands of crack propagation gauge
T	Transverse
w	Panel width
σ	Tensile stress
σ_o	Gross stress
σ_n	Net section stress
σ_{max}	Maximum cyclic gross stress
σ_{min}	Minimum cyclic gross stress
σ_H	Hoop tension stress
σ_y	Uniaxial yield strength
σ_{yB}	Biaxial yield strength
σ_u	Uniaxial ultimate tensile strength
σ_{uB}	Biaxial ultimate tensile strength

Section 1

SUMMARY

An experimental and analytical investigation was conducted to determine the plane-stress flaw growth behavior of 2219-T87 aluminum and 5Al-2.5Sn (ELI) titanium alloys as cryogenic tank wall materials under uniaxial and biaxial stresses at room temperature, -320° and -423°F.

Fatigue crack propagation behavior and plane-stress fracture toughness were established for a wide range of stress environments. Equations were developed from the experimental results which can be used to predict crack-growth behavior in pressurized tanks. Graphs were constructed which showed the relationship between stress, crack-growth rate, fatigue life, and stress intensity (K).

Uniaxial data were obtained by cycling precracked panels and observing crack growth visually and electromechanically. Precracked cylindrical specimens were used for the biaxial tests, and the crack growth was monitored electromechanically. Correlation factors between actual crack size and electromechanical indications were determined during the uniaxial tests and were applied to the biaxial data. Empirical equations developed during the program were found which accurately described the crack-growth behavior of all tests.

Section 2

INTRODUCTION

Service requirements of some projected space vehicles call for multiple loading of cryogenic propellant tanks and extended exposure to meteoroid flux in space. While most pre-existing flaws which might escape detection prior to service are embedded within the wall of a structure or are open to one surface only, cracks open to both surfaces may develop under repeated loading in the wall of a propellant tank, or if penetration is achieved by meteoroids. Such a tank can fail in service after growth of the through-the-thickness crack to critical length.

In cases where leaks are detected in damaged tanks, it may be technically and economically feasible to repair the leak in space by patching or caulking. If the remaining duration of useful service life of the damaged tank were known, or could easily be determined to be sufficient for the mission, repair of the crack would not be needed for structural considerations.

Propellant systems that utilize internal insulation might experience very minor leakage or none at all as a result of penetration of the tank wall. Continued use of the tank containing such damage will cause propagation of the through-the-thickness crack. Provision for sufficient tank life under repeated loads should, if possible, be made when the tank is designed. Design activity devoted to this end would include selection of material and the maximum operating cyclic stress levels on the basis of minimum weight for safe service life.

Much effort has been devoted to the study of cracks and their behavior under both monotonic and repeated loading. The majority of the data so generated, however, relate to low stress intensities, to plane-strain conditions, to the uniaxial stress state, to testing at room temperature, and to materials not presently considered for cryogenic tankage (ref. 1-8). The research program reported in this document was designed to provide data on through-the-thickness crack propagation in two alloys directly applicable to cryogenic propellant tanks, 2219-T87 aluminum and 5Al-2.5Sn titanium (ELI). Testing was planned for liquid nitrogen and liquid hydrogen temperatures in addition to room temperature. Both uniaxial and biaxial testing were included. The major objectives of the program were to establish a correlation between uniaxial and biaxial crack propagation under repeated loads similar to those which would be experienced by an actual vehicle and to present the data in a form convenient for use by the designer.

Section 3

PROGRAM PLAN

The objective of this program required that design data be generated on, and analytical methods be developed for the effects of uniaxial and biaxial stresses on the flaw-growth characteristics of typical cryogenic tank materials. One aluminum alloy (2219-T87, 0.060-in. thick) and one titanium alloy (Ti-5Al-2.5Sn extra low interstitial, 0.020-in. thick) were selected for evaluation. The materials have characteristics that indicate that they may be well suited for use in cryogenic propellant tanks. The 2219-T87 is currently being used for large spacecraft structures (S-IC), and the use of the titanium alloy appears attractive for future, high-performance cryogenic propellant tanks (ref. 9). Thicknesses of the materials tested are representative of future upper-stage design requirements. The thicknesses represented plane-stress conditions for both alloys.

The program was divided into five discrete tasks in order to accomplish the program objectives. Uniaxial tests were conducted in Task I; preparation was made for biaxial tests in Task II; biaxial tests were conducted in Task III; data were reduced and analyzed in Task IV; reports were prepared and presented in Task V. Testing schedules for Tasks I and III are shown in Tables 3-I and 3-II. A more detailed description of each task is given below.

(1) TASK I--UNIAXIAL TESTING

Task I consisted of design and fabrication of the uniaxial test fixture, the procurement of material for all test specimens, the design of uniaxial test panels, the establishment of baseline properties for 2219-T87 and Ti-5Al-2.5Sn ELI, and conducting uniaxial tests shown in Tables 3-I and 3-II.

(2) TASK II--BIAXIAL MANUFACTURE

Task II consisted of the design and manufacture of the biaxial test apparatus and the biaxial specimens. Fatigue precracks were produced in the biaxial specimens. Preliminary checkouts were made of the biaxial testing systems.

(3) TASK III--BIAXIAL TESTING

Room temperatue and cryogenic biaxial tests were conducted in Task III according to the schedule shown in Table 3-II.

(4) TASK IV--DATA REDUCTION AND ANALYSIS

Task IV consisted of reducing the data produced in Tasks I and III, analysis using various analytical and empirical techniques, and the development of a method of presentation of the results in a form usable for design.

TABLE 3-I

STATIC TEST PLAN

Material	Test temperature (°F)	Number of uncracked specimens	Number of 16 in. x 42 in. cracked* specimens
2219-T87 0.060-in. thickness	70	62	2
	-320	2	2
	-423	2	2
Ti-5Al-2.5 Sn (ELI) 0.020-in. thickness	70	62	2
	-320	2	2
	-423	2	2

*All specimens had 5-in. initial crack lengths.

TABLE 3-II

CRACK PROPAGATION TEST PLAN

TABLE 3-II

Material	Test temperature (°F)	$\sigma_{max.}$	R $\frac{\sigma_{min.}}{\sigma_{max.}}$	Number of specimens		
				Uniaxial 16 in. x 42 in.	10-in. diam biaxial	4-in. diam biaxial
2219-T87 0.060-in. thick	70	σ_1(a)	0.05 0.5	2 2	2 -	- -
		σ_2(b)	0.05 0.5	2 2	- -	- -
		σ_3(c)	0.05 0.5	2 2	2 -	2 -
	-320	σ_1	0.05 0.5	2 2	2 2	
		σ_2	0.05 0.5	2 2	- -	
		σ_3	0.05 0.5	2 2	2 2	
	-423	σ_1	0.05 0.5	2 2	2 1	
		σ_2	0.05 0.5	2 2	- -	
		σ_3	0.05 0.5	2 2	2 1	
Ti-5Al-2.5Sn ELI 0.020-in. thick	70	σ_1	0.05 0.5	2 2	2 -	
		σ_2	0.05 0.5	2 2	- -	
		σ_3	0.05 0.5	2 2	2 -	
	-320	σ_1	0.05 0.5	2 2	2 1	
		σ_2	0.05 0.5	2 2	- -	
		σ_3	0.05 0.5	2 2	2 1	
	-423	σ_1	0.05 0.5	2 2	2 2	
		σ_2	0.05 0.5	2 2	- -	
		σ_3	0.05 0.5	2 2	2 2	

Notes:

(a) $\sigma_1 \leq \frac{\sigma_u}{1.4}$, $\sigma_1 \leq \frac{\sigma_y}{1.1}$

(b) $\sigma_2 = \frac{\sigma_1 + \sigma_3}{2}$

(c) σ_3 = Breaking stress of a uniaxial 16 in. x 42 in. specimen with a 5-in. initial crack.

Section 4

APPARATUS AND PROCEDURES

Testing for this program was conducted at two different sites. Uniaxial tests were conducted at the Douglas Santa Monica facility on a specially-designed fixture which would permit visual observations of the crack during cryogenic testing. Room temperature biaxial tests were also conducted at Santa Monica where hydraulic loading could be utilized. Cryogenic biaxial tests were conducted at a remote test site in Orange County, California, to eliminate danger to populated areas which may be present when pressure vessels are burst in large quantities of liquid hydrogen.

4.1 UNIAXIAL FLAW-GROWTH TESTS

Uniaxial flaw-growth tests were conducted at room temperature, -320° and -423° F. All tests were made on a hydraulic fatigue machine especially designed to accommodate the 16-in. -wide by 42-in. long specimens. Crack growth was monitored both visually and electro-mechanically in each test.

4.1.1 Baseline Property Determinations

Since small variations in chemistry and rolling history may have significant effects on the crack-propagation characteristics of aluminum or titanium alloys, extensive measurements were made to ensure the homogeneity of the test material and its specific mechanical and physical properties.

Specimens for mechanical property tests at room temperature were selected both perpendicular to (transverse) and parallel with (longitudinal) the sheet rolling direction. Specimens for mechanical testing at -320° and -423° F were selected to correspond with the orientation of the precracked uniaxial flaw growth panels; all cryogenic test specimens of 2219-T87 were transverse and all cryogenic test specimens of Ti-5Al-2.5Sn ELI were longitudinal.

4.1.1.1 Chemical Analysis

Samples for chemical analysis were selected from each sheet of test material. Analysis of the percent of iron, carbon, and nitrogen content was made for each sheet of Ti-5Al-2.5Sn ELI. Independent analysis of the percent of copper and iron in 2219-T87 was made with a spectrograph, an X-ray spectrograph, and by wet chemical analysis. The redundant analysis was made because sheet-to-sheet variation in these critical elements seems to exist even though the material is from one lot.

4.1.1.2 Pole Figure Analysis

Independent investigations at Douglas (ref. 10) have shown that the Ti-5Al-2.5Sn alloy has preferred crystallographic orientation, and that this texturing affects the biaxial mechanical properties. X-ray pole-figure analysis was made for five selected sheets using the back reflection technique to characterize this orientation and to record variations in crystallographic orientation from sheet to sheet.

4.1.1.3 Mechanical and Physical Property Measurements

Standard tensile tests were conducted on each sheet of test material. Properties recorded for the 2219-T87 aluminum alloy were: 0.2% offset yield strength, ultimate strength, % elongation in 2-in., Young's modulus, and elastic Poisson's ratio. The same properties were measured for the Ti-5Al-2.5Sn ELI with the following exceptions:

(1) Subsize specimens (1-in. gauge length) were used for the longitudinal mechanical property measurements in 12 sheets (A through L) due to a shortage of larger size pieces in this direction.

(2) No Poisson's ratio measurements were made on the subsize specimens.

(3) Measurements were made of plastic Poisson's ratio for most sheets in both the longitudinal and transverse directions. The only exceptions were for Sheets A through L in the longitudinal direction.

Standard ASTM procedures were used for the mechanical property tests. Modulus determinations were made using an extensometer (ASTM Classification B-1) to measure strain. Elastic and plastic Poisson's ratios were measured using a Budd Co. C6-121-R2T biaxial strain gauge. Mechanical property measurements were also made at -320° and -423° F on selected sheets of each alloy.

4.1.2 Specimen Design and Preparation

Specimen design and preparation are discussed in the following sections.

Specimen orientation with respect to sheet rolling direction for precracked uniaxial panels was based upon the need for correlation of crack-growth direction between uniaxial and biaxial specimens. All uniaxial 2219-T87 panels were prepared with a transverse orientation (long dimension perpendicular to the rolling direction); the Ti-5Al-2.5Sn ELI panels were longitudinal.

4.1.2.1 Specimen Geometry

Precracked uniaxial specimens 16-in. wide by 42-in. long were used for both static and cyclic tests, Figure 4-1. The 16-in. width was selected as the minimum size which would permit testing Ti-5Al-2.5Sn ELI at room temperature and still be within the dimensional limitations for a plane-stress specimen noted in ref. 11. These limitations are as follows:

$$16 < \frac{w}{t} < 45$$

$$\ell_o = 1/3\ w \text{ (for static test to measure } K_c \text{ only)}$$

$$\sigma_n < 0.9\ \sigma_y$$

$$L = 4\ w \text{ (pin-loaded specimens)}$$

$$\ell_c \leq 0.6\ w$$

where

w = specimen width

ℓ_o = initial crack length (for static test specimen)

σ_n = net section stress

σ_y = yield strength of the material at 0.2% offset

L = specimen length

The one limitation violated was that $\frac{w}{t}$ be held less than 45. In order to compensate for this necessary deviation, aluminum angle stiffeners were clamped on each side of the specimen approximately 1 in. above and below the crack. Buckling, which is the prime reason for the upper $\frac{w}{t}$ limitation, was thereby minimized. Friction grips were used on the specimen so that a uniform stress field could be obtained with a specimen shorter than the $L = 4\ w$ suggested for a pin-loaded specimen.

4.1.2.2 Precracking Procedure

Starter slots were machined in all specimens and then fatigue tipped on a 30,000-lb. capacity fatigue machine, Figure 4-2. The crack was monitored visually until it reached the desired size. Measurements of the initial crack length were made at 2X magnification using a steel scale graduated in 0.01-in. increments. Precracking stress history was then recorded on a data sheet, Figure 4-3, which accompanied each specimen throughout the program.

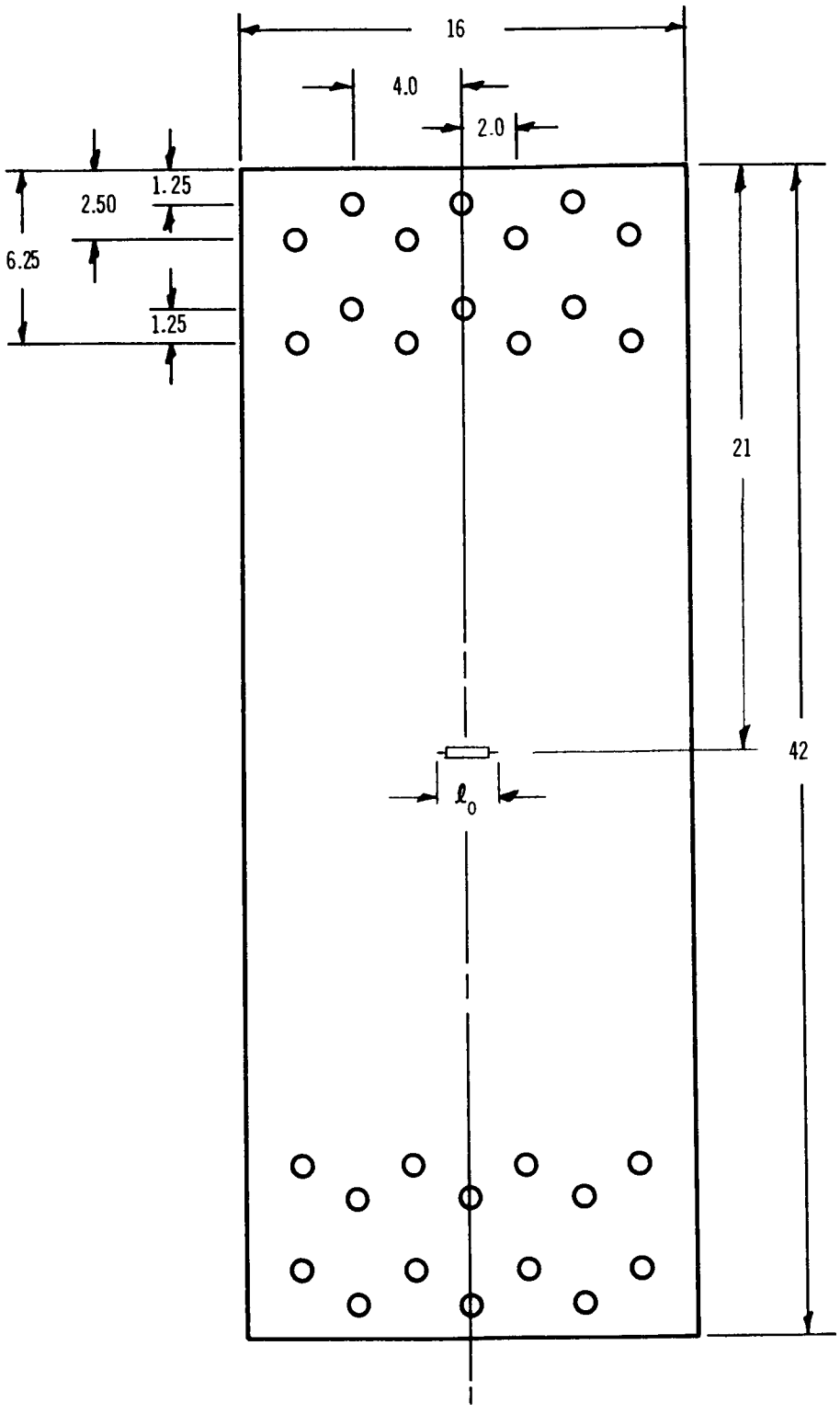

Figure 4-1. Uniaxial Test Specimen
(Dimensions in inches)

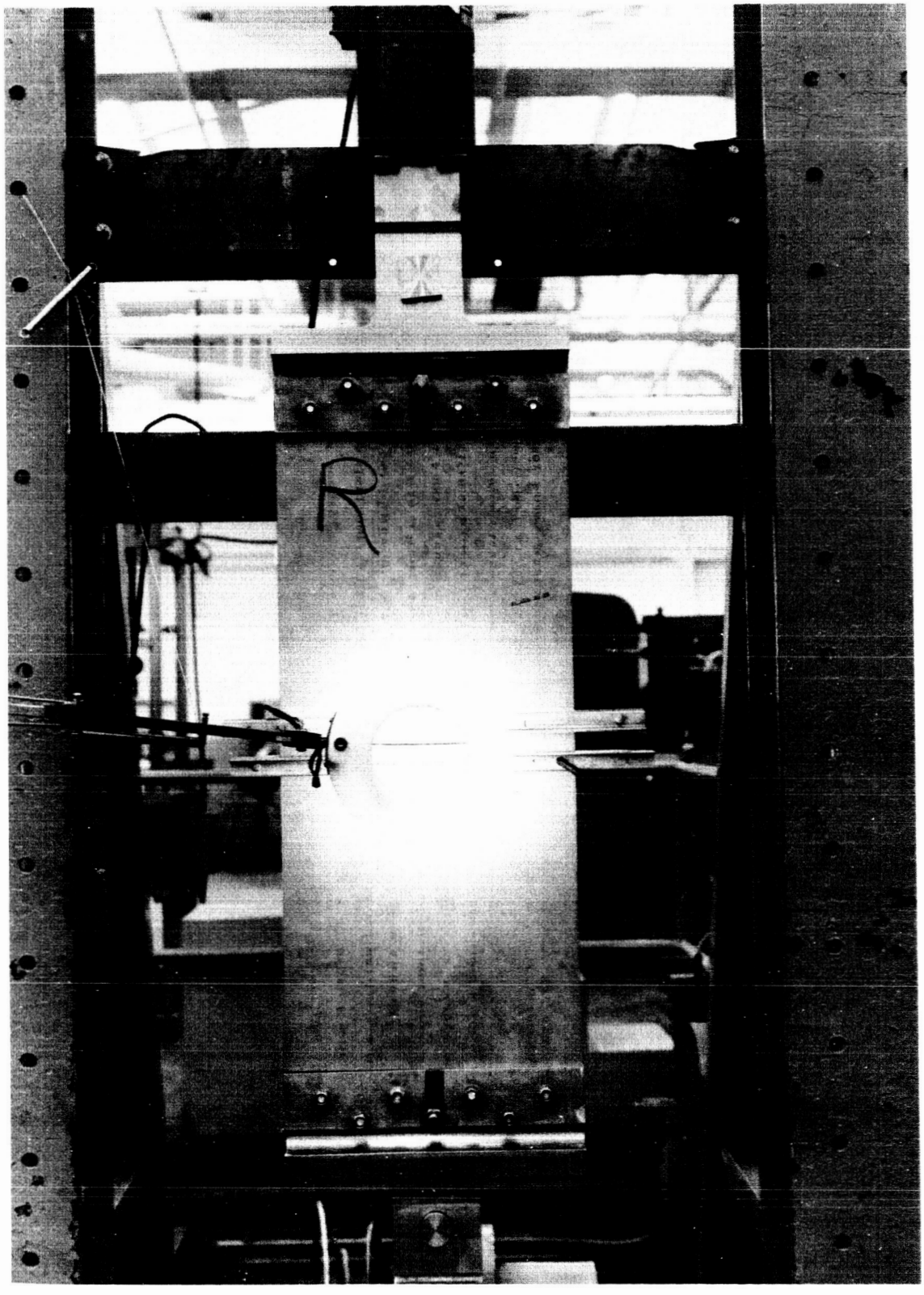

Figure 4-2. Precracking Uniaxial Panel

DATA SHEET

SPECIMEN NUMBER EA

Contract NAS 3-4192

MATERIAL - 2219-T87

WIDTH = 15.992 THICKNESS = 0.0595 AREA = 0.9515

ORIGINAL SLOT LENGTH 1.590

FATIGUE CRACK LENGTH 2.000

MAX LOAD 9000 #

MIN LOAD 900 #

CYCLES 12175

GAGE DATA

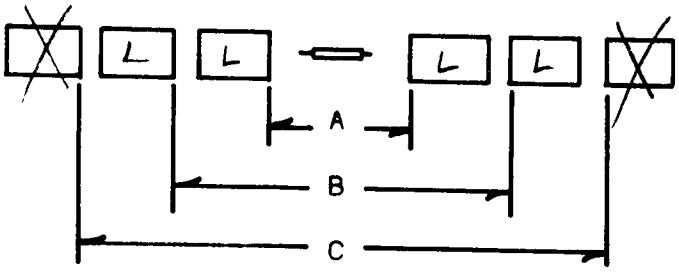

A = 2.14

B = 6.14

C =

TEST DATA -

TEMP. R.T.

$\sigma_{MAX.}$ 21.9

R 0.05

% of Cal. distance

$$\frac{\sigma \text{ Max} \times \text{Area} \times 100}{\text{Cal}} = \frac{21.9 \times .9515 \times 100}{24.205} = 86.09\%$$

Cal. Dist. = 4.0

(Circle correct calibration)

CALIBRATION: (25K = 24,205 lbs)

10K = 60,530 lbs

BROKEN STRAND (Count away from crack)

Number Gage

N/A

REMARKS:

Figure 4-3. Uniaxial Data Sheet Sample

4.1.2.3 Pretest Preparation

After precracking, crack-propagation gauges were bonded to one surface of the specimen, and a grid with lines 0.1-in. apart was drawn on the opposite surface. A 6H drafting pencil was used to scratch the layout dye for marking the grid so that longitudinal scratches would not be made in the metal.

Two sizes of crack-propagation gauges were used, depending on the expected final crack size in the test. Schematics of the gauges are shown in Figure 4-4. Bonded large gauges are shown in Figure 4-5. Measurements were made of the distance between the first strands of each set of gauges and of the distance between the first two grid marks ahead of the crack front.

4.1.3 Selection of Cyclic Stress Levels and Starting-crack Sizes

Selection of the maximum stress levels for cyclic tests was made with two prime objectives. The first was to conduct tests with as wide a range of stress levels as possible. Secondly, it was considered necessary to restrict the final crack size in the specimen so that edge effects would not influence the results. Therefore, the maximum peak stress was selected as typical in a design application for a manned vehicle, i.e., the ultimate strength divided by 1.4 or the yield strength divided by 1.1, whichever was less. The lower peak stress was selected as the maximum stress attained in a static test of a specimen with a 5-in.-long precrack. A third peak stress level was selected which was half-way between the highest and the lowest cyclic stresses.

After conducting two static tests for each alloy at each test temperature, starting crack sizes were selected for all uniaxial tests. Starting crack sizes were selected so that K_o, the initial maximum stress intensity, would be less than 0.6 K_c. In this way, a period of stable crack growth was ensured for each test.

4.1.4 Test Apparatus

Test apparatus is discussed in the following paragraphs.

4.1.4.1 Load Fixture

A 150,000-lb capacity hydraulic fatigue machine was constructed for this program. The entire loading apparatus was suspended in a large frame (Figure 4-6) and could be moved up and down to position the cryostat. The bottom half of the loading apparatus was submerged during cryogenic tests.

The first step in assembling the load cage was to weld the top, bottom, and middle plates to the support tubes. Holes for the hydraulic cylinder, load train, and bottom clevis were then precision jig-bored to assure alignment during testing. The middle plate served as a lid for the cryostat, and everything below it was submerged during testing. An insulation coupling was installed in the load train immediately below the load cell to eliminate thermal gradients in the load cell.

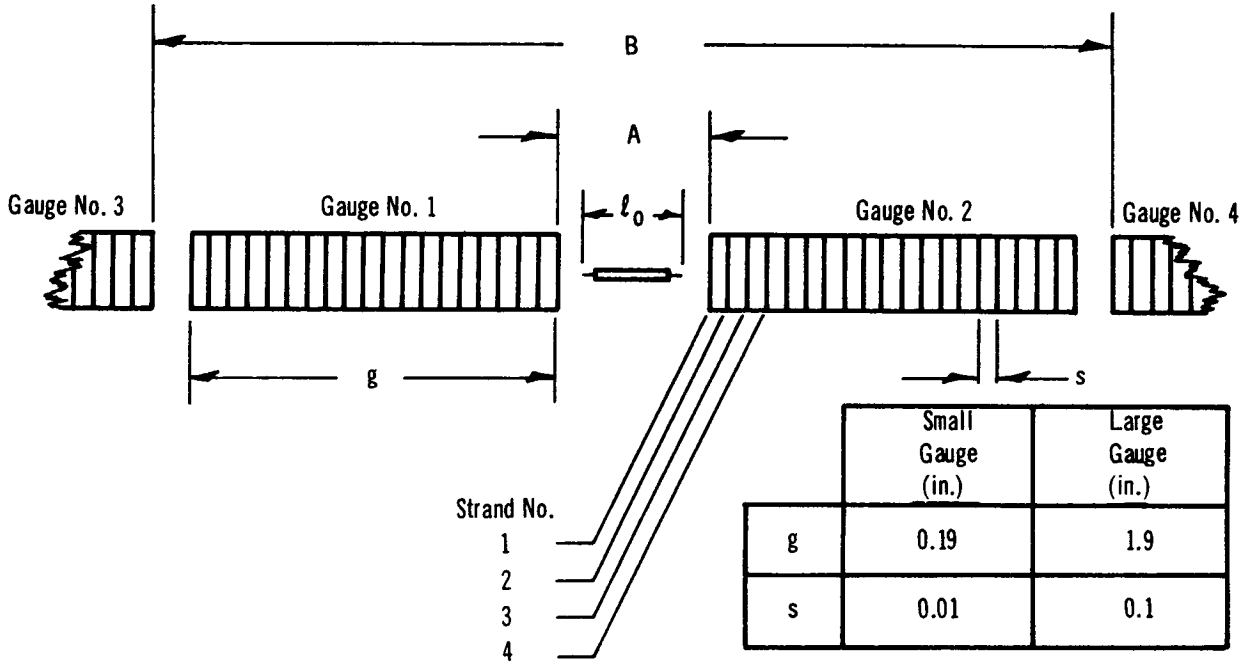

	Small Gauge (in.)	Large Gauge (in.)
g	0.19	1.9
s	0.01	0.1

Figure 4-4. Schematic of Crack Propagation Gauge Arrangement

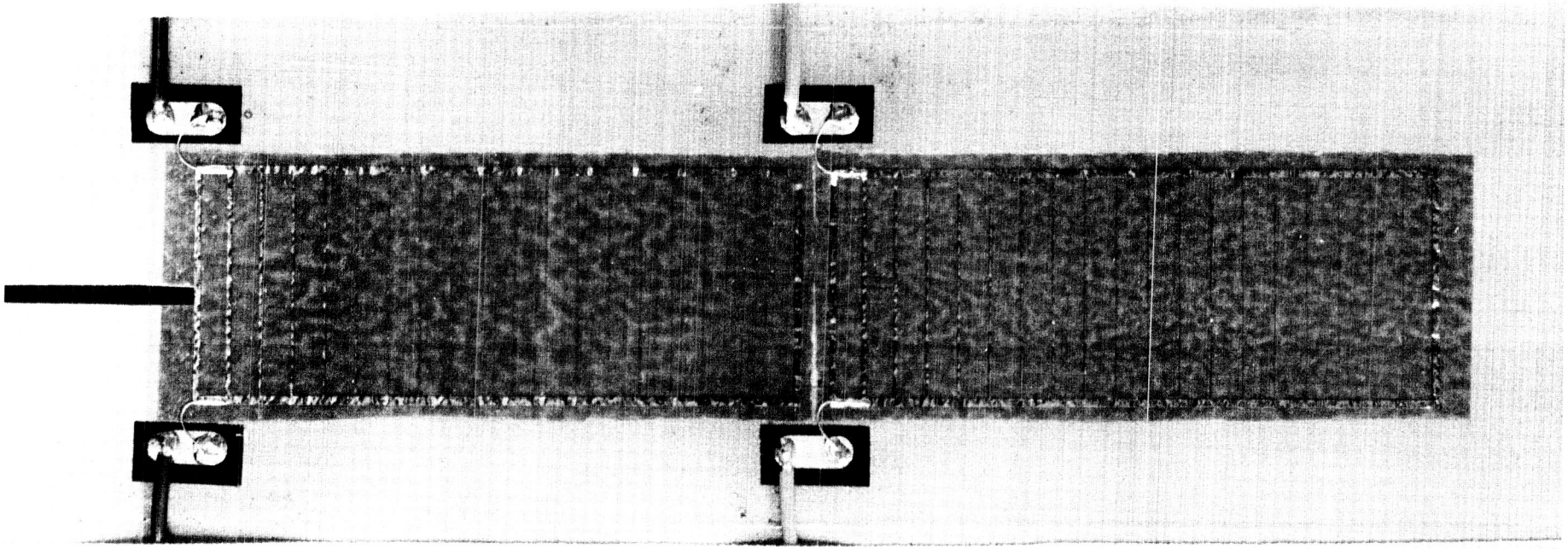

Figure 4-5. Large Crack Propagation Gauges Bonded on Uniaxial Specimen

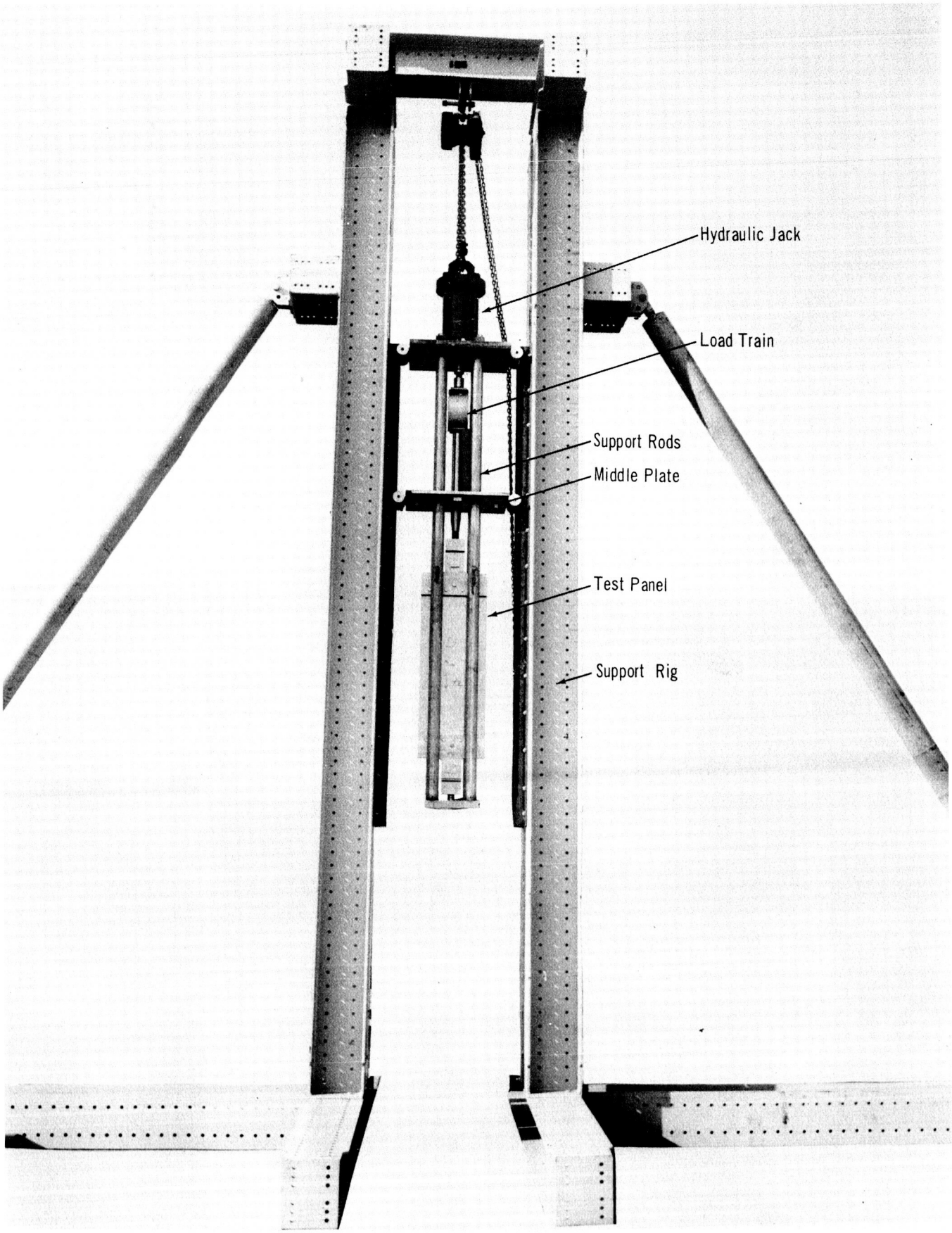

Figure 4-6. Uniaxial Testing Apparatus

4.1.4.2 Liquid Hydrogen Cryostat

An 80-gal capacity liquid hydrogen cryostat with a 6-in.-diam observation port was used for cryogenic testing as shown in Figure 4-7. The seal around the observation port became a problem early in the program. A temporary seal which lasted through most of the -320° F tests was obtained with a gasket made from a polyurethane adhesive (Narmco 7343) and a pyrex window. Several new installations of this configuration were required to complete testing. A warp in the retaining seat for the observation port compounded the problem, so that the window had a tendency to shatter during thermal cycling.

An adequate seal for -423° F testing was not obtained and condensation on the observation port obscured the crack during testing. As a result, visual observations had to be made by interrupting the test, eliminating the liquid hydrogen from the cryostat, and measuring the length of the crack in the specimen. The cryostat was then refilled with liquid hydrogen, and the test was continued to failure.

Attempts were made to use telescopes, television, and photographs to monitor the crack at -423° F. The photographic technique appeared to be the most applicable but was not used after it was found that the observation port lost vacuum and clouded during liquid hydrogen fill.

4.1.4.3 Instrumentation

Data during testing were recorded on 7-in.-wide paper on a Consolidated Electrodynamics Corporation high-speed oscillograph, Model CEC-124.

Both the load and the crack growth were recorded simultaneously. A schematic of a typical recording is shown in Figure 4-8. Galvanometers used in the oscillograph had a 0 to 60 cps full-scale, flat response, so that load spikes and/or rapid crack progression could be recorded accurately.

Two sizes of load cells (60, 000 and 250, 000-lb capacity) were used during testing. The smaller unit was used whenever possible as the error in load measurements may be ±1% of rated capacity.

Crack growth was measured both visually and electromechanically. Visual measurements were made by observing the crack while holding a switch in each hand. As the crack front passed a grid mark to the right or left of center, the corresponding switch was activated. An event mark was made on the oscillograph trace whenever a switch was activated.

Crack-propagation gauges were also used to measure the crack length. When the crack broke a strand in the gauge, there was an abrupt resistance change which was recorded on the oscillograph. Special circuits were designed to modify the output of these gauges to linearize their output. Schematics of these circuits are shown in Figures 4-9 and 4-10.

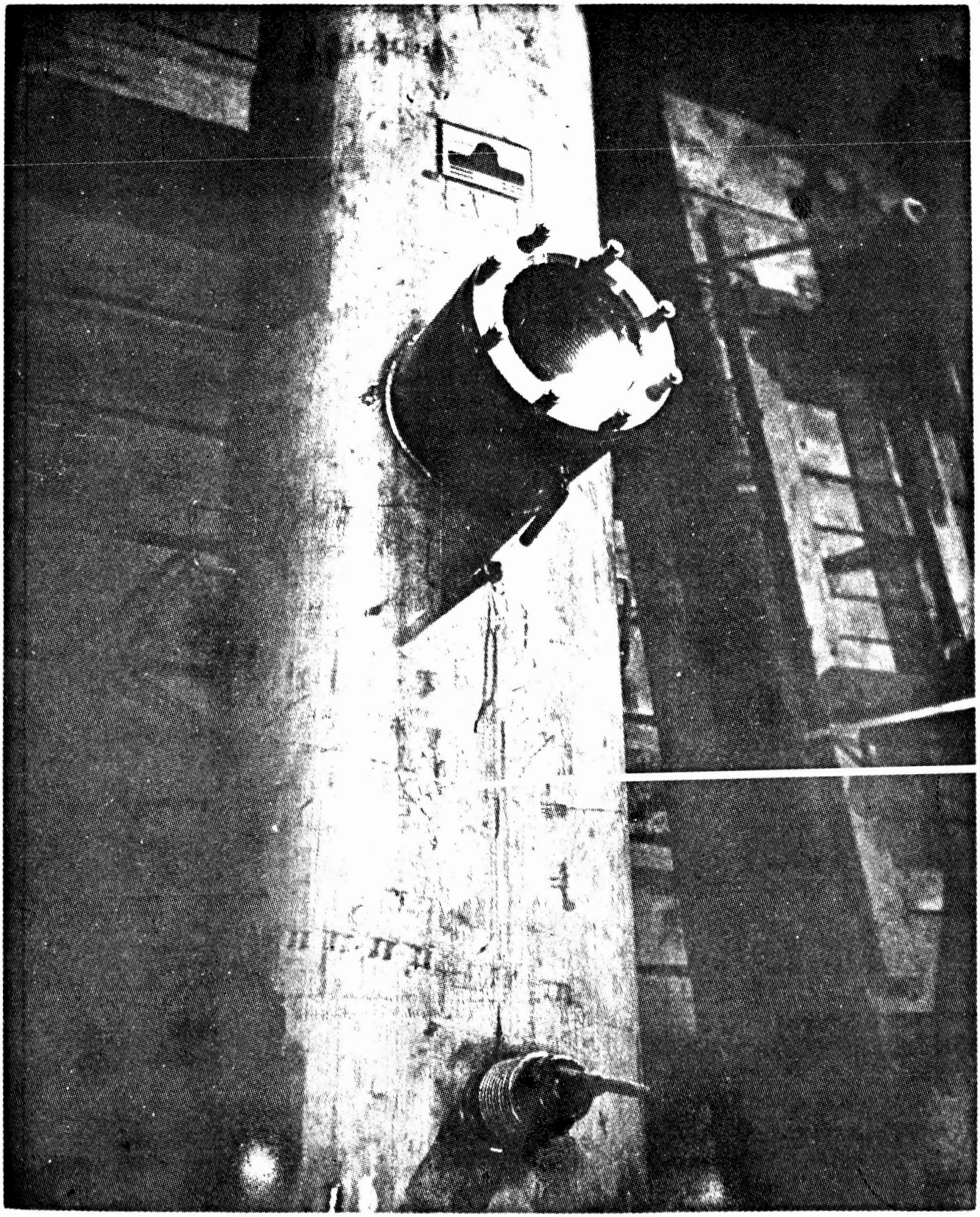

Figure 4-7. Uniaxial Cryostat

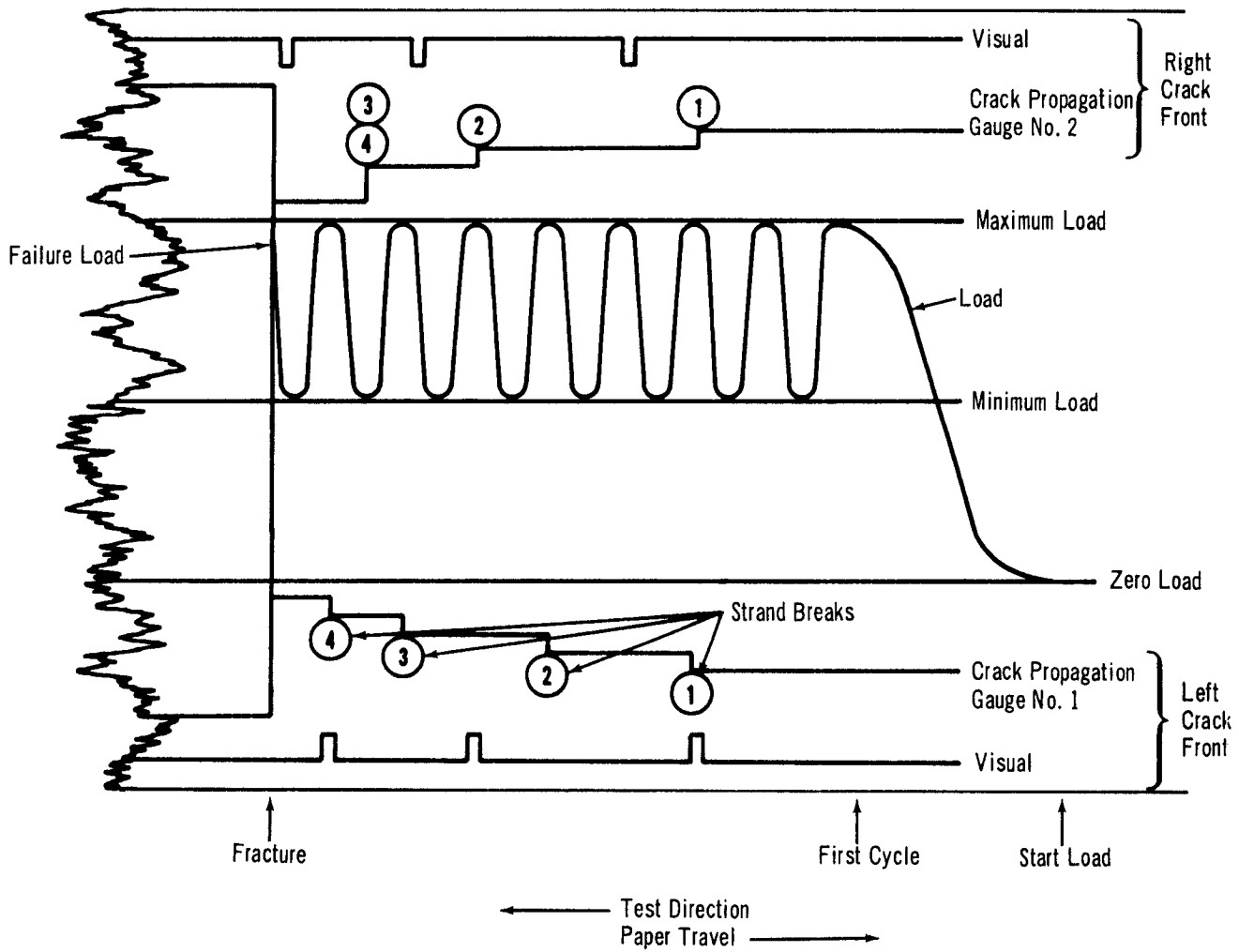

Figure 4-8. Idealized Schematic of Oscillograph Trace

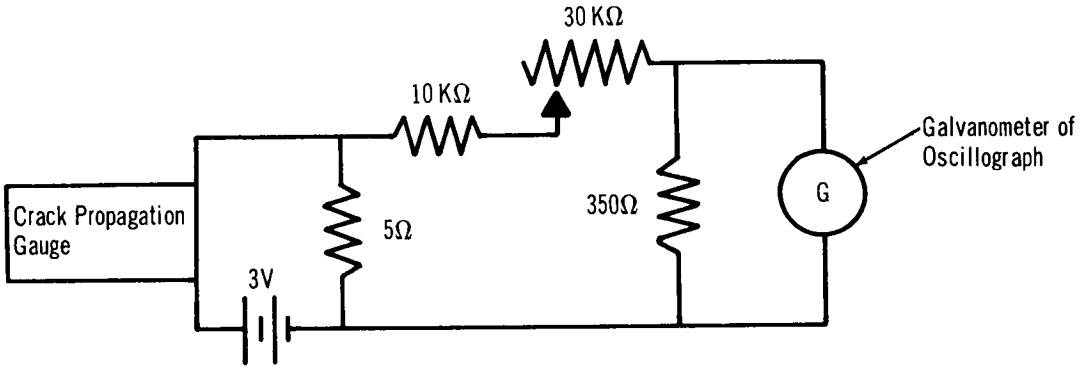

Figure 4-9. Electrical Circuit for Large Crack Propagation Gauge (0.1-in. Strand Spacing)

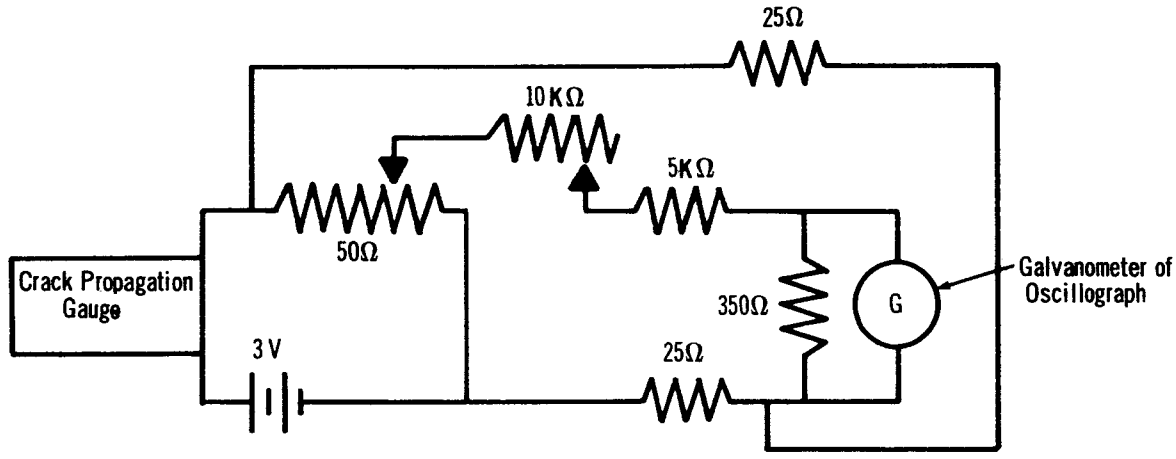

Figure 4-10. Electrical Circuit for Small Crack Propagation Gauge (0.01-in. Strand Spacing)

Preliminary tests were conducted at the beginning of the program to find an optimum adhesive for these gauges. For room temperature tests, crack propagation gauges were bonded to the specimens using Budd Type RTC room temperature cement. For tests at -320° and -423° F, Minnesota Mining and Manufacturing Company, Inc., EC 2219 adhesive was used. Application of the gauges was preceded by a thorough cleaning of the specimen surface. After a light sand blast, the surface was cleaned with alcohol. No further cleaning of the 2219-T87 specimens was performed. However, Ti-5Al-2.5Sn ELI specimens then received a dilute hydrofluoric wash and were rinsed in water; a final wash in British Etch (15% by volume sulfuric acid, 12 oz. per gal sodium dichromate, remainder water) and a rinse in water followed by alcohol completed the surface preparation. Adhesive and gauges were then applied and cured 1 hour at 175° F in an air oven.

4.1.5 Test Procedure

A detailed check list was made for the preliminary static tests. Additions to this list were made for fatigue testing, liquid nitrogen tests, and liquid hydrogen tests.

At the beginning of each test, the instrumentation was connected and the galvanometer recording load was calibrated. Reference traces were set for zero load, maximum load, and minimum load. Channels for recording visual measurements were set on the extreme edge of the recording paper and checked for continuity. Galvanometers recording the crack-propagation gauge readings were adjusted so that a total of 5.7 in. were traversed when the gauge had been completely broken. After all zero positions had been set, the specimen was installed in the loading fixture.

The specimen was placed in the friction grips and held in position by the top and bottom center bolts. A small load (100 to 300 lb) was applied and the specimen was aligned with a surveyor's transit. The remaining bolts were put in position and all bolts were torqued to approximately 150 ft-lb. For cryogenic tests, the load cage was then raised, the cryostat was placed in position, and the load cage was lowered into the cryostat. Wires from the crack-propagation gauges were connected to a terminal board and a final check was made for continuity. A liquid nitrogen line was connected and the cryostat was filled. The liquid level was monitored by the thermocouples placed at the bottom, middle, and top of the cryostat.

For the liquid hydrogen tests, the cryostat was filled with liquid nitrogen to precool the system and immediately emptied. Warm, dry air was introduced into the cryostat until all thermocouples were just above the temperature of liquid air. The cryostat was then purged with argon for 5 min. to eliminate any remaining oxygen. Liquid hydrogen fill was started after the argon purge.

In order to prevent air or moisture from freezing in the hydrogen elimination system, a small positive pressure of helium (1 psig) was maintained in the elimination system throughout the test. Testing was started no sooner than 5 min. after the middle thermocouple read -423° F and when the top thermocouple read -423° F.

After filling the cryostat, the oscillograph was checked to ensure that the electrical systems had not drifted. Data recording for the test started at this point and was not stopped until after the test. Calibration switches were turned on and off in sequence so that an autographic record of each channel was made at the start of the test.

A technician stood near the specimen to observe crack growth in all but the liquid hydrogen tests. Measurements during the tests were made as described in Section 4.1.4.3.

At the beginning of each test, the specimen was loaded to maximum load by manual operation of the hydraulic valves. Automatic cycling was begun at a low frequency, then increased gradually until a speed of 45 to 60 cpm was reached. Continuous adjustments of the maximum and minimum loads were made throughout the test to compensate for changes in hydraulic oil temperature and an increase in the compliance of the specimen. During the last few cycles of testing both maximum and minimum loads decreased rapidly due to the large increase in compliance, and large adjustments had to be made. When the crack growth rate approached 0.1 in./10 sec. the oscillograph paper speed was increased from 0.25 in./sec to 1 in./sec until failure occurred.

After specimen failure, the load cell calibration was checked to determine if there had been any zero shift or change in sensitivity.

When liquid hydrogen was being used, a siphon system was turned on and the cryostat contents were sprayed into the air within 10 to 20 min. Warm air was then used to heat the cryostat above the temperature of liquid air. The specimen could then be disassembled safely by the test personnel.

4.2 BIAXIAL TESTS

Biaxial tests were conducted on precracked cylinders of Ti-5Al-2.5Sn ELI and 2219-T87 at room temperature, -320° and -423° F. Room temperature tests and precracking operations were conducted using hydraulic oil as a pressurizing medium. Cryogenic tests were conducted at a remote test location with the specimens filled with, and completely immersed in, the cryogen being used.

4.2.1 Biaxial Specimen

A discussion of biaxial specimen design, fabrication, and preparation is detailed in the following paragraphs. Specimen blanks for the 2219-T87 cylindrical specimens were sheared in such a way that the hoop direction of the cylinder was perpendicular to the sheet rolling direction, whereas in the Ti-5Al-2.5Sn ELI cylinders the hoop direction was parallel with the sheet rolling direction. These orientations correlated with those of the uniaxial specimens so that, for a given alloy, the crack growth direction was the same with respect to rolling direction in both uniaxial and biaxial specimens.

4.2.1.1 Specimen Design

The biaxial specimens used in this program were cylindrical with a length-to-diameter ratio equal to or greater than 3. This ratio is considered adequate to eliminate stress field discontinuities caused by the rigid end closures. When this specimen is pressurized, a uniform stress (1:2) field is attained in the center section. Both 4-in.-diam and 10-in.-diam specimens were used in the program.

4.2.1.2 Specimen Fabrication

The fabrication sequence for the biaxial specimens was as follows:

(1) Shear blanks of Ti-5Al-2.5Sn ELI and 2219-T37 to final circumferential dimensions.

(2) Roll form 10-in.-diam cylinders (brake form 4-in.-diam 2219-T37 cylinders).

(3) Heat treat the 2219-T37 to T87 temper.

(4) Weld longitudinal seam. Tungsten inert gas process was used for both the Ti-5Al-2.5Sn ELI and the 2219-T87. No filler wire was used for the Ti-5Al-2.5Sn; 2319 filler wire was used for the 2219-T87.

(5) Inspect all welds using X-ray and dye penetrant techniques.

(6) Trim cylinders to 36 in. long with a circle shear.

(7) Make a circumferential weld bead on the ends of the cylinders.

(8) Scrub each Ti-5Al-2.5Sn ELI cylinder thoroughly with acetone for 15 min. using white cotton gloves and clean white rags.

(9) Stress relieve the Ti-5Al-2.5Sn ELI cylinders at 1,000°F for 3 hours.

(10) Mill starter slots in all specimens.

(11) Bond doublers on the longitudinal weld of the 2219-T87 cylinders scheduled for high stress tests.

Details of the biaxial specimens are shown in Figure 4-11.

4.2.1.3 Specimen Preparation

Crack detector wires were bonded on each cylinder near both ends of the slot but separated by a distance corresponding to the desired length of precrack. A stainless steel shim was placed inside the specimen to seal the starter slot. The shim was held in place by Mylar tape. The specimens were then assembled in end closures which were specifically made for room temperature tests. A schematic of the assembled specimen is shown in Figure 4-12. The biaxial specimens were filled with oil and hydraulically fatigued at pressures below those to be used in the test program until the desired precrack length was reached as denoted by signals from the crack detector wires. The precrack size was then carefully measured while under reduced pressure.

On some occasions, specimens with small starter slots did not precrack easily. It was necessary to burn a small hole (1/16-in. diam) through the specimen with a TIG welding torch with no shielding gas. Small cracks were then more readily obtained for specimens scheduled for high stress testing. Care was taken to be sure that the precrack had extended out of contaminated material. Specimens were then disassembled and cleaned, and crack-propagation gauges were applied. Data sheets similar to those used for uniaxial specimens accompanied each specimen.

4.2.2 Selection of Cyclic Stress Levels

Originally, the stresses planned for the biaxial specimens were to be those noted in Table 3-II. The stress levels were identical with those in the highest and the lowest stress uniaxial tests. However, it was necessary to reduce the stress levels for particular specimens in some cases. This was due to errors in the selection of the size of the precrack.

Sizes of precracks for the room temperature biaxial tests were selected by using the Christensen-Denke equation with a correction after Kuhn*.

*These equations are described in Section 6.1.1.

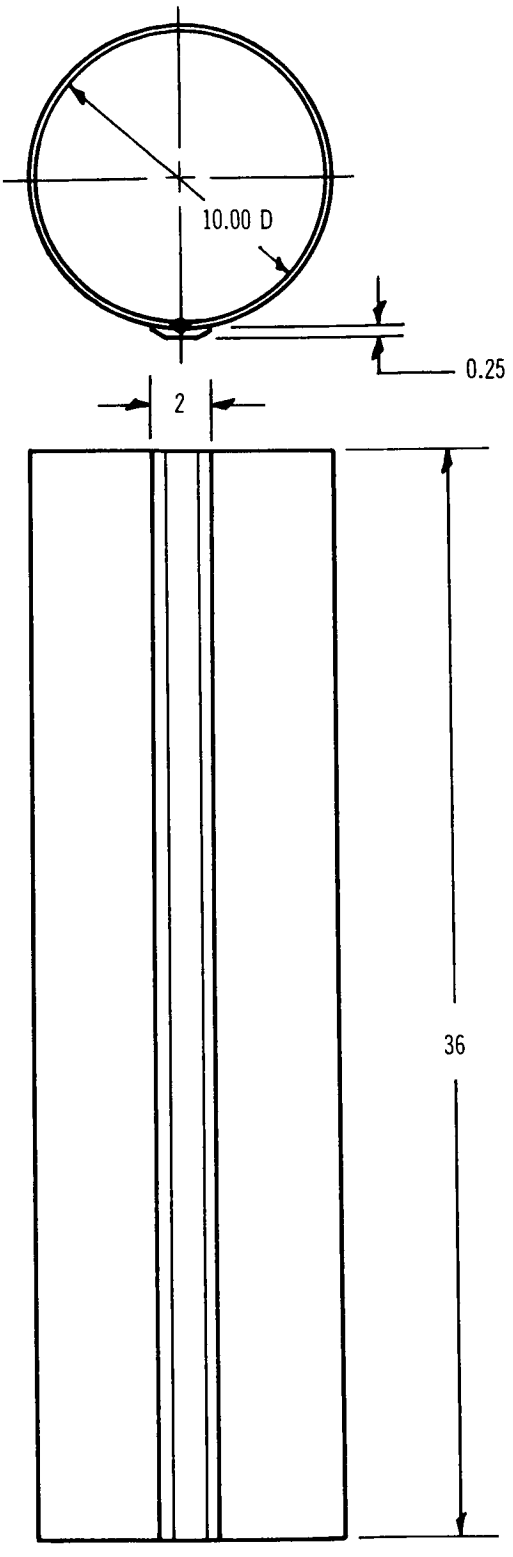

Figure 4-11. Biaxial Specimen With Doubler
(Dimensions in inches)

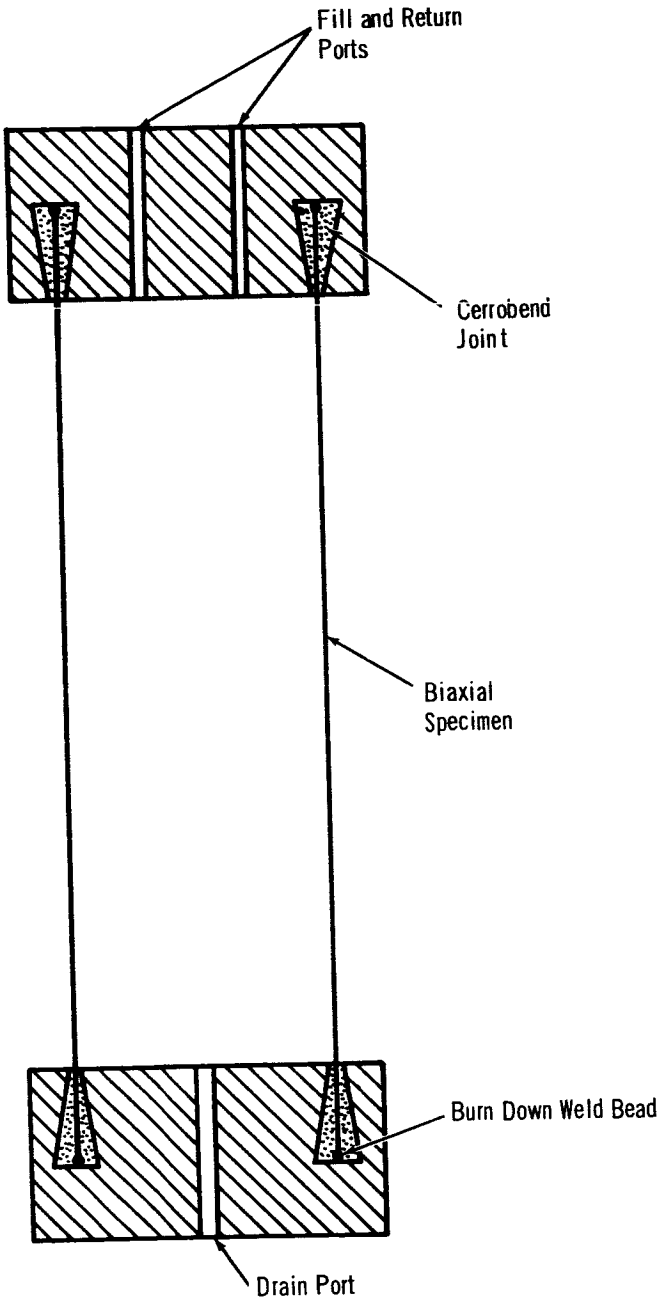

Figure 4-12. Assembled Room Temperature Biaxial Specimen

The results of this equation were then compared with calculations using the Irwin criteria (K_c) and a bulge coefficient correction developed by Anderson* (ref. 12).

Results of these calculations are shown in Figures 4-13 and 4-14. The data points on the above figures are taken from the room temperature dynamic tests. Since the Christensen-Denke equation agreed with the data and no biaxial data were available to obtain a value for the bulge coefficient needed for the Anderson-Irwin equation, it was decided that the Christensen-Denke equation provided an adequate first approximation. Conservative precrack sizes were then selected to account for some experimental error in precracking.

During initial tests at -320°F and -423°F, it was found that the calculated critical crack sizes for Ti-5Al-2.5Sn ELI were much larger than those actually achieved. As a result, it was necessary to reduce the experimental cyclic stress from those which were originally planned in order to achieve a period of stable crack-growth. Results of the biaxial tests are presented in Section 6.1.

4.2.3 Room Temperature Tests

4.2.3.1 Test Apparatus

Specimens were cycled at room temperature by pressurization with hydraulic oil. A schematic of the hydraulic system is shown in Figure 4-15. Special end-closures were made for room temperature pressurization. A schematic of an assembled room temperature specimen is shown in Figure 4-11. Specimen assembly was accomplished by heating an end cap to 180°F with hot water and filling the wedge-shaped groove with liquid cerrobend. The specimen was then placed into position and the assembly was quenched with cold water.

Cerrobend is an alloy of lead, tin, bismuth, and cadmium and melts at 158°F. This alloy undergoes a solid state reaction at room temperature which results in an increase in volume of approximately 0.5% within 2 hours after solidification. As a result, a leak-tight seal is formed around the specimen.

A 55-gal oil reservoir was used to fill the specimen with oil. To pressurize the specimens, an actuator which was driven by a 3,000 psi hydraulic supply acted on a load cylinder which forced oil through the system. A pressure switch was installed in the system to prevent over-pressurization in the event of a malfunction in the control console. Pressure was measured with a Statham 300 psig or 1,000 psig capacity pressure transducer and monitored on an oscilloscope during precracking and on a CEC-124 oscillograph during room temperature tests. The accuracy of the pressure transducers was within ±1% of full-scale capacity.

*The bulge coefficient was estimated from one biaxial static test in which failure occurred by circumferential tearing due to an initial crack size of 5 in.

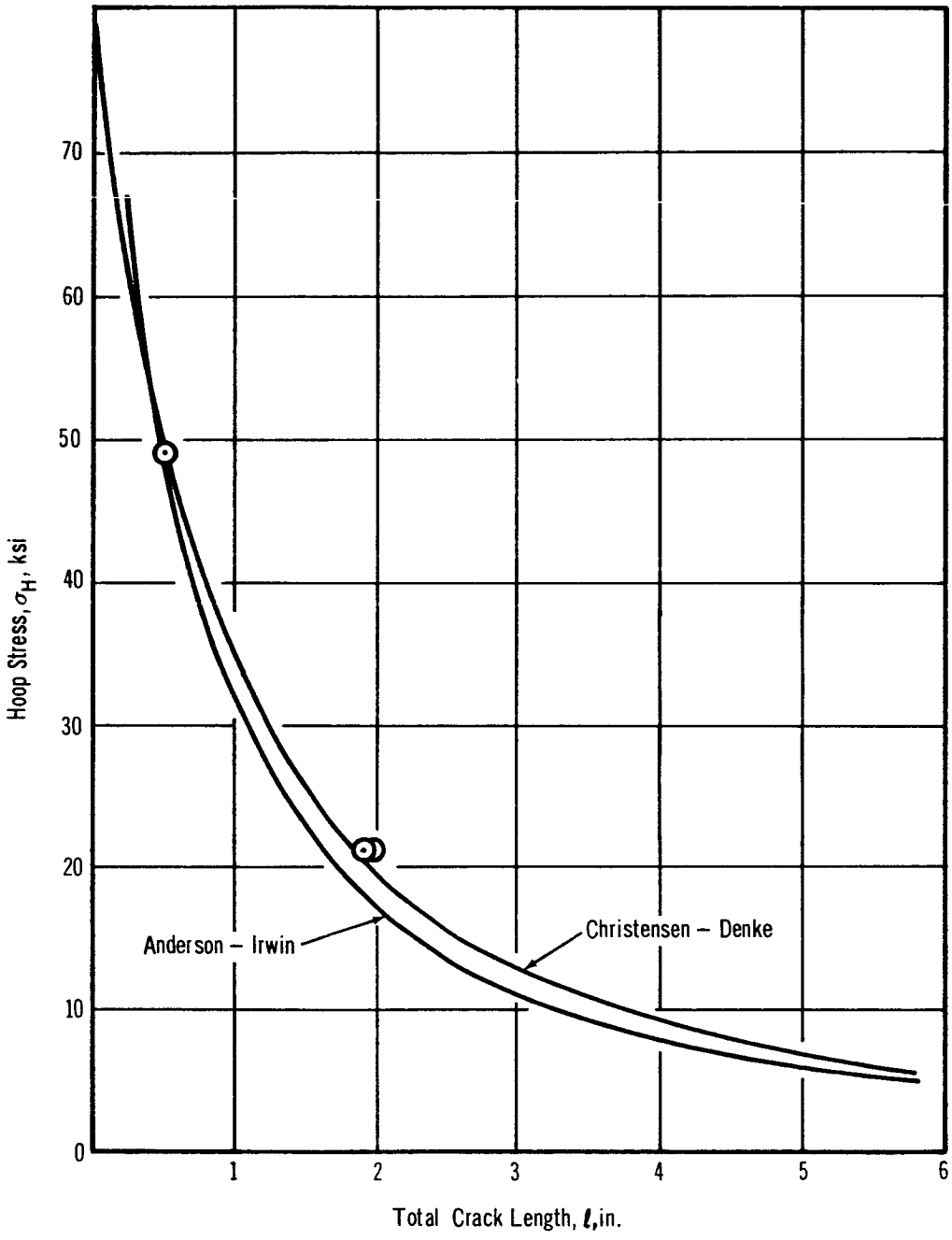

Figure 4-13. Failure Prediction for 10-in. Diam 2219-T87 Aluminum Alloy Cylinders at 70°F

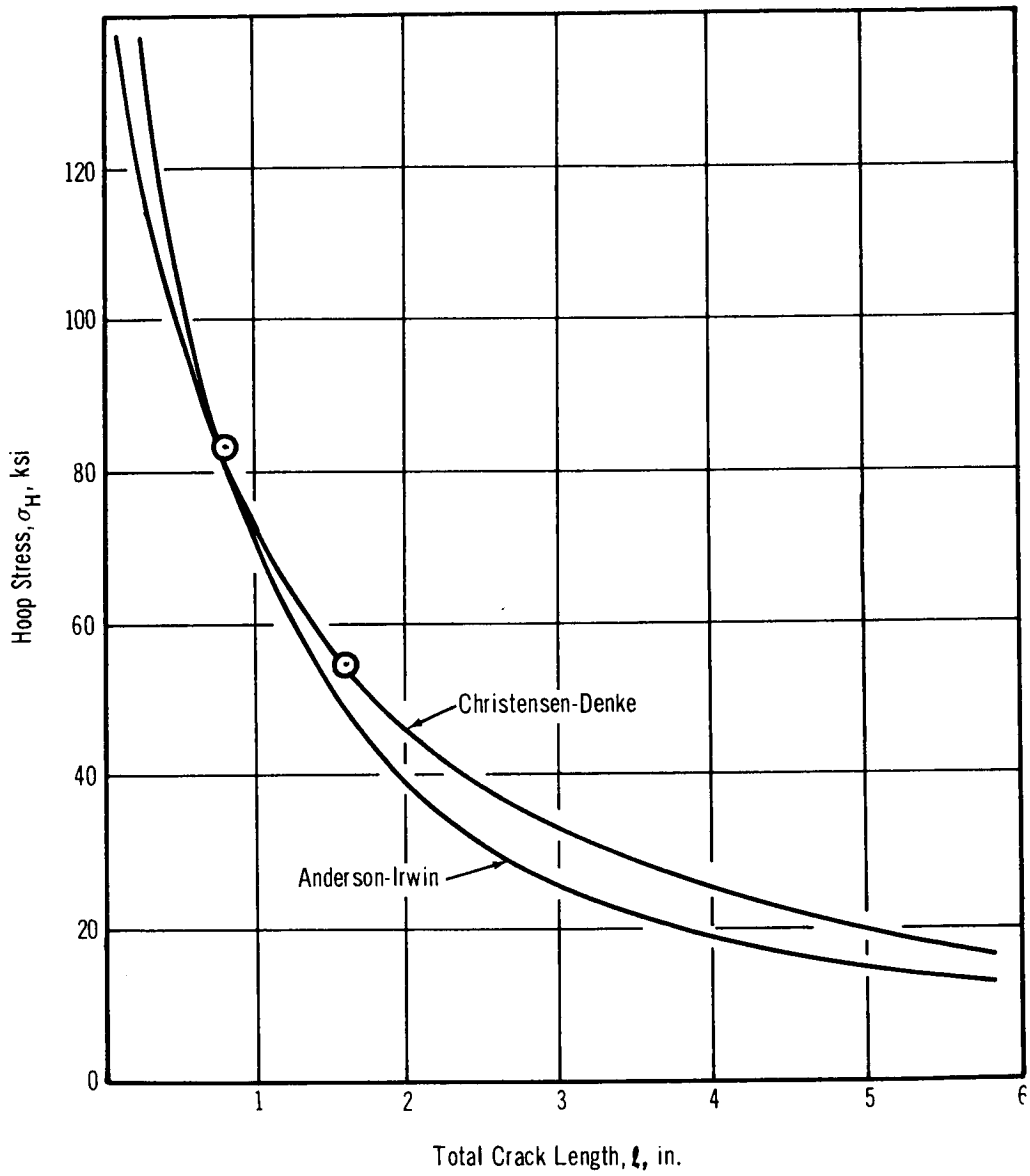

Figure 4-14. Failure Prediction for 10-in. Diam Ti-5Al-2.5Sn ELI Titanium Alloy Cylinders at 70°F

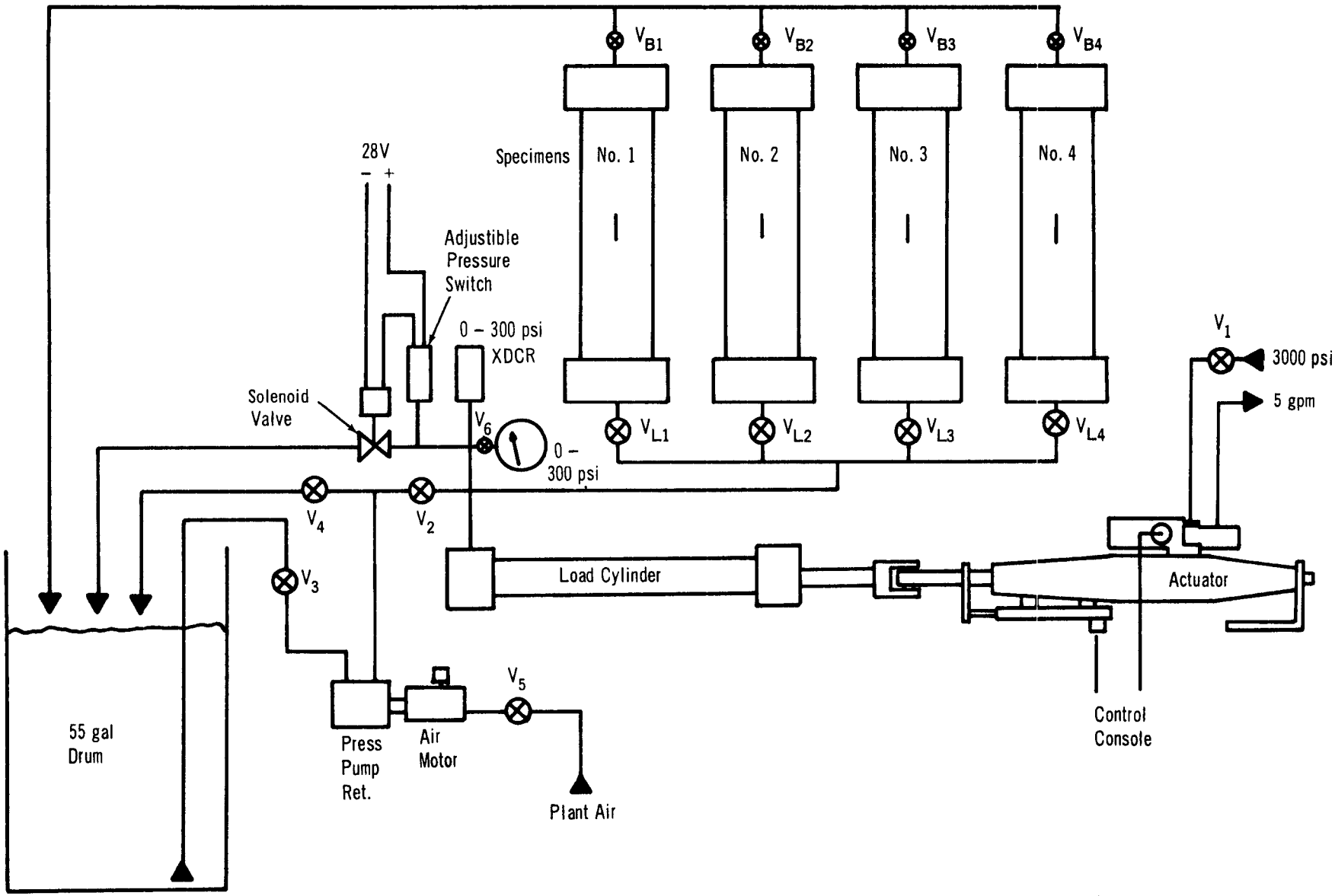

Figure 4-15. Schematic of Hydraulic System for Room Temperature Biaxial Tests

The control console contained a function generator and several servo amplifiers to control the speed and travel distance of the actuator. Instrumentation for data acquisition was the same as for uniaxial tests and has been described in Section 4.1.4.3.

4.2.3.2 Room Temperature Biaxial Test Procedure

At the beginning of each test, the specimen was plumbed into the hydraulic system and filled with oil. A pressure transducer and crack propagation gauges were plugged into an oscillograph. The pressure transducer was set on zero pressure and calibrated. Reference traces were positioned on the oscillograph paper for zero, minimum pressure, and maximum pressure. The zero position and sensitivity of the crack-propagation gauge circuits were adjusted.

All valves to and from the specimen were then closed. A pressure relief switch was set at 5 to 10 psig above maximum test pressure to prevent accidental over-pressurization. A specimen being tested at room temperature is shown in Figure 4-16.

The oscillograph was started and calibration readings were recorded at the beginning of the data trace. The pressure was raised to a point just below the mean stress and cycling at approximately 10 cpm was started. The amplitude of the pressure cycle was adjusted and shifted until both maximum and minimum pressures were those desired. Cycling speed was then increased slowly while adjusting the pressures until a speed of 30 cpm was reached. The pressure was continuously monitored and pressure adjustments were made throughout the test.

After specimen failure, the pressure transducer calibration was checked to be sure that no changes in sensitivity or zero position had occurred during the test.

4.2.4 Cryogenic Tests

4.2.4.1 Apparatus

Cryogenic tests were conducted by pressurizing with the cryogenic test fluid. Special end closures were designed for these tests. A schematic of an assembled specimen is shown in Figure 4-17.

A groove filled with cerrobend was used to attach the specimen to the end closures. This joint provided an adequate seal at room temperature and -320°F but invariably cracked and leaked when cooled to -423°F. Radial cracks in the cerrobend were observed after several -423°F tests. The size of the cracks and the amount of leakage were variable and the maximum pressure attainable in each test varied. In several cases, pressures as high as 700 psig were attained before the leak rate equaled the rate of displacement by the pressurizing shaft.

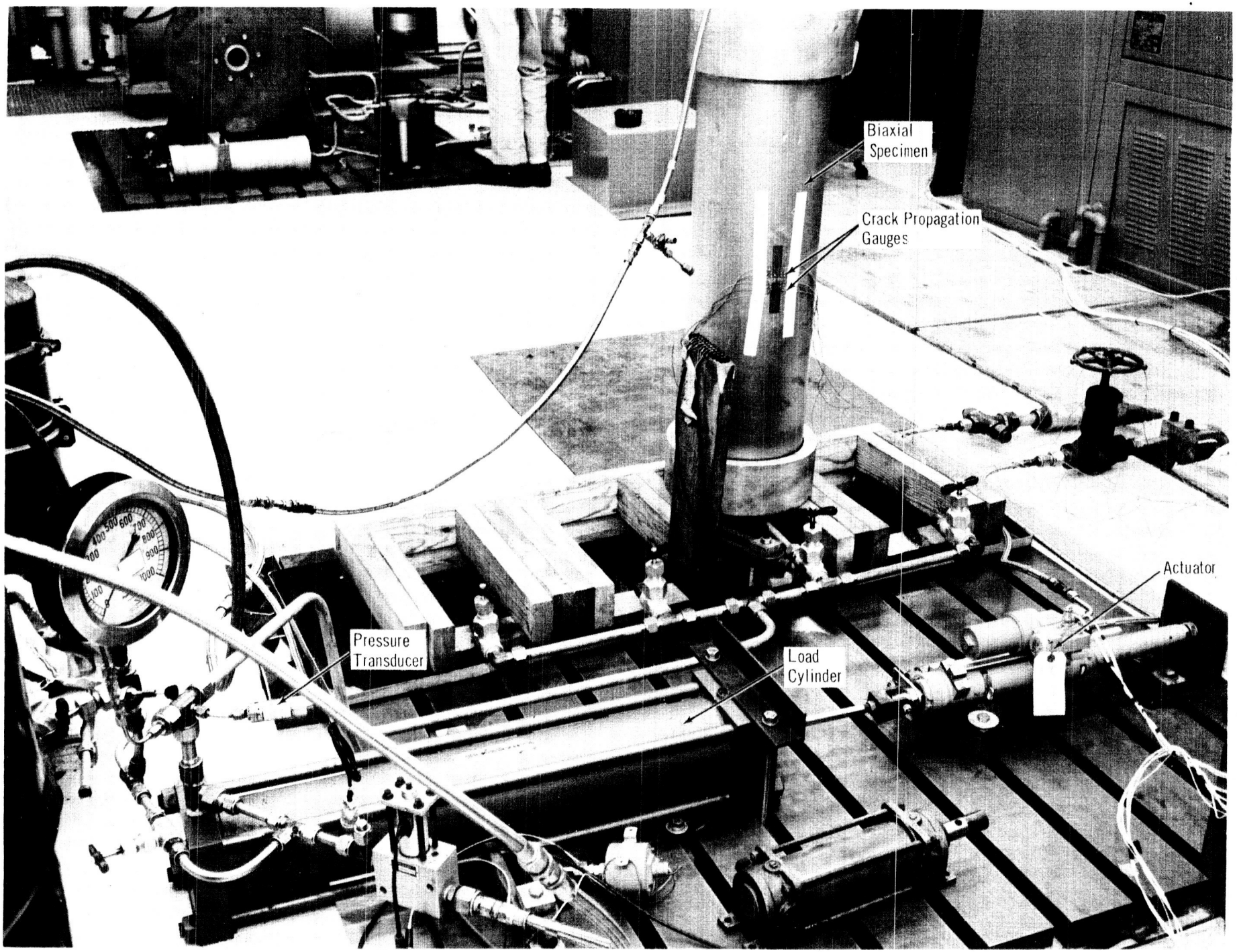

Figure 4-16. Room Temperature Biaxial Test

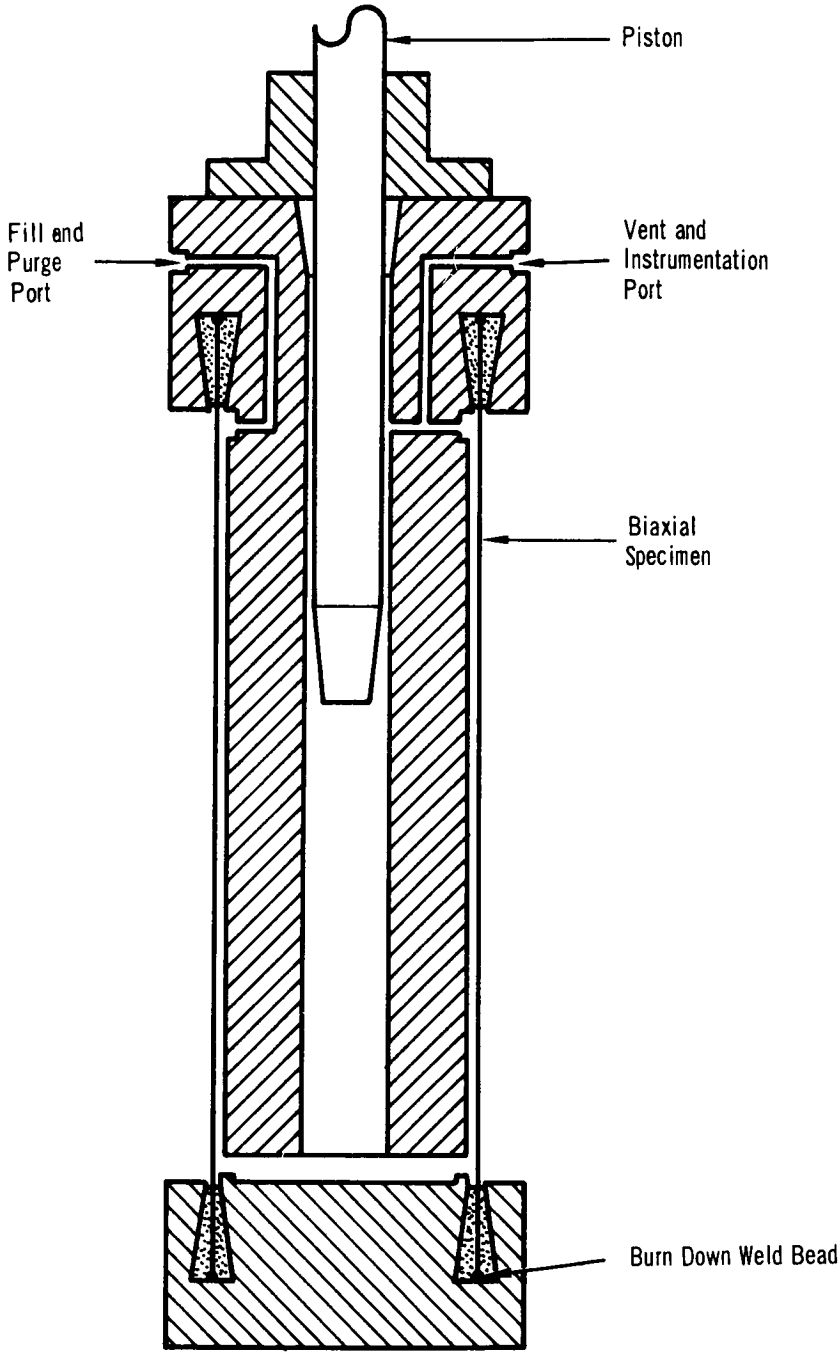

Figure 4-17. Assembled Cryogenic Biaxial Specimen

The inner volume of the specimen was a solid core of aluminum with fractional clearances between the cylinder and the core. The core center was bored out to accept a vertical-stroking piston. An attempt was made to use piston rings made of glass impregnated Teflon on the shaft to achieve pressurization. These attempts failed due to the inability to maintain exact alignment during testing. A modification of the design was made to include the housing at the top of the specimen (Figure 4-18). This housing contained bronze alignment bushings and a set of Kel-F chevron seals. This housing, along with the connectors on the shaft, provided the necessary alignment and sealing for pressurization. The shaft could then be driven into the specimen and the displacement resulted in pressurization. The housing before assembly is shown in Figure 4-19. Two contracting piston rings were also located in the bottom of the housing. One of these is shown in Figure 4-19.

A typical test setup for liquid nitrogen testing is shown in Figure 4-20. Several changes in the plumbing at the specimen were made to permit remote purging of check valves during testing. A flow chart of the final arrangement is shown in Figure 4-21.

Cryogenic fluids were piped to the specimen and cryostat through a 25-ft long vacuum jacketed hose. Flow to both the specimen and cryostat was controlled by gas operated, vacuum jacketed valves. Check valves and pressure relief valves were incorporated between the specimen and the specimen fill valve to prevent inadvertent pressurization of the fill system. Provisions for purging the piping system prior to liquid hydrogen tests were made. All of the gas operated valves were mounted on the cryostat lid and were controlled remotely from a blockhouse.

The cryostat, which was around the specimen during testing, was a 120-gal capacity vacuum jacketed container. A drain spout was located at the bottom of the cryostat to permit rapid draining of fluids.

The cryogenic piping, valves, and cryostat were built to specification by Hoffman Laboratories, Inc., under subcontract number DAC-A-65-503.

The portion of the test apparatus which pressurized the specimen consisted of a vertically mounted hydraulic jack driven by a 5,000 psig capacity pumping unit. The hydraulic ram was used to drive the pressurization shaft into the specimen. The hydraulic pumping unit was controlled and operated from a blockhouse. The bottom of the hydraulic cylinder was pressurized with dry nitrogen at approximately 200 psig in order to return the pressurization shaft to its original position.

Crack-growth instrumentation for the cryogenic biaxial tests was identical to that used in the uniaxial tests and is described in Section 4.1.4.3.

4.2.4.2. Cryogenic Biaxial Test Procedure

Both liquid nitrogen and liquid hydrogen biaxial tests were conducted using similar procedures.

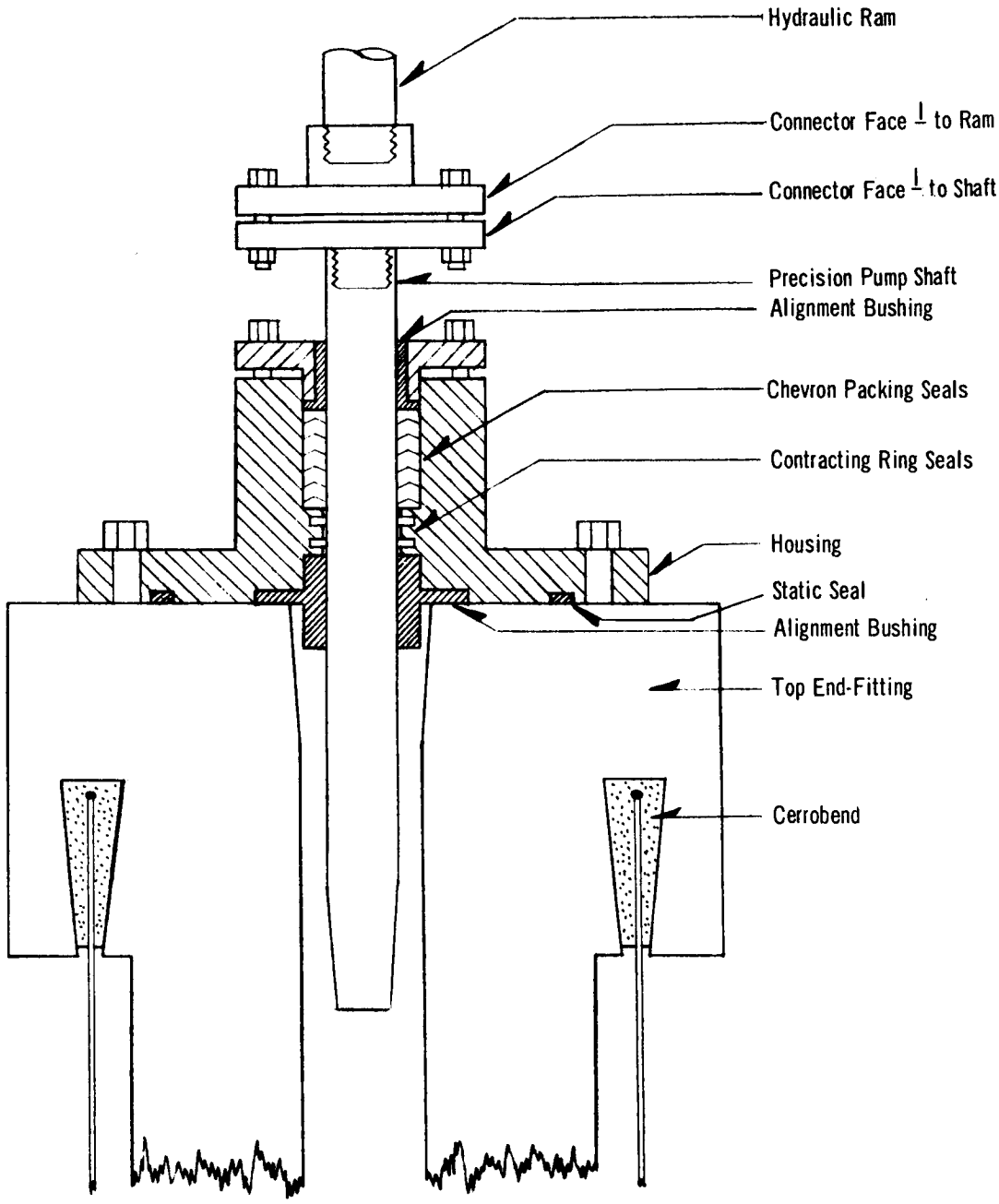

Figure 4-18. Cryogenic Biaxial Test System Alignment and Sealing Devices

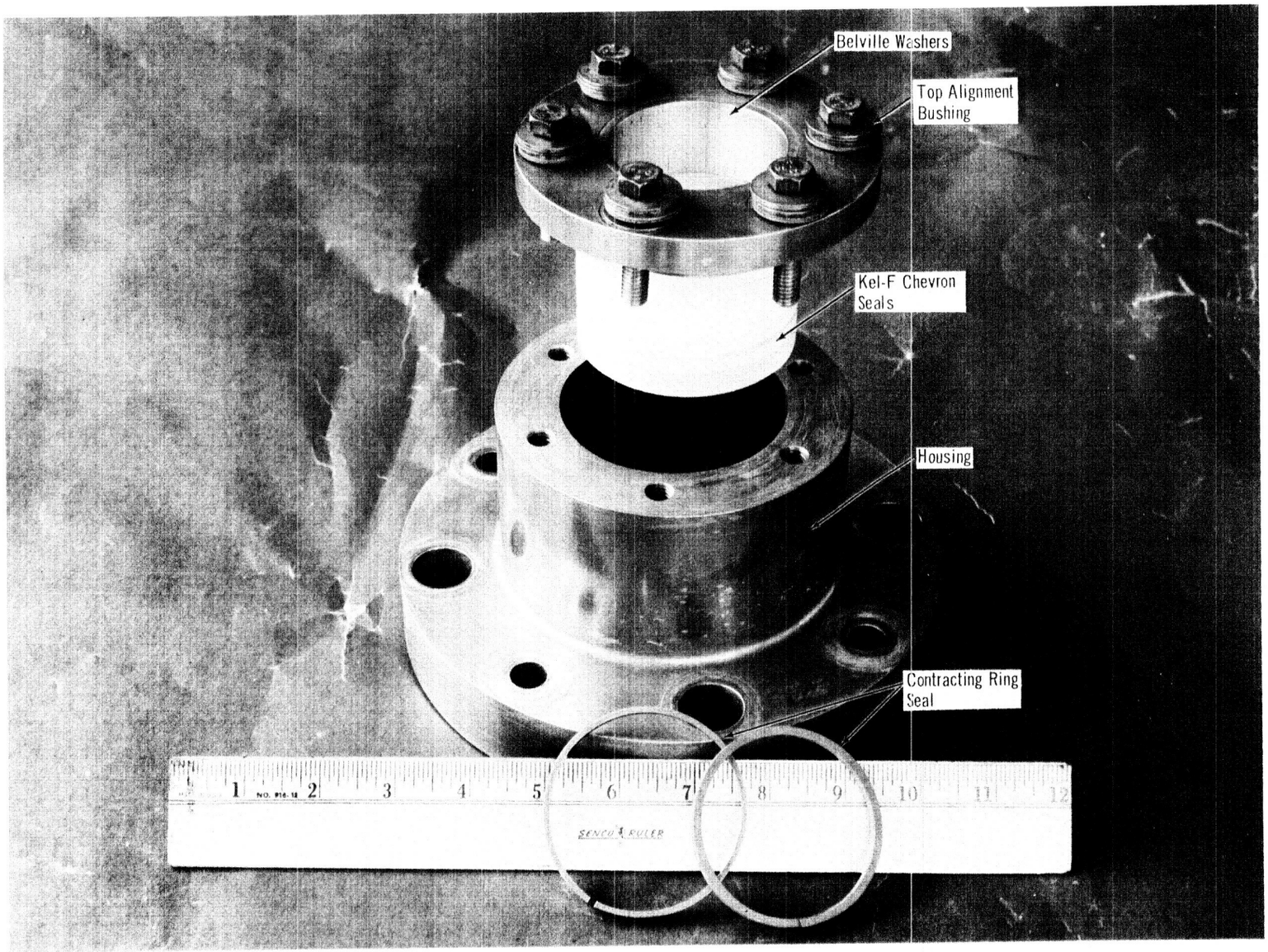

Figure 4-19. Housing for Cryogenic Tests

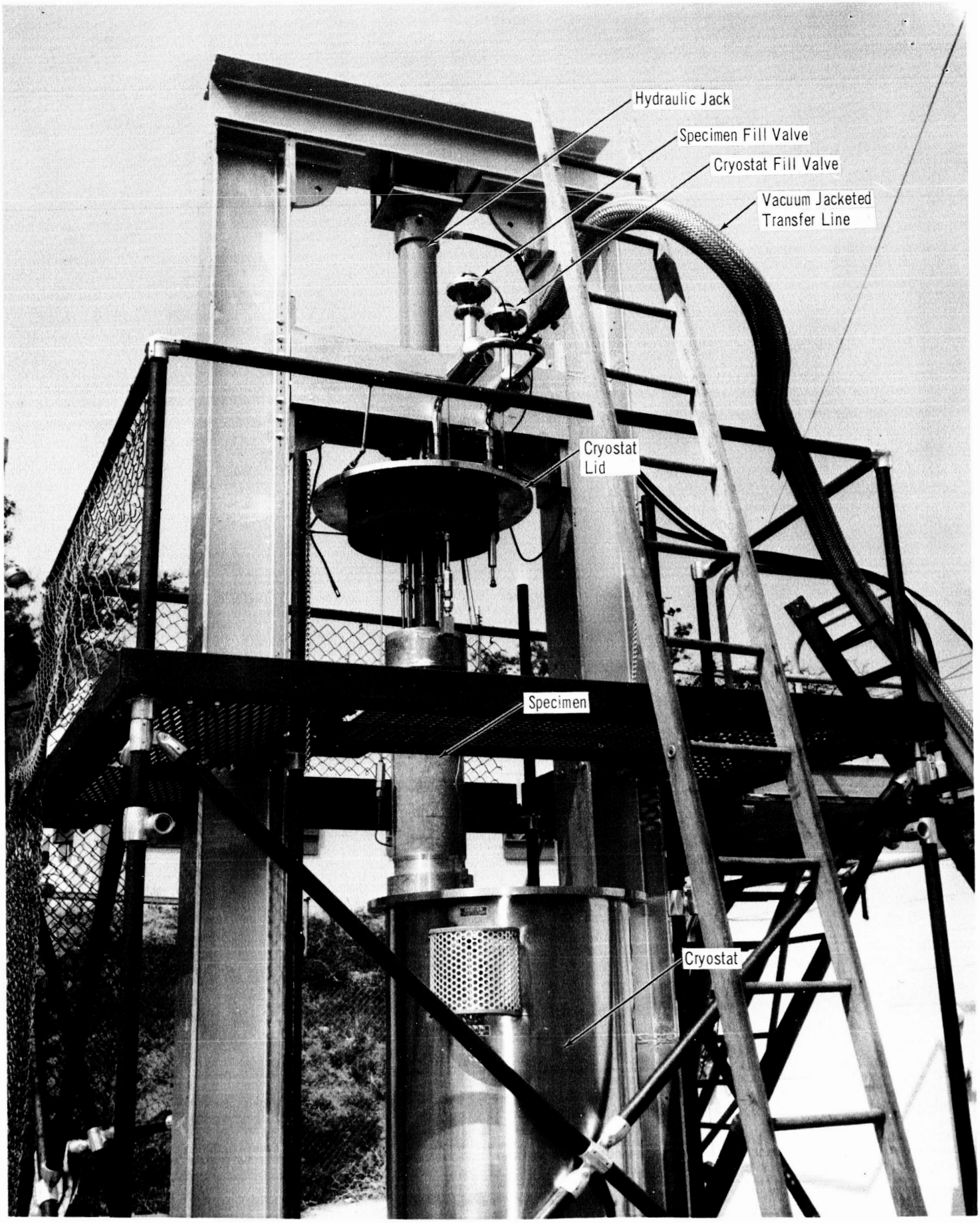

Figure 4-20. Typical Test Setup for Liquid Nitrogen Testing

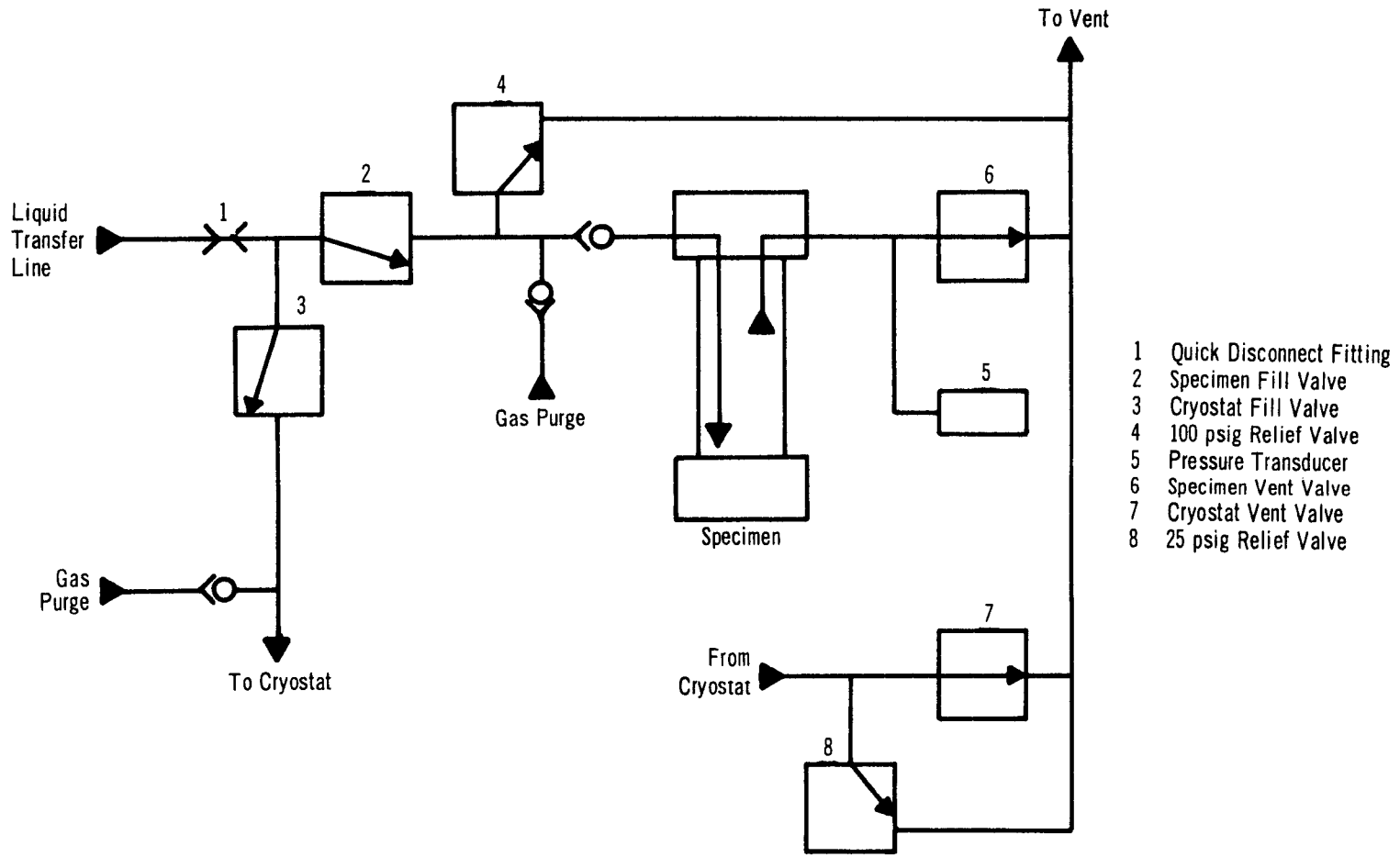

Figure 4-21. Cryogenic Flow System

Before the specimen was placed in position for testing, the following steps were taken:

(1) The pressurization shaft and alignment bushings were polished with 0-grade metallographic paper.

(2) The chevron seals were cleaned with acetone and polished with 2/0 metallographic paper.

(3) The top surface of the top cryogenic end fitting was sanded smooth with 180 grit sandpaper.

(4) The housing was assembled and placed in position.

(5) Bolts holding the housing to the top end fitting were torqued to 80 ft-lb.

(6) The pressurization shaft was placed in position and the seals were torqued to 75-in. -lb.

The specimen was then transported to the test stand for assembly. A careful leak check was made of all fittings and seals. After all lines had been connected to the specimen, a screen was then placed around the specimen to keep pieces of tape used to seal the existing precrack from getting into the cryostat and plugging the cryostat drain tube.

Wires on the crack-propagation gauges were connected and a complete check was made of all instrumentation. The procedure for setting up the instrumentation was the same as previously described for the room temperature tests (Section 4. 2. 4. 1).

The specimen was then adjusted for alignment to the hydraulic ram. This adjustment was made by turning the bolts which held the specimen until the face of the connector on the end of the shaft and the face of the connector on the end of the hydraulic ram were parallel (Figure 4-22).

Parallelism was set with a feeler gauge and was better than ±0. 001-in. across the connector face. After the alignment, the cryostat was raised into position and bolted down.

Both the specimen and the cryostat were purged for approximately 5 min. with dry nitrogen gas to drive off any acetone which may have been left in the lines after cleaning.

The bottom drain on the cryostat was capped and the cryostat and specimen were filled with liquid nitrogen. The specimen was considered full when the cryostat overflowed and liquid came out of the specimen vent line.

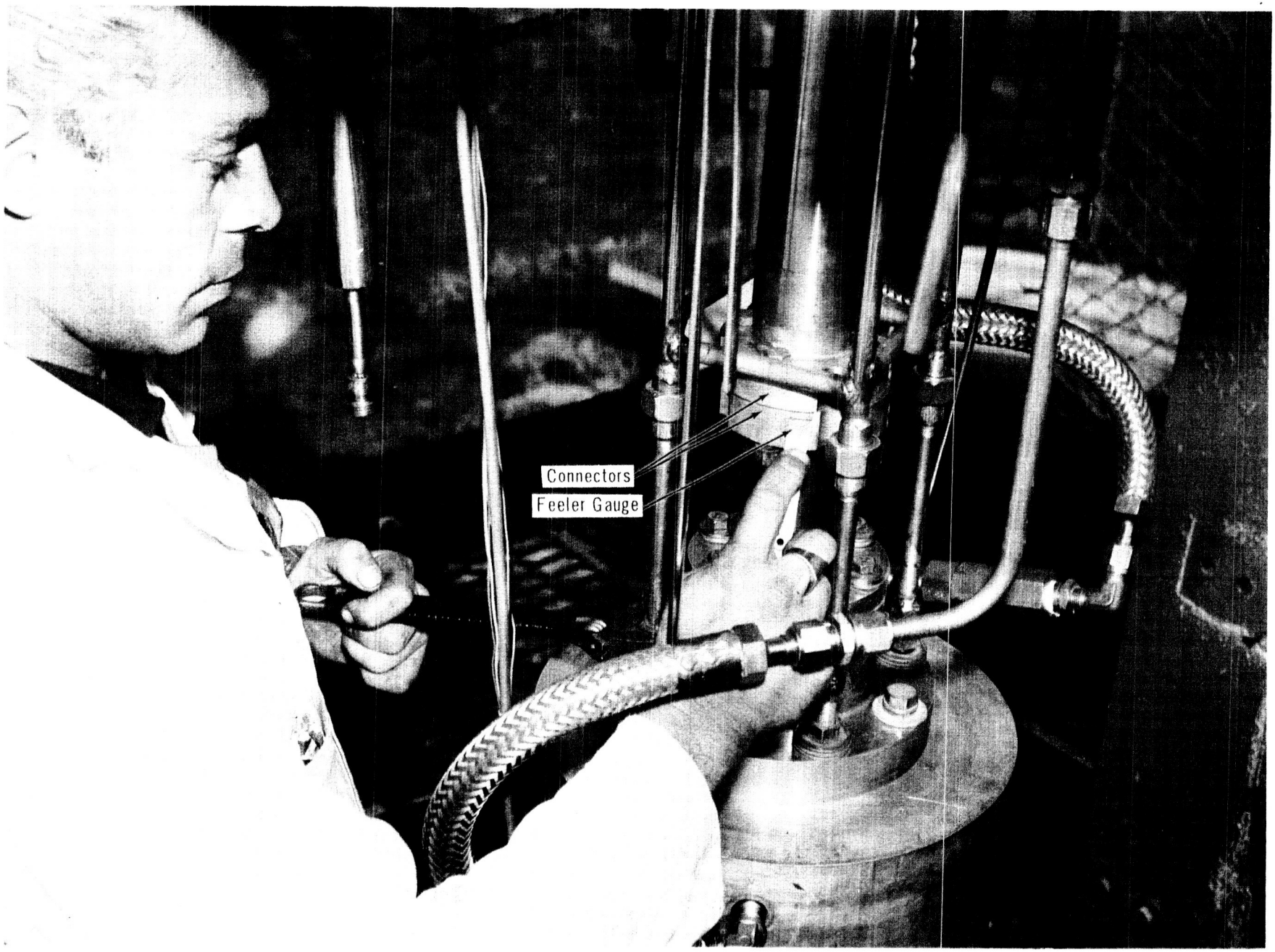

Figure 4-22. Aligning Cryogenic Biaxial Specimen

For each liquid hydrogen test, the cryostat and specimen were filled with liquid nitrogen which was then drained from the cryostat. The piston was lowered to be sure that no residual nitrogen would impede its progress into the specimen. Both the specimen and the cryostat were purged with gaseous nitrogen after all the liquid had drained from the cryostat.

A helium purge sequence which cleared nitrogen from fill lines and valves was started. Personnel on the site were notified that the area was closed to traffic.

After a 10-min. helium purge, the specimen and cryostat were filled with liquid hydrogen. When liquid overflowed from the cryostat and was coming out of the specimen vent line, the specimen was considered full. The top end fitting on the specimen was approximately 25 in. below the lid of the cryostat. The pressurizing shaft was raised and the instrumentation checked to be sure that there had been no temperature effects.

The hydraulic pump was started, and a switch was activated which closed the return line on the hydraulic pump. The pressure on the hydraulic pump was increased until the specimen reached maximum load. The return line was then opened until the specimen reached the minimum pressure for the test. Cycling speed was gradually increased to approximately 20 cpm and was manually controlled throughout the test. Different automatic cycling mechanisms were tried early in the program but were not as satisfactory as the manual control due to drift during testing operations.

Because of an increase in the amount of gas in the specimen, and/or small leaks, the pressurization shaft moved lower on each pressure cycle. When the limit of travel of the shaft was reached, the pressure was dropped to zero, the shaft raised to its maximum height, and the specimen and the cryostat were refilled. In most cases the cryostat began spilling over immediately and, therefore, did not require further refilling.

After specimen failure, the hydrogen in the cryostat was eliminated by blowing large quantities of gaseous nitrogen through the fill line and by blowing warm air into the bottom of the cryostat. The nitrogen flow was stopped after approximately 15 to 20 min., and the air was allowed to flow overnight to warm the system for handling.

4.3 DATA HANDLING PROCEDURES

Procedures were developed to simplify data reduction and to obtain the maximum possible accuracy. Load calibration and data traces were measured to within ±1/4% of their calibration scale. Independent measurements were made of the maximum and minimum cyclic loads and the load at failure.

Plots of crack length versus cycles were developed by plotting the growth of each crack front versus cycles and adding the curves from each crack front, Figure 4-23.

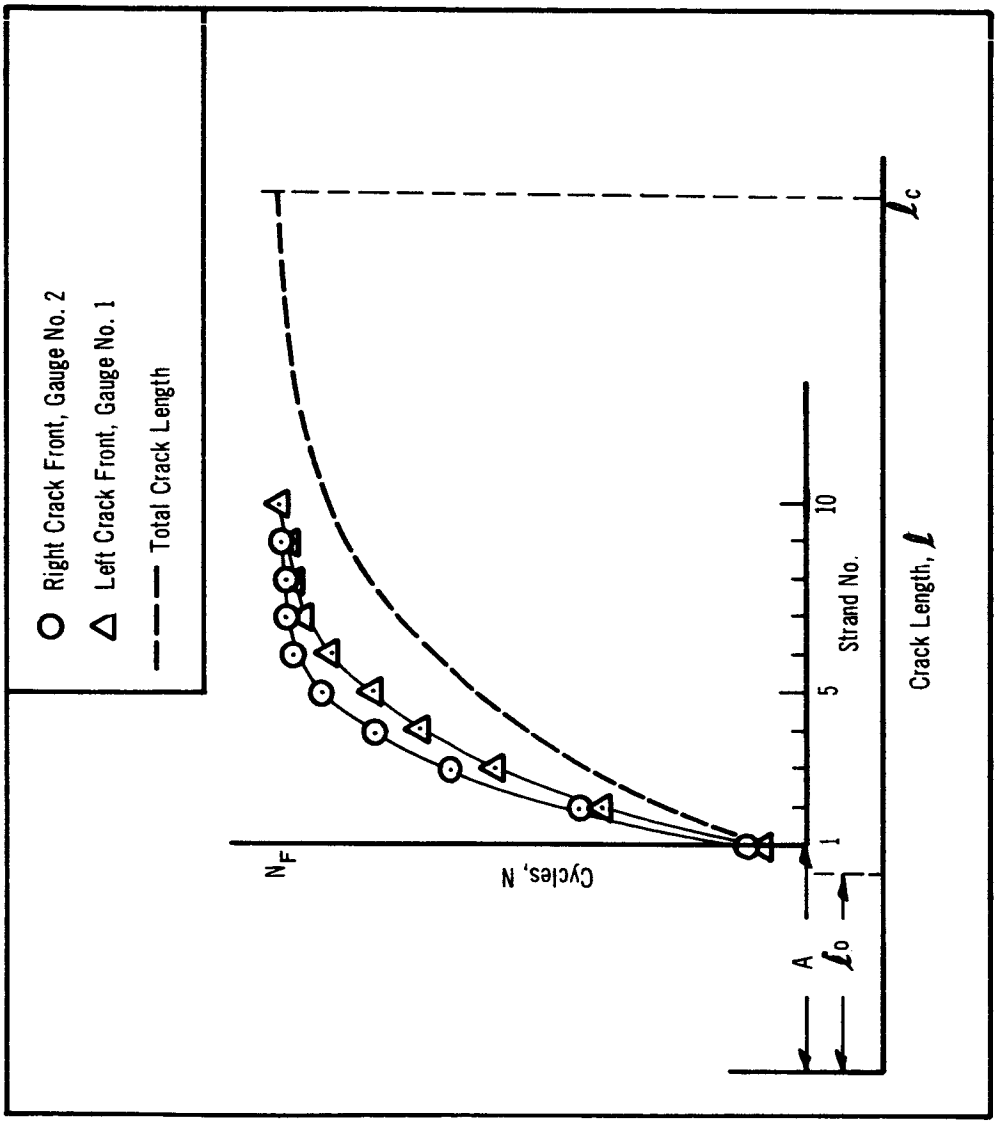

Figure 4-23. Idealized Plot of Crack Propagation Data

An equation was developed which fit each crack-growth curve. This equation, which is discussed in Section 5, was used as a procedural tool for analysis. By expressing the data mathematically, it was possible to calculate $d\ell/dN$, σ gross, σ net, and various functions of K at any point in the test. A Royal-McBee Corporation computer, model LGP-30, was used for this task.

A preliminary and final series of calculations were made. The preliminary calculations did not contain corrections for crack-propagation gauge readings and for the stress on the final cycle of the test but were merely used as an initial step in discovering meaningful parameters.

Section 5
UNIAXIAL TEST RESULTS

5.1 BASELINE PROPERTY TESTS

Baseline mechanical properties and fracture toughness parameters were established for both test materials at all test temperatures. These properties were determined by static (load-to-failure) tests. Conformance of the chemical composition of each alloy to specified limits were verified. Results of chemical analyses and a typical pole figure are reported in Appendix A. Pole figure analyses performed on five sheets of Ti-5Al-2.5Sn ELI indicated a high degree of texturing due to sheet rolling with the basal (0001) crystallographic planes oriented in the plane of the sheet.

Measurements of sheet thickness indicated that a wide variation of thickness existed in the Ti-5Al-2.5Sn ELI material from sheet to sheet and within some individual sheets. The thickness range for the lot of Ti-5Al-2.5Sn ELI sheets was 0.016 to 0.024 in. Within some Ti-5Al-2.5Sn ELI sheets, the thickness varied as much as ±10%. The thickness range for the lot of 2219-T87 sheets was 0.059 to 0.065 in. Sheet thickness variation for 2219-T87 did not exceed ±2% in any sheet.

5.1.1 Mechanical Properties

Mechanical property tests at room temperature were performed on each sheet of test material. The properties were measured for the longitudinal and transverse directions and included 0.2% offset yield strength, ultimate tensile strength, elongation, elastic modulus, and Poisson's ratio. Plastic Poisson's ratio was also measured on some of the Ti-5Al-2.5Sn ELI specimens. Mechanical property tests were also performed at -320° and -423°F on 2219-T87 (transverse specimens) and on Ti-5Al-2.5Sn ELI (longitudinal specimens). The average mechanical properties are given in Figures 5-1 and 5-2. The results of individual tests are presented in Appendix B.

5.1.2 Fracture Toughness Test

To establish the stress levels and initial flaw sizes for the cyclic test portion of the program, static (load-to-failure) tests were performed on centrally cracked, 16-in.-wide panels. Each panel contained a central slot which had been fatigue-cracked to a total length of 5 in. A minimum of two panels was tested for each test material at room temperature, -320°F and -423°F. Individual test results are tabulated in Tables 5-I and 5-II.

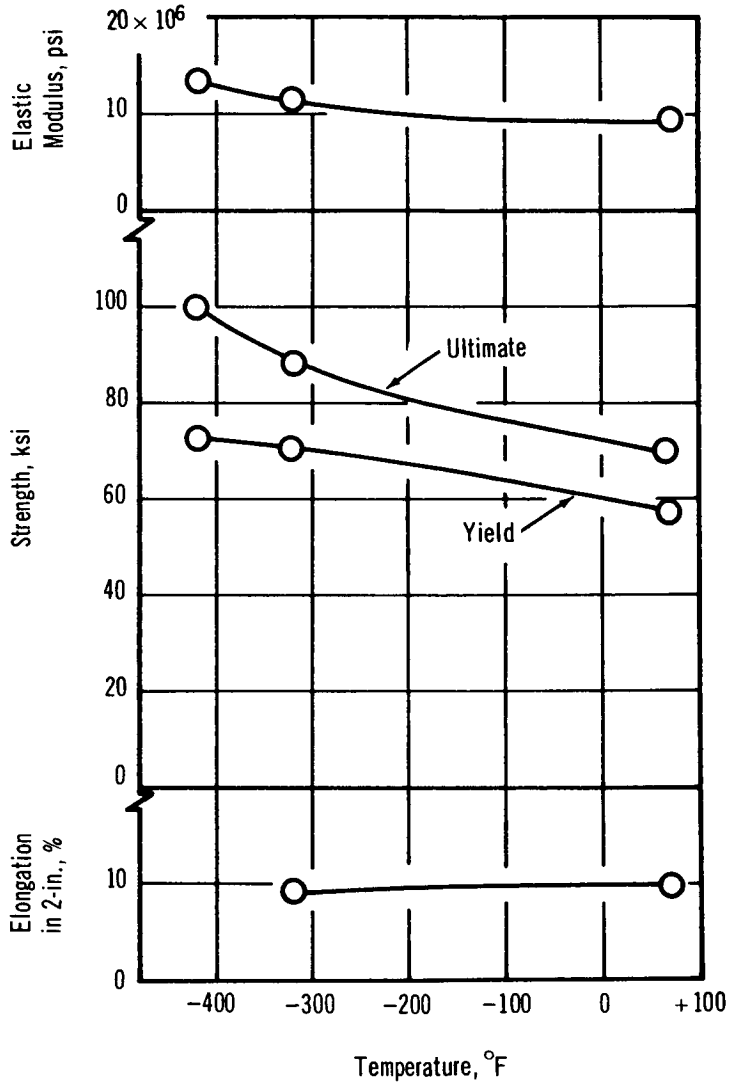

Figure 5-1. Average Transverse Mechanical Properties of 0.060-in. 2219-T87 Sheet

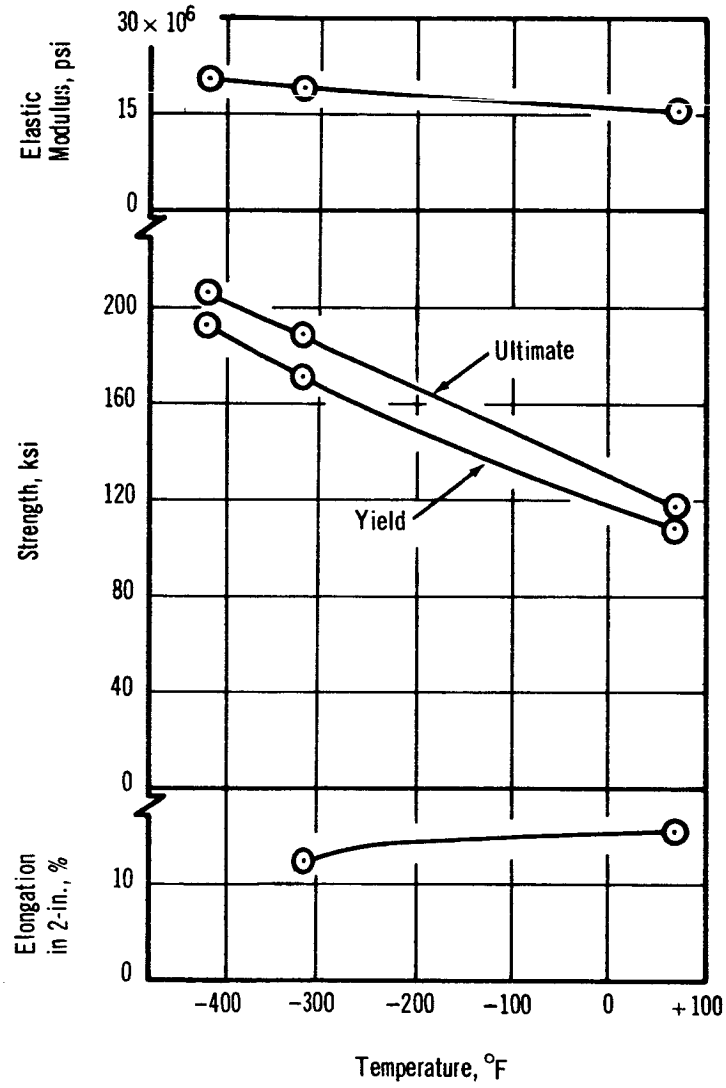

Figure 5-2. Average Longitudinal Mechanical Properties of 0.020-in. Ti-5Al-2.5Sn ELI Sheet

TABLE 5-I

RESULTS OF UNIAXIAL STATIC TESTS PERFORMED ON 2219-T87 0.060-IN. SHEET[1]

Specimen			Crack Length		Stress				
No.	Width (in.)	Thickness (in.)	Initial ℓ_o (in.)	Critical ℓ_c (in.)	Gross σ_o (ksi)	Net σ_n (ksi)	σ_n/σ_y [2]	K_c ksi (in.)$^{1/2}$	R_p (in.)
			Test Temperature, 70°F						
AC	15.93	0.061	5.00	6.28	22.76	37.56	0.65	81.89	7.56
MA	16.29	0.062	4.98	5.91	23.09	36.24	0.62	79.42	6.68
DD	16.29	0.062	5.00	6.36	21.55	35.35	0.61	77.27	6.74
			Test Temperature, -320°F						
NA	15.99	0.062	5.00	6.70	28.07	48.31	0.67	105.88	8.55
KA	15.99	0.061	5.00	6.52	27.52	46.47	0.65	101.39	7.46
			Test Temperature, -423°F						
DC	15.93	0.062	5.06	6.41	26.32	44.05	0.59	94.86	4.53
GA	15.99	0.061	5.00	5.98	26.25	41.94	0.56	90.01	3.77

(1) Transverse specimens: crack growth direction parallel with rolling direction of sheet.

(2) Net section stress to yield strength ratio.

TABLE 5-II

RESULTS OF UNIAXIAL STATIC TESTS PERFORMED ON Ti-5Al-2.5Sn.ELI 0.020-IN. SHEET[1]

Specimen			Crack Length		Stress				
No.	Width (in.)	Thickness (in.)	Initial ℓ_o (in.)	Critical ℓ_c (in.)	Gross σ_o (ksi)	Net σ_n (ksi)	σ_n/σ_y [2]	K_c ksi (in.)$^{1/2}$	R_p (in.)
Test Temperature, 70°F									
DIO	16.39	0.018	5.07	6.66	58.67	98.84	0.90	236.34	51.84
SM	15.95	0.018	5.06	6.78	54.49	94.78	0.86	219.45	35.99
Test Temperature, -320°F									
DIP	15.94	0.018	5.00	5.40	44.62	67.49	0.39	139.99	2.34
XM	16.23	0.020	4.98	5.61	44.83	68.51	0.40	143.75	2.58
Test Temperature, -423°F									
AIO	15.93	0.019	4.98	5.28	29.22	43.70	0.22	88.99	0.75
RP	15.93	0.016	4.98	5.48	32.84	50.07	0.25	102.56	1.03

(1) Longitudinal specimens: crack growth direction perpendicular to rolling direction of sheet.

(2) Net section stress to yield strength ratio.

In these tests, the growth of the crack during loading was monitored by means of the crack propagation gauges bonded to the specimen surface at the extremities of the fatigue precrack. As the crack grew with increasing applied tensile load, it severed the strands of the gauge in succession and caused the electrical resistance of the gauge to increase in discrete jumps. These jumps in resistance were recorded on an oscillograph simultaneously with the tensile load. The length of the crack at maximum load, when catastrophic fracture began, was then established as the critical crack length, ℓ_c, by analysis of the oscillographic trace.

5.1.2.1 Methods of Analysis

In static fracture toughness tests, the maximum gross stress at failure, σ_o, and the critical crack length, ℓ_c, are employed in calculations of parameters representative of the resistance of the test material to propagation of cracks. The critical stress intensity, K_c, is one such parameter utilized in this program. As introduced by Irwin (ref. 13), the critical stress intensity for centrally cracked flat panels of finite width is

$$K_c = \sigma_o \left[w \tan \left\{ \frac{\pi}{2w} \left(\ell_c + \frac{K_c^2}{\pi \sigma_y^2} \right) \right\} \right]^{1/2} \qquad (5\text{-}1)$$

where

σ_o = gross stress

w = specimen width

ℓ_c = total length of critical crack

σ_y = 0.2% yield strength (uniaxial)

Because eq. (5-1) was developed on the basis of linear elastic theory, its usefulness is limited to approximately elastic conditions. For accuracy, certain restrictions upon specimen configuration and testing conditions have been suggested (ref. 11). Notable among these is that the net stress at failure should not exceed about 90% of the uniaxial yield strength.

A second parameter employed in this program is the notch resistance factor, R_p, introduced at Douglas by Christensen and Denke (ref. 6). This parameter was developed empirically in studies of through-cracks in panels and is defined mathematically as

$$R_p = \frac{3\ell_c}{\left[\frac{\sigma_u}{\sigma_o} \left(1 - \frac{\ell_c}{w} \right) \right]^2 - 1} \qquad (5\text{-}2)$$

where σ_u is the uniaxial ultimate tensile strength and the other symbols are as defined for eq. (5-1).

5.1.2.2 Selection of Conditions for Cyclic Tests

Maximum stress levels planned for the uniaxial dynamic tests were to be selected on the basis of the strengths of an uncracked panel and of a panel containing a 5-in. initial precrack. The highest maximum cyclic stress would correspond with the tensile ultimate strength divided by 1.4 or the tensile yield strength divided by 1.1, whichever was lower. The lowest maximum cyclic stress would correspond with the gross stress at failure of a panel containing a 5-in.-long initial precrack, as determined by static tests. The intermediate maximum cyclic stress would be a stress halfway between the highest and the lowest maximum cyclic stresses.

Initial crack lengths for the cyclic tests were selected on the basis of the critical stress intensity, K_c, determined by the static tests. The limitation placed upon initial conditions for cyclic tests was that the initial maximum stress intensity should not exceed 60% of the critical stress intensity. The longest permissible initial crack lengths for the selected maximum cyclic stresses were calculated with eq. (5-1) used in the following form

$$\ell_o = \frac{2w}{\pi}\left[\left\{\arctan\left(\frac{K_o^2}{\sigma_{max.}^2\, w}\right)\right\} - \frac{K_o^2}{2w\sigma_y^2}\right] \qquad (5\text{-}3)$$

where

ℓ_o = total initial crack length

K_o = initial stress intensity

= $0.6\, K_c$

$\sigma_{max.}$ = maximum cyclic stress

Panels for the cyclic tests were slotted and precracked in fatigue to crack lengths slightly less than the values calculated by means of eq. (5-3).

5.2 CYCLIC TESTS

Cyclic tests were performed in a manner similar to that used in the static tests except that the tensile load was cycled between the predetermined maximum and minimum stresses. The progress of crack propagation was monitored by gauges at all test temperatures. In addition, visual measurements of the crack length throughout the cyclic tests at room temperature and at -320°F were made and recorded on the oscillographic trace simultaneously with the load and crack propagation gauge readings (Section 4.1.4.3). Visual measurements at -423°F were made in selected tests by interrupting

the loading sequence after a number of cycles and, after siphoning off liquid hydrogen to protect test personnel, measuring the length of the crack visually; after the measurement was completed, the cryostat was refilled and the test continued.

Comparison of the visual measurements and the crack propagation gauge measurements revealed that, in all cases, the gauge crack length exceeded the visual crack length. The amount of error in the gauge readings increased at the higher maximum stresses and varied with test temperature. The results of this comparison are shown in Figure 5-3, in which the average correction factor for crack propagation gauge readings is shown as a function of maximum stress for each test temperature. These average values were employed in correcting all gauge-measured crack lengths. Only corrected, or true, crack lengths are reported here.

The conditions and results of cyclic tests are tabulated in Tables 5-III and 5-IV.

5.2.1 Methods of Analysis

Much previous effort has been devoted to the development of theoretical and empirical expressions for the crack growth rate of cracked panels subjected to cyclic loading (refs. 6 and 14 through 17). Various equations have been published to relate the effects of stress and crack length on the growth rate. Often in these efforts, integration of the crack growth rate equations has produced analytical expressions defining the panel's life, or the number of loading cycles before catastrophic failure will occur.

Just the opposite has been true in this program; that is, an expression for panel life was first developed empirically which, when differentiated, provides a crack growth rate equation suitable for describing the data resulting from these tests. Whether or not these empirical techniques can be extended to results of other test programs and materials has not been investigated. However, examination of the empirical equations developed in this program provides some interesting insights into crack behavior under cyclic loading conditions.

There are several reasons why the primary analytical approach in this program has been to define cyclic life rather than crack growth rate. First, crack growth rate is a complex function of the stresses, crack length, specimen geometry and fracture toughness, fatigue resistance, and other properties of the material. This complexity compounds the difficulties involved in correlating crack growth rates of panels containing various initial crack lengths, each tested at different maximum and alternating stresses and at different temperatures. Second, the physical measurement of crack growth rate with a tangent straight-edge and a cycles versus crack length curve is, to a large degree, open to personal interpretation. In addition, manual measurement of growth rates at numerous intermediate crack lengths for a large number of specimens is tedious and time-consuming. Third, the ultimate objective and the most practical result of

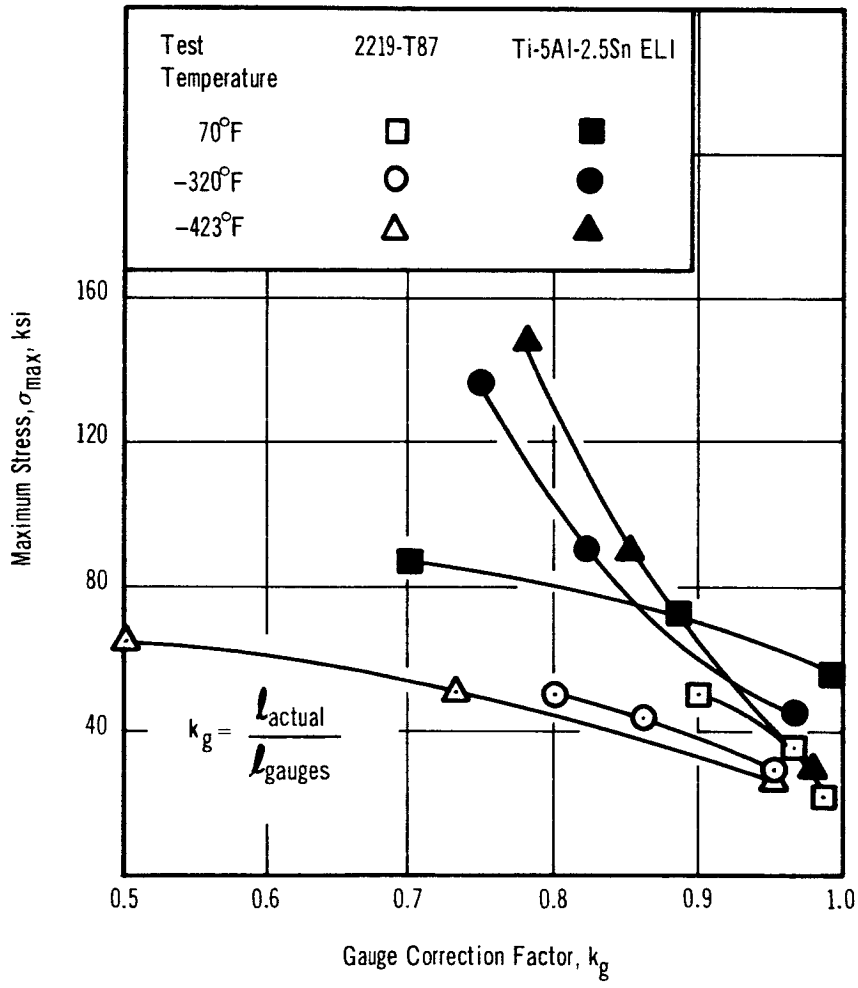

Figure 5-3. Correction Factor for Crack Propagation Gauge Readings as a Function of Maximum Stress and Test Temperature

TABLE 5-III

RESULTS OF UNIAXIAL CYCLIC TESTS PERFORMED ON 2219-T87 0.060-IN. SHEET (TRANSVERSE SPECIMENS)

Specimen			Crack length		Stress					Cycles to fail		
No.	Width (in.)	Thick-ness (in.)	Initial ℓ_o (in.)	Critical ℓ_c (in.)	Maximum σ_{max} (ksi)	Minimum σ_{min} (ksi)	Ratio	Gross at failure σ_o (ksi)	Net at failure σ_n (ksi)	N_F	K_c ksi(in)$^{1/2}$	R_p (in.)
Test temperature, 70°F												
LA	15.99	0.061	0.26	1.10	50.04	2.78	0.06	48.65	52.24	13	79.98	4.15
SB	16.01	0.063	0.25	1.00	49.96	2.57	0.05	49.66	52.97	71	78.65	4.02
JD	15.93	0.062	0.26	1.12	49.26	24.63	0.50	49.10	52.82	184	81.91	4.43
SD	16.01	0.063	0.54	1.00	50.37	25.30	0.50	48.77	52.02	10	76.47	3.70
HD	15.92	0.061	0.72	2.62	36.26	1.81	0.05	36.01	43.10	121	83.23	4.79
AD	15.93	0.062	0.72	2.62	36.11	1.70	0.05	35.86	42.92	103	82.78	4.72
IA	15.92	0.061	0.72	2.82	36.75	18.47	0.50	35.73	42.42	689	85.80	5.27
EC	15.99	0.059	0.73	2.58	35.97	17.99	0.50	35.26	42.05	591	80.35	4.37
EA	15.99	0.060	2.00	6.66	22.50	1.14	0.05	21.79	37.33	423	81.28	7.94
BD	15.93	0.061	2.00	6.63	22.00	1.12	0.05	20.81	35.65	243	76.98	6.90
KD	15.93	0.062	2.15	6.08	22.34	11.17	0.50	23.27	37.65	1220	82.10	7.36
DB	15.93	0.062	2.17	6.81	22.35	11.18	0.50	21.54	37.63	1185	81.69	8.22
Test temperature, -320°F												
RE	16.01	0.063	0.25	1.71	50.26	2.87	0.06	48.90	54.75	40	92.60	3.19
IA	15.93	0.062	0.26	1.64	(1)	(1)	(1)	62.53	66.90	1	102.18	4.18
FA	15.93	0.060	0.26	1.12	(1)	(1)	(1)	61.64	66.30	1	103.75	4.31
CB	15.93	0.061	0.25	2.01	49.25	24.55	0.50	48.79	55.83	1326	100.51	3.99
ED	15.99	0.059	0.73	2.10	45.75	2.42	0.05	43.98	50.63	20	89.99	3.07
FC	15.92	0.060	0.72	2.00	45.70	2.21	0.05	43.89	50.19	12	87.47	2.85
AB	15.98	0.061	0.72	1.96	46.08	3.74	0.08	45.45	51.81	14	90.45	3.07
HB	15.92	0.061	0.73	2.61	43.42	22.02	0.51	43.27	51.75	199	99.06	4.07
KC	16.00	0.062	2.12	6.52	28.06	1.36	0.05	27.07	45.70	72	99.49	7.13
GB	15.92	0.061	2.10	6.29	28.26	1.41	0.05	26.64	44.03	73	95.26	6.18
AA	15.93	0.062	2.15	5.94	28.17	13.66	0.49	27.80	44.34	360	96.02	5.95
KB	15.99	0.062	2.12	6.32	28.12	13.91	0.50	27.26	45.08	477	98.02	6.65
Test temperature, -423°F												
CA	15.99	0.061	0.13	(2)	(2)	(2)	(2)	74.90	(2)	1	(2)	(2)
QC	16.01	0.063	0.13	(2)	(2)	(2)	(2)	70.61	(2)	1	(2)	(2)
CC	15.93	0.062	0.13	0.70	66.13	3.45	0.05	64.39	66.91	149	88.86	1.70
IB	15.94	0.061	0.13	0.76	65.47	32.98	0.50	64.98	68.23	838	90.67	1.94
QE	16.01	0.063	0.43	1.89	51.12	2.73	0.05	49.15	55.73	38	97.18	2.51
RC	16.01	0.063	0.43	1.65	51.58	4.88	0.10	49.90	55.63	45	92.32	2.18
RF	16.01	0.063	0.43	1.67	51.15	25.50	0.50	50.70	56.60	357	94.86	2.32
SH	16.01	0.063	0.45	1.82	51.01	25.50	0.50	50.25	56.69	358	98.06	2.54
QA	16.00	0.063	1.95	7.14	26.32	1.40	0.05	25.66	46.32	147	99.86	5.77
RG	16.01	0.063	1.95	7.55	26.43	1.29	0.05	24.90	47.12	177	101.03	6.38
RD	16.01	0.063	1.95	7.16	25.73	12.38	0.48	24.39	44.13	1855	94.56	5.12
QB	16.01	0.063	1.95	7.16	24.87	12.43	0.50	24.35	44.07	2565	94.40	5.10

(1) Specimen failed during loading on first cycle; ℓ_c readable.

(2) Specimen failed during loading on first cycle; ℓ_c not readable.

TABLE 5-IV

RESULTS OF UNIAXIAL CYCLIC TESTS PERFORMED ON Ti-5Al-2.5Sn ELI 0.020-IN. SHEET (LONGITUDINAL SPECIMENS)

Specimen			Crack length		Stress					Cycles to fail		
No.	Width (in.)	Thickness (in.)	Initial ℓ_o (in.)	Critical ℓ_c (in.)	Maximum σ_{max} (ksi)	Minimum σ_{min} (ksi)	Ratio	Gross at failure σ_o (ksi)	Net at failure σ_n (ksi)	N_F	K_c ksi(in)$^{1/2}$	R_p (in.)
Test temperature, 70°F												
VO	15.93	0.018	0.23	3.73	84.09	4.20	0.05	81.15	105.95	1482	246.82	44.80
VN	15.93	0.021	0.73	3.80	85.45	4.40	0.05	78.85	103.55	187	239.15	36.93
QM	15.93	0.019	0.73	3.90	84.60	42.41	0.50	79.02	104.63	2062	244.08	41.52
XP	15.93	0.023	0.73	3.80	83.79	41.89	0.50	79.60	104.53	1796	242.59	40.12
BIO	15.93	0.020	1.35	6.20	71.36	3.64	0.05	54.86	89.81	224	205.50	24.98
ZM	15.93	0.018	1.35	5.95	74.42	3.78	0.05	61.98	98.93	213	234.00	40.82
AIN	15.93	0.017	1.35	6.30	71.18	36.41	0.51	59.04	97.65	3209	229.53	39.74
BIN	15.93	0.017	1.35	6.30	71.14	34.90	0.49	58.31	96.46	3138	225.66	36.86
ZP	15.93	0.019	2.11	7.50	58.58	4.17	0.07	54.20	102.45	246	240.61	65.31
ZN	15.93	0.018	2.13	7.28	56.81	3.45	0.06	56.49	103.98	225	247.24	72.17
UP	15.93	0.019	2.10	8.72	58.19	29.41	0.51	48.31	106.75	4760	245.08	108.36
UO	15.93	0.020	2.10	7.46	57.65	29.22	0.51	53.17	100.01	4098	232.80	54.55
Test temperature, -320°F												
WP	16.01	0.019	0.13	(1)	(1)	(1)	(1)	135.36	(1)	1	(1)	(1)
RN	15.93	0.017	0.13	0.80	134.86	6.63	0.05	132.56	139.56	375	177.89	2.84
RO	15.94	0.017	0.13	0.90	135.21	65.02	0.48	123.70	131.10	2481	171.55	2.48
QP	15.93	0.019	0.13	0.80	135.47	66.99	0.50	134.47	141.58	1275	181.58	3.03
UN	15.93	0.019	0.25	1.62	91.21	5.69	0.06	89.38	99.50	1224	154.44	1.85
BIM	15.93	0.018	0.26	1.80	89.20	4.73	0.05	87.79	98.97	1517	159.70	2.02
TP	15.95	0.017	0.26	1.75	90.87	45.44	0.50	90.42	101.56	4602	162.88	2.11
XN	15.94	0.020	0.26	1.80	91.28	45.64	0.50	87.00	98.08	3494	158.03	1.97
AIP	15.93	0.017	1.35	6.07	46.85	2.33	0.05	45.92	74.19	4551	155.59	3.28
XO	15.93	0.022	1.35	5.65	46.88	2.34	0.05	45.09	69.87	3616	145.63	2.65
TM	15.93	0.019	1.35	6.22	46.34	23.17	0.50	46.13	75.67	12875	158.93	3.52
BIP	15.93	0.017	1.35	6.88	47.01	23.62	0.50	45.42	79.95	17262	167.83	4.43
Test temperature, -423°F												
VM	15.94	0.020	0.09	0.14	147.21	19.83	0.14	146.22	147.52	16	81.08	0.44
AIM	15.94	0.018	0.09	(1)	(1)	(1)	(1)	146.83	(1)	1	(1)	(1)
SP	15.94	0.018	0.09	0.14	(2)	(2)	(2)	148.13	150.27	1	87.98	0.47
SO	15.94	0.019	0.09	0.20	149.24	73.59	0.49	149.24	151.09	8	98.49	0.70
WO	16.01	0.021	0.21	0.78	91.03	4.85	0.05	86.92	91.37	126	101.62	0.58
YO	16.01	0.020	0.18	0.59	90.42	14.07	0.16	89.02	92.39	288	90.32	0.45
YP	16.01	0.019	0.18	0.59	92.29	47.86	0.52	90.27	93.70	1067	91.75	0.46
YN	16.01	0.020	0.18	0.64	87.03	43.51	0.50	86.27	89.88	1579	91.45	0.45
PN	16.01	0.016	1.55	(3)	(3)	(3)	(3)	30.97	(3)	1	(3)	(3)
PM	16.01	0.016	1.55	5.24	31.41	1.53	0.05	30.12	44.78	4324	91.31	0.78
PO	16.01	0.017	1.55	3.76	32.85	16.54	0.50	32.38	42.32	12496	81.21	0.50
PP(4)	16.01	0.019	1.55	2.28	32.73	16.37	0.50	42.05	49.04	6390	81.28	0.41

(1) Specimen failed in grips.

(2) Specimen failed during loading on first cycle.

(3) Specimen accidentally broken in compression when unloading to interrupt test as a result of lack of sufficient liquid hydrogen.

(4) Specimen accidentally overloaded after 6389 cycles when unloading to interrupt test; critical crack length based on fracture appearance.

analysis of crack propagation tests in this program is knowledge concerning the life of the cracked structure. For these reasons, emphasis has been placed on obtaining a relationship which would aid in the prediction of life remaining in a cracked panel at any crack length and under any maximum stress within the experimental limits of the program.

5.2.1.1 Geometrical Aspects of Crack Growth Curves

Certain similarities in the shapes of crack growth curves for specimens tested at the same stress, but containing different initial crack lengths, suggests that a common growth curve exists for a given gross stress, regardless of the length of the starting flaw. In particular, the similarity of shape of the growth curve at equal crack lengths is striking, as shown by the schematic curves of Figure 5-4, an often-used method of presentation of crack propagation test results. In the figure, the curve for Test No. 2 has a shape identical with that portion of the curve for Test No. 1 beyond a crack length equal to ℓ_{o2}, the initial crack length for Test No. 2. The shape of that portion of the curve for Test No. 1 at crack lengths less than ℓ_{o2}, however, is unique. The common shape exists, then, at the terminal portion of the two test curves; that is, from the critical crack length (common for both tests since the maximum stress is the same for both tests), proceeding backwards to the initial crack length of Test No. 2.

In Figure 5-5, the two curves are superimposed to form a common crack growth curve representative of the stress schedule employed. Test No. 2 is shown to be equivalent to Test No. 1 in number of cycles and length of crack grown for all crack lengths between ℓ_{o2} and ℓ_c.

In summary, it may be assumed that under a given stress schedule in panels of a given material, crack propagation proceeds along a common growth curve which is independent of initial crack length (for $0 < \ell < \ell_c$). This assumption requires that the initial crack itself be a fatigue crack or a mechanical notch of equivalent sharpness.

5.2.1.2 Analysis of The Common Growth Curve

Data for crack growth curves are usually acquired by measuring the length of the crack at various intervals after the start of the test. Direct plotting of such data (length versus cycles after start) results in curves such as those shown in Figure 5-4. Such plotting of the data reveals little evidence of the commonality of growth curves because there are no points on the plot common to both curves. Hence, mathematical treatment involves a family of curves for each stress schedule.

By converting the cyclic data to "cycles remaining to failure," however, commonality may be observed. The end point (length = ℓ_c, cycles remaining to failure = 0) is common to both tests and the terminal shapes are identical. Mathematical treatment thus involves a single curve for each stress schedule.

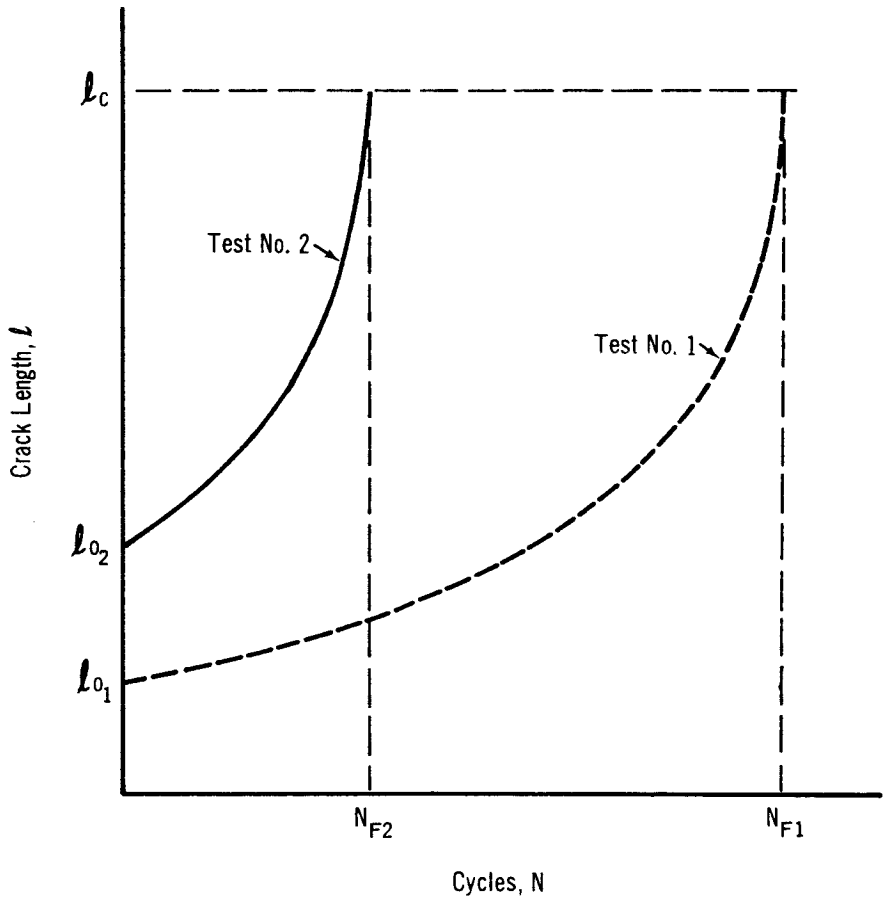

Figure 5-4. Idealized ℓ vs N Curves for Tests Performed Under Identical Stress Schedules but with Different Initial Crack Lengths

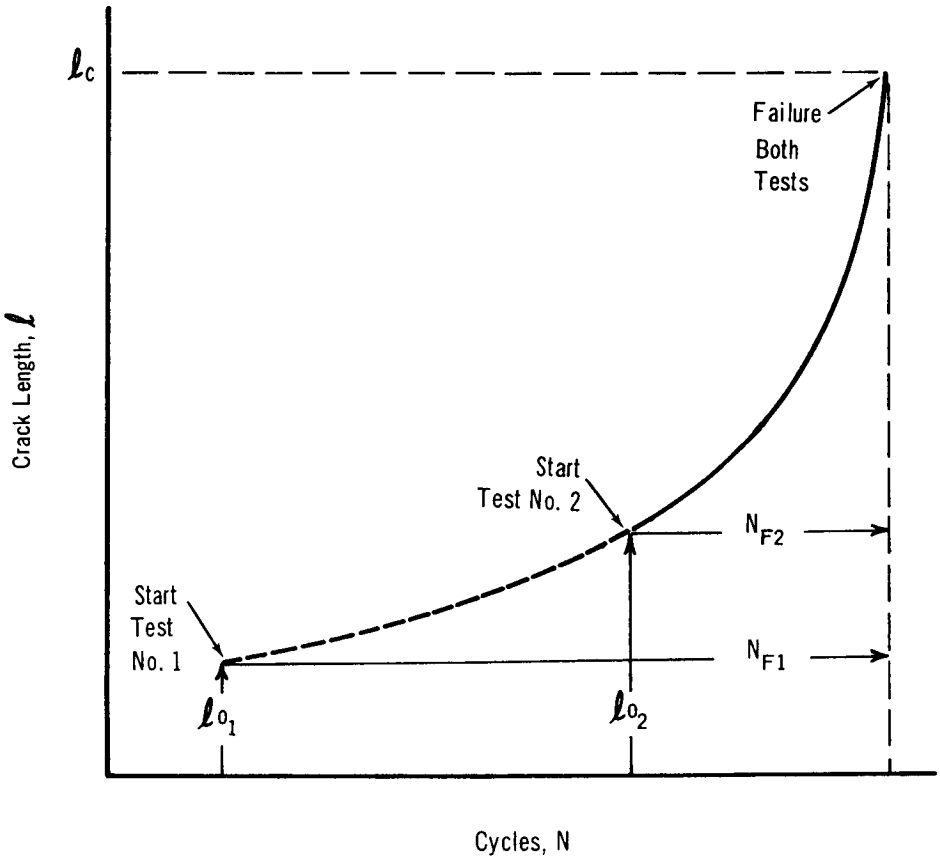

Figure 5-5. Same Curves Shown in Figure 5-4 Superimposed to Form Common Growth Curve

Determination of crack growth rate is not impaired by this conversion. As shown in Figure 5-6, crack growth rates at any crack length are numerically equal (but opposite in sign) for the curves, one plotted versus cycles from start, N, the other versus cycles remaining, N_R.

In mathematical terms,

$$N_R = N_F - N \tag{5-4}$$

and

$$\frac{d\ell}{dN} = - \frac{d\ell}{dN_R} \tag{5-5}$$

where

N_R = cycles remaining to failure

N_F = cycles to failure from start of test

N = cycles after start

$\frac{d\ell}{dN}$ = crack growth rate

A fourth-power relationship between cycles remaining and the crack length was inferred from log-log plots of cycles remaining, N_R, versus crack growth remaining, $\ell_c - \ell$. These plots yielded relatively straight lines having a slope of 4. The data was, therefore, replotted as the fourth root of cycles remaining, $N_R^{1/4}$, versus crack length, ℓ. The method is demonstrated in Figure 5-7. Solid straight lines are drawn through the data points and are extrapolated (dashed lines) to a point of common intersection.

Each line represents the common crack growth curve for a particular maximum stress. The intercept on the crack-length axis (at $N_R = 0$) is the critical crack length characteristic of that maximum stress.

The general equation for this family of common growth curves is

$$N_R^{1/4} = \frac{F\,(\ell_c - \ell)}{\ell_c - \ell_F} \tag{5-6}$$

where F and ℓ_F are the coordinates of the common point of intersection.

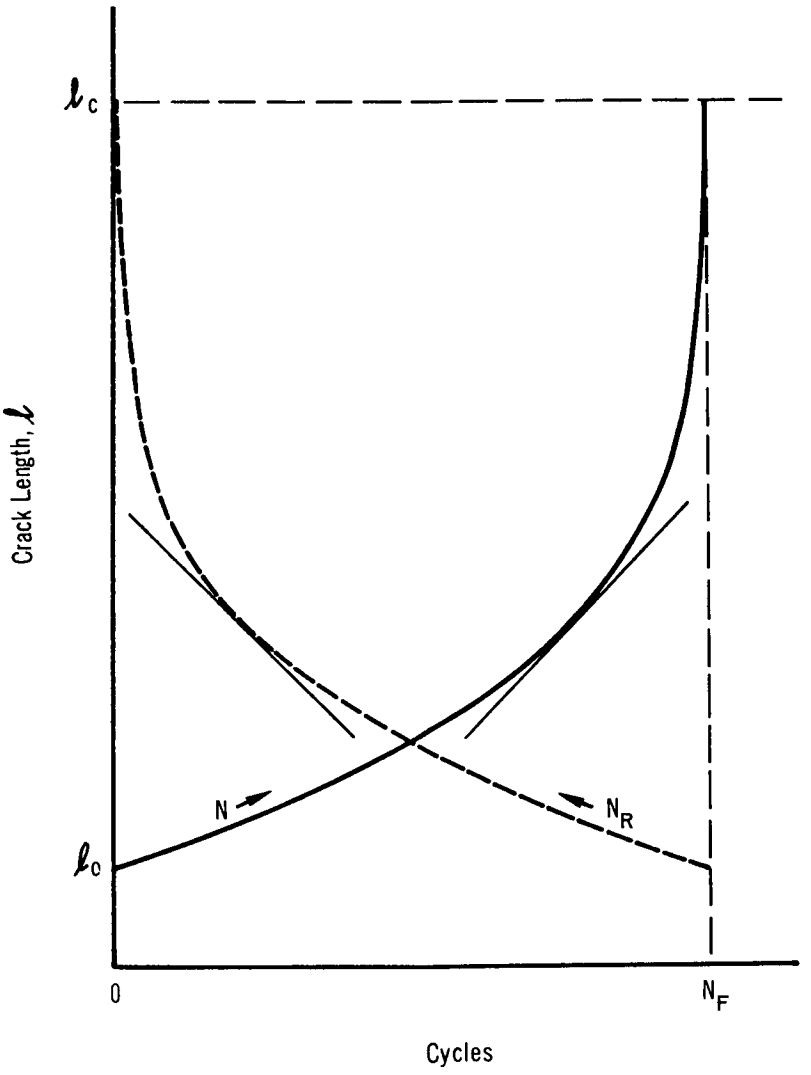

Figure 5-6. Idealized Crack Propagation Curve Illustrating Growth Rate Equivalance for ℓ vs N and ℓ vs N_R

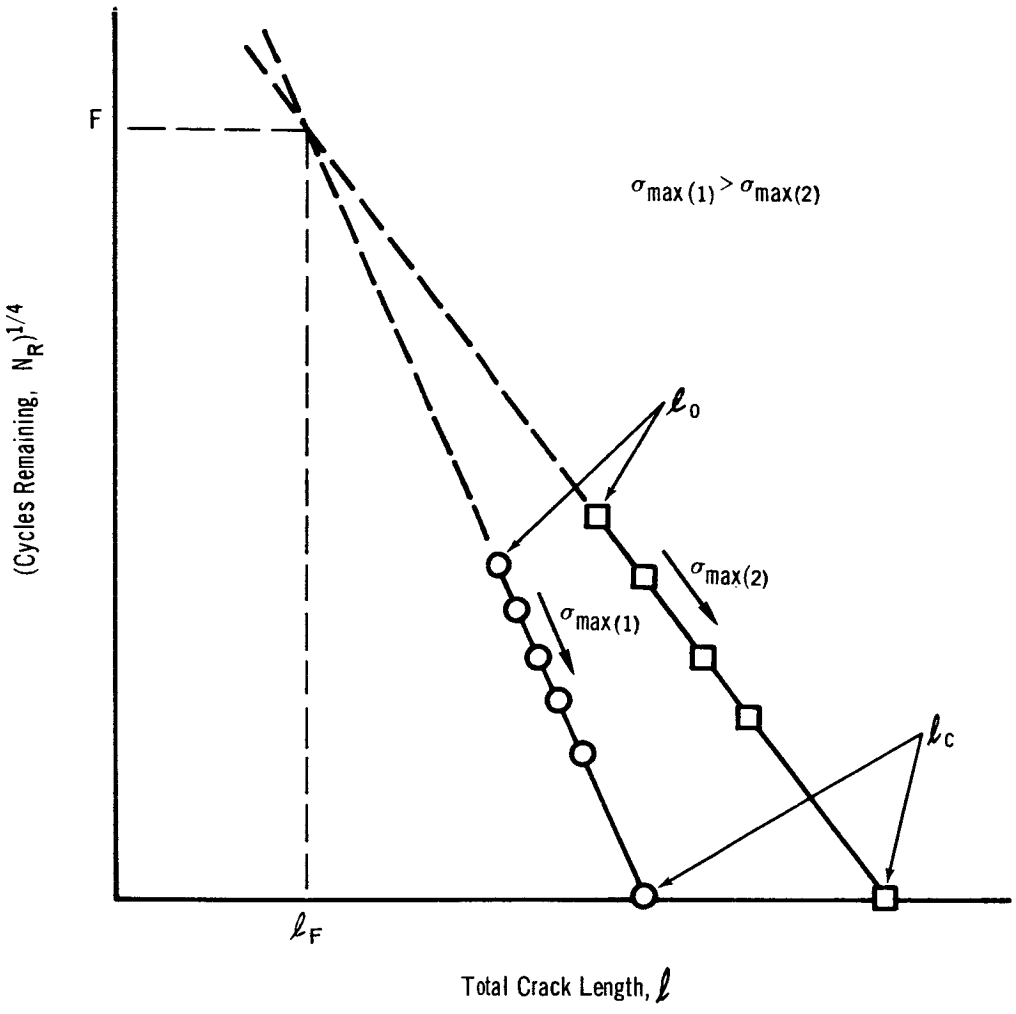

Figure 5-7. Idealized Crack Propagation Data from Two Tests

5.2.2 Test Results

The results of individual uniaxial cyclic tests are presented in Appendix C. Average critical stress intensity factors, K_c, for both static and cyclic tests are shown as a function of test temperature in Figures 5-8 and 5-9. For 2219-T87, K_c increases from 80.6 ksi $(in.)^{1/2}$ at 70°F to 97.3 ksi $(in.)^{1/2}$ at -320°F. At -423°F, the K_c for 2219-T87 decreased slightly to 93.9 ksi $(in.)^{1/2}$. For Ti-5Al-2.5Sn ELI, K_c decreased with decreasing temperature from 234.9 ksi $(in.)^{1/2}$ at 70°F to 159.8 ksi $(in.)^{1/2}$ at -320°F and to 90.9 ksi $(in.)^{1/2}$ at -423°F.

Theoretical critical crack length (based on average K_c) is shown as a function of maximum gross stress in Figures 5-10 and 5-11. The theoretical curves, calculated by means of eq. (5-1), are in agreement with the experimental values which are included in the figures. Crack growth curves for the cyclic tests were plotted with the method explained above and are shown in Appendix C. The F coordinate of the common point of intersection is tabulated in Table 5-V. A value of -1.0 for ℓ_F is suitable for both materials at all test temperatures. The value of F, however, varies with stress ratio, material, and test temperature.

5.2.3 Crack Growth Rates

Eq. (5-6) can be differentiated to give an expression for crack growth rate in the following manner. Rearranging eq. (5-6)

$$\ell = \ell_c - \left[\frac{N_R^{1/4} (\ell_c + 1)}{F} \right] \tag{5-7}$$

and differentiating with respect to N_R

$$\frac{d\ell}{dN_R} = - \left[\frac{\ell_c + 1}{4F N_R^{3/4}} \right] \tag{5-8}$$

Cubing eq. (5-6)

$$N_R^{3/4} = \left[\frac{F(\ell_c - \ell)}{\ell_c + 1} \right]^3 \tag{5-9}$$

and substituting in eq. (5-8)

$$\frac{d\ell}{dN_R} = - \left[\frac{(\ell_c + 1)^4}{4F^4 (\ell_c - \ell)^3} \right] \tag{5-10}$$

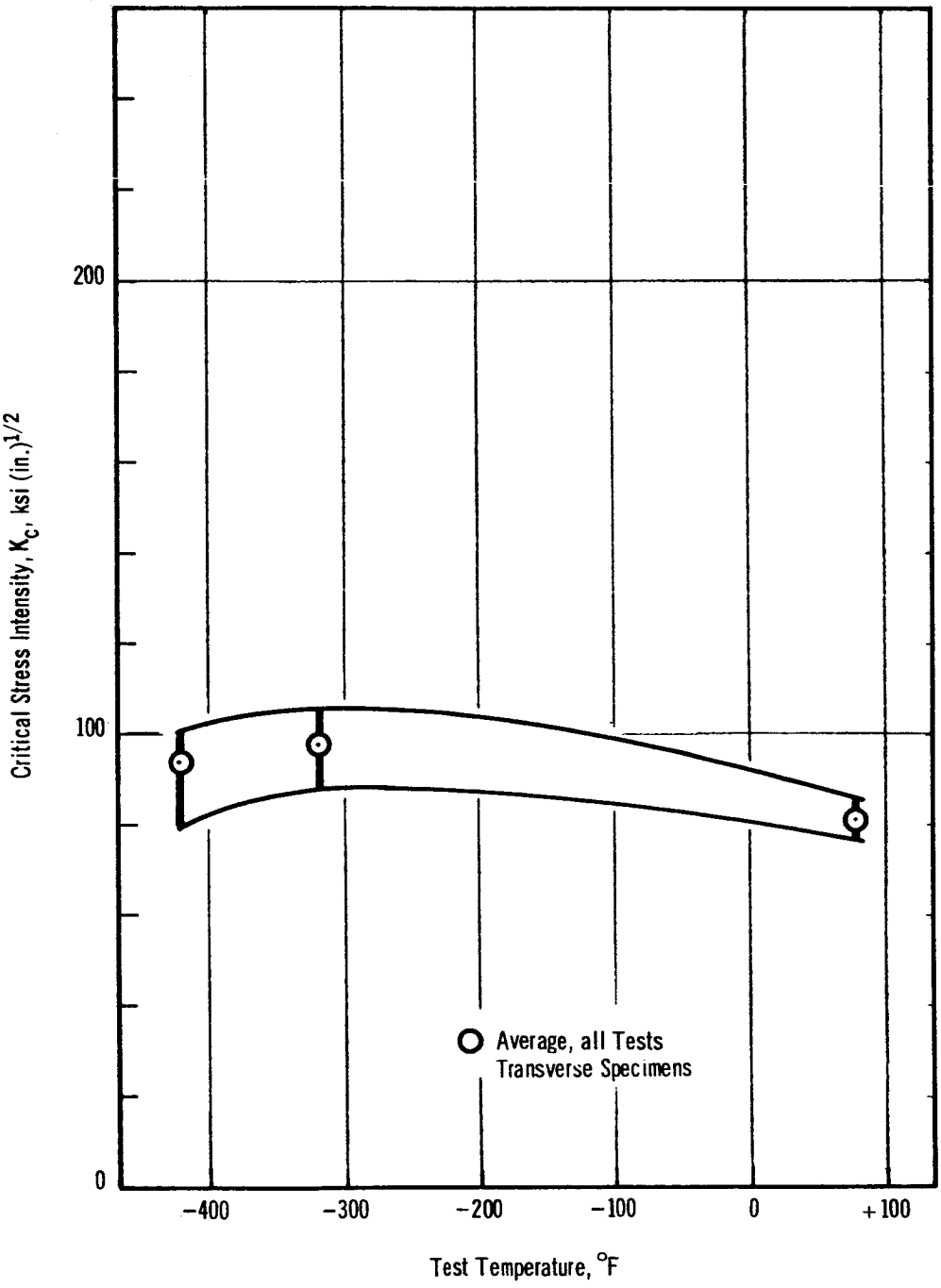

Figure 5-8. Plane Stress K_c Range for 2219-T87 From Uniaxial Tests

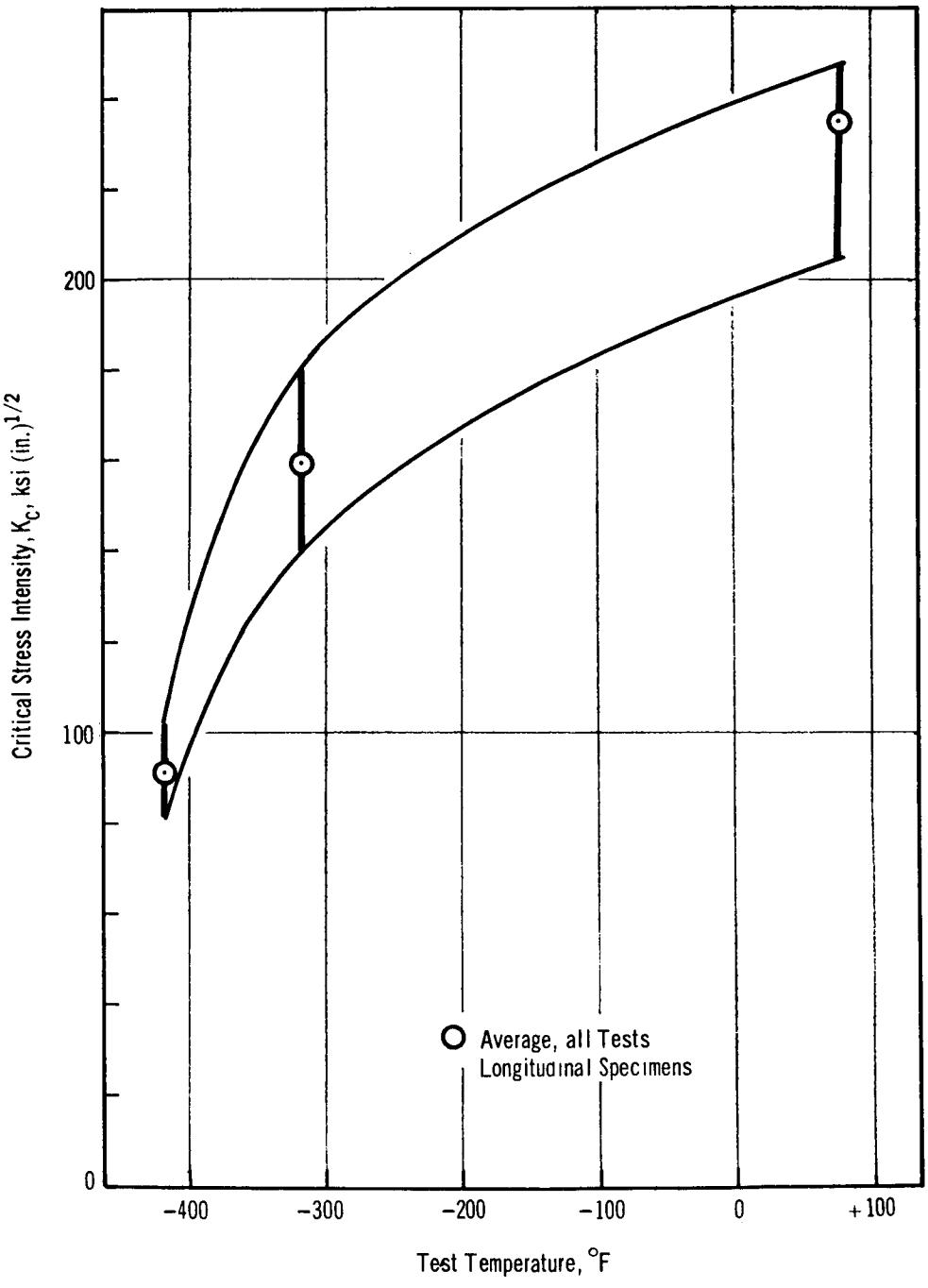

Figure 5-9. Plane Stress K_c Range for Ti-5Al-2.5Sn ELI From Uniaxial Tests

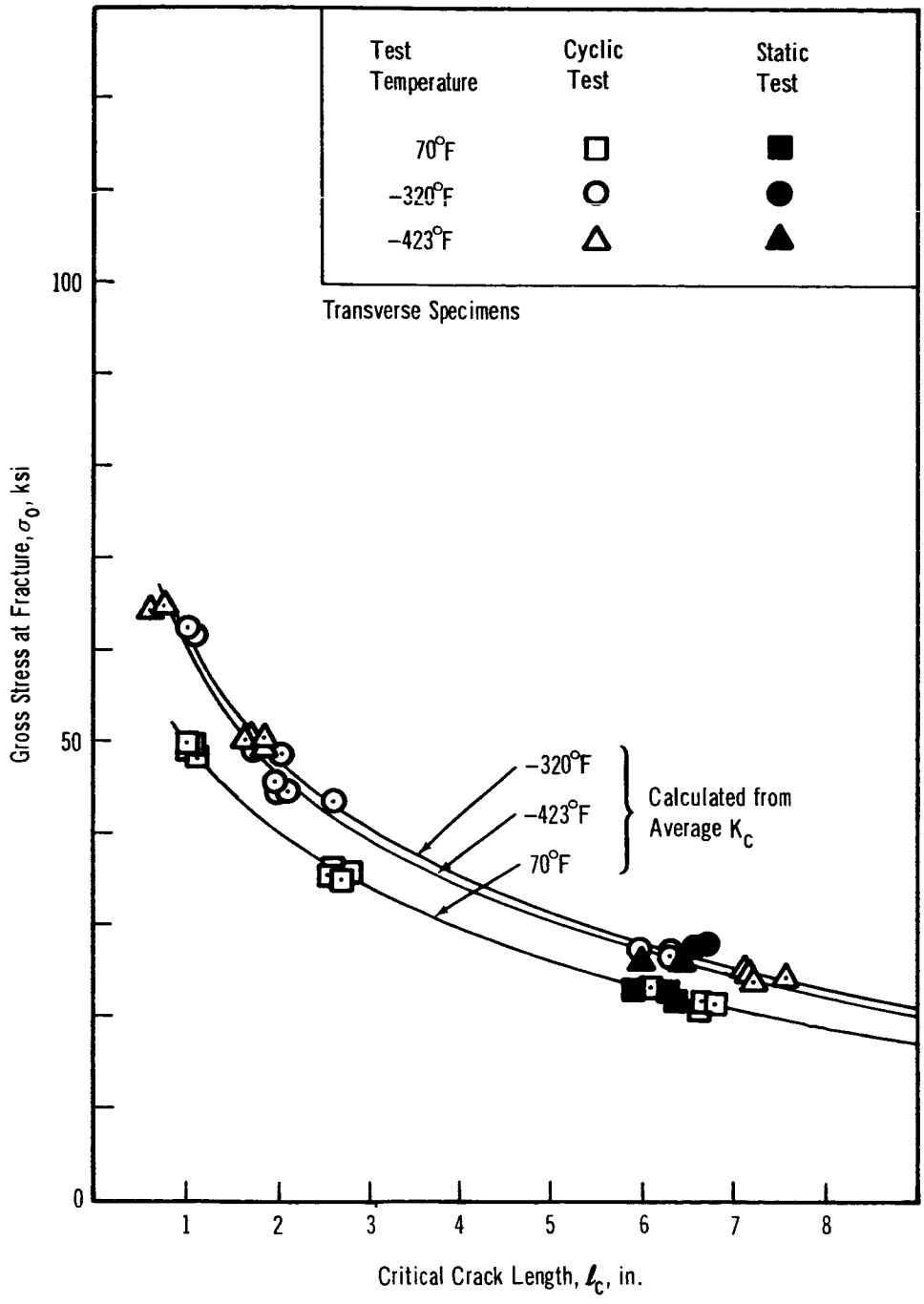

Figure 5-10. Gross Fracture Stress vs Critical Crack Length for Uniaxial Tests of 2219-T87

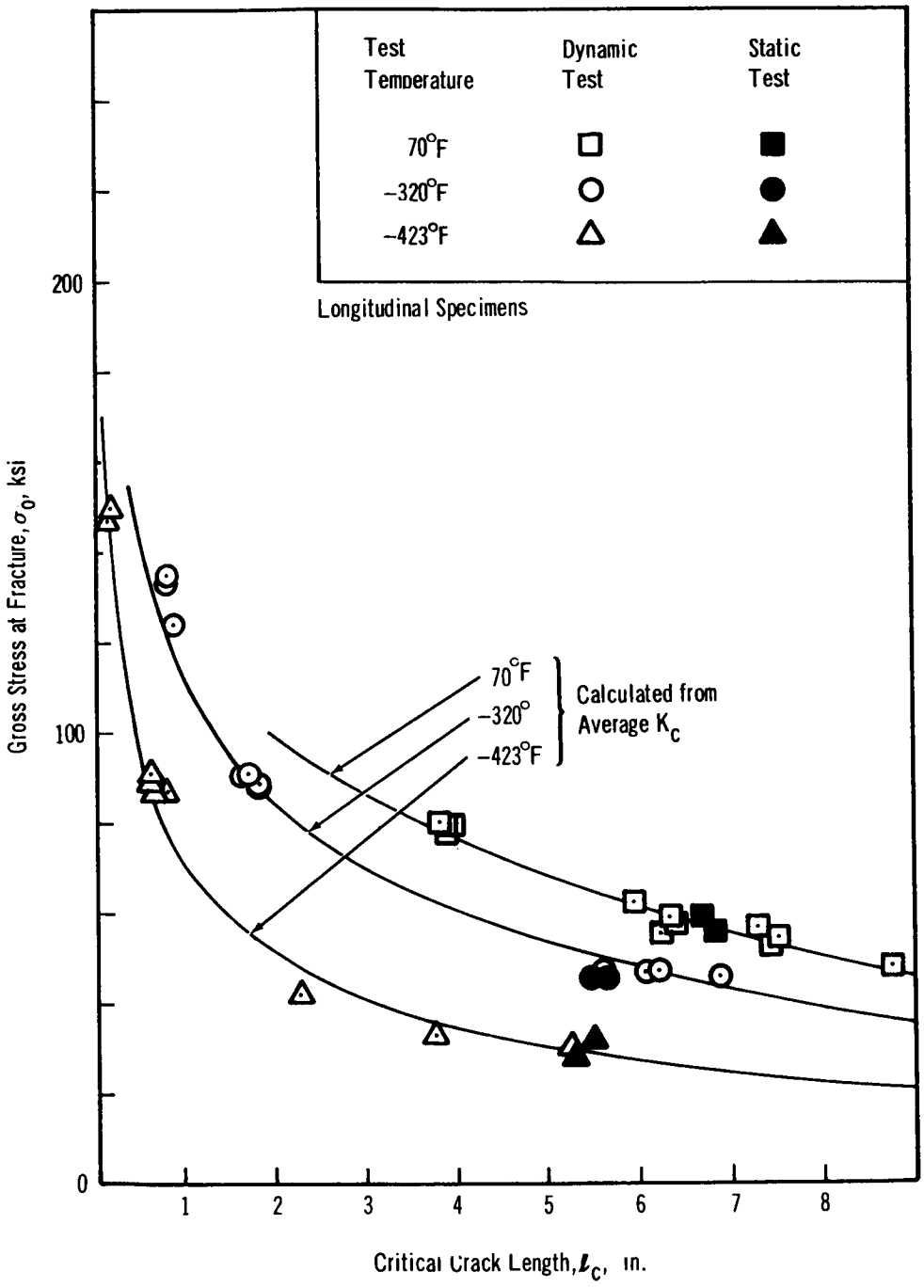

Figure 5-11. Gross Fracture Stress vs Critical Crack Length for Uniaxial Tests of Ti-5Al-2.5Sn ELI

TABLE 5-V

AVERAGE F VALUES DETERMINED FROM UNIAXIAL CYCLIC TESTS

Alloy	Test Temperature (°F)	F	
		$\frac{\sigma_{min.}}{\sigma_{max.}} = 0.05$	$\frac{\sigma_{min.}}{\sigma_{max.}} = 0.50$
2219-T87 Transverse	70	6.5	10.5
	-320	5	8
	-423	6	10.5
Ti-5Al-2.5Sn ELI Longitudinal	70	6.5	13
	-320	12	16
	-423	14	19

The crack growth rate with respect to N, from eq. (5-5), is

$$\frac{d\ell}{dN} = \frac{(\ell_c + 1)^4}{4F^4 (\ell_c - \ell)^3} \qquad (5\text{-}11)$$

Examination of uniaxial crack growth rates, both experimental and theoretical, revealed that eq. (5-11) satisfactorily describes the test experience within the limits of the program.

5.2.3.1 Effect of Crack Length

Under any given stress schedule, the crack growth rate increases with increasing crack length. In all uniaxial tests, the growth rate increased by several orders of magnitude before failure occurred. This effect is predicted by eq. (5-11). Examples of the effect of crack-length are presented in Figure 5-12.

5.2.3.2 Effect of Maximum Cyclic Stress

At any given crack length and stress ratio, the crack growth rate is greater the higher the maximum stress. While this effect can be studied experimentally only by testing specimens with equal crack lengths at various maximum stresses, the effect can be inferred from results of tests of specimens with differing crack lengths. In some of the tests in this program, the initial crack length for a test at a lower maximum stress was less than the critical crack length for a test at a higher maximum stress. These tests provide the opportunity to examine the effect of maximum cyclic stress at equal crack lengths.

The effect of higher maximum stress on increasing the crack growth rate at equal crack lengths is predicted by eq. (5-11), as shown in Figure 5-13.

5.2.3.3 Effect of Stress Ratio

For any given crack length and maximum cyclic stress, the crack growth rate is greater the lower the minimum stress. This effect was unmistakable in the results of the uniaxial tests because specimens containing the same crack length were tested at the same maximum stress but at stress ratios of 0.5 and 0.05. The crack growth rate for the 0.05 stress ratio was greater in every case. Examples are given in Figure 5-14.

Eq. (5-11) predicts this effect since the F value for the lower stress ratio was always less than that for the higher stress ratio. Because F^4 appears in the denominator, $d\ell/dN$ must increase inversely with F^4.

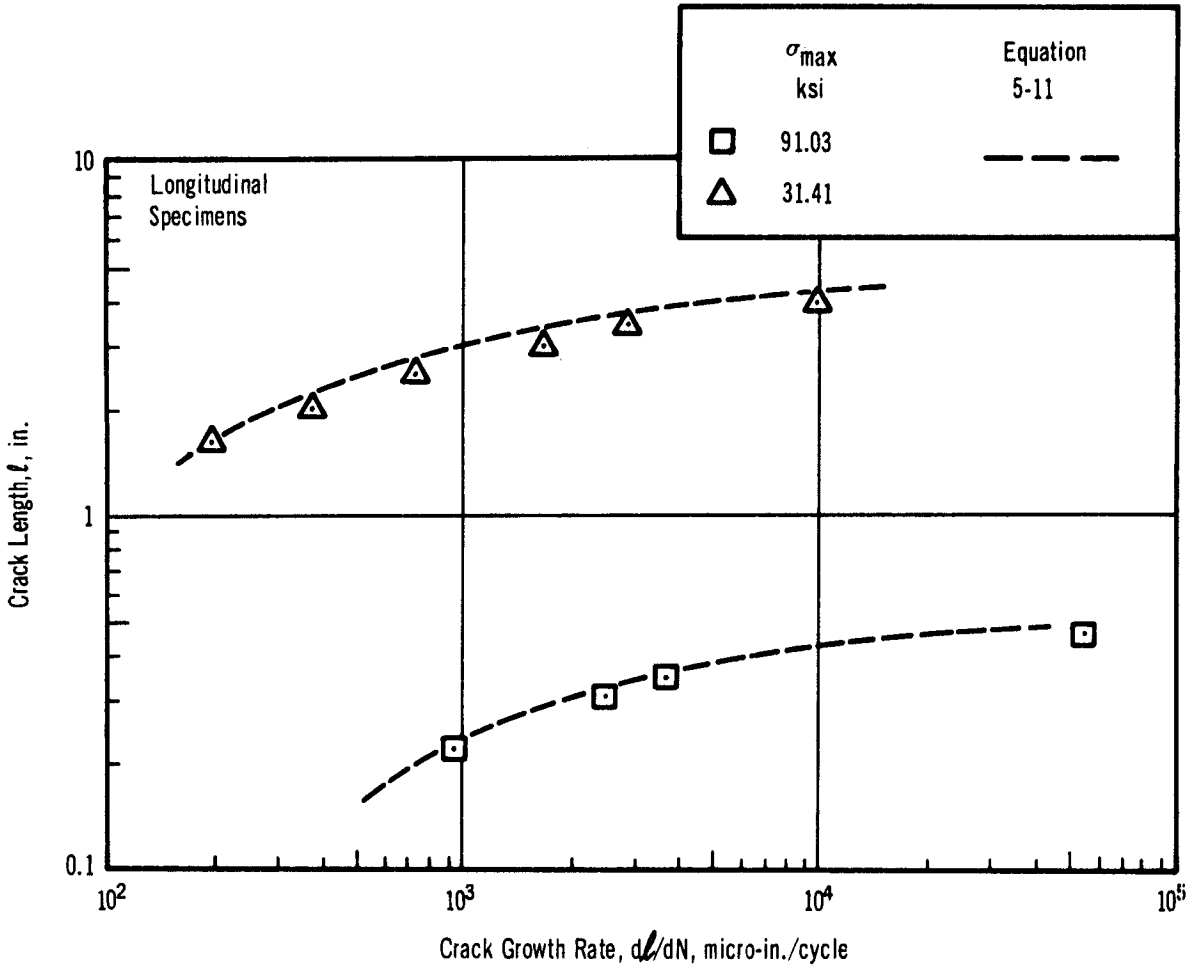

Figure 5-12. Effect of Crack Length on Uniaxial Crack Growth Rate at Constant Maximum Stress for Ti-5Al-2.5Sn ELI at −423°F and 0.05 Stress Ratio

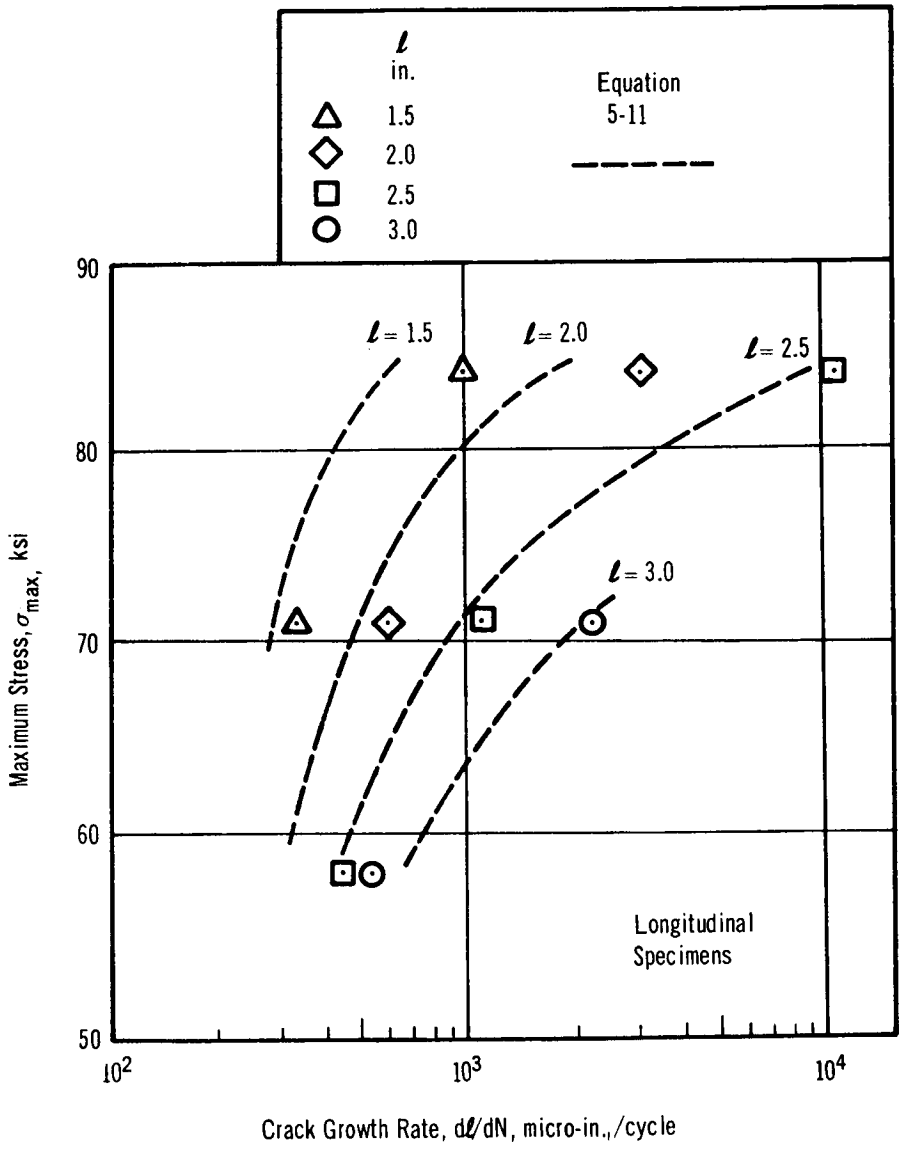

Figure 5-13. Effect of Maximum Stress on Uniaxial Crack Growth Rate at Equal Crack Lengths for Ti-5Al-2.5Sn ELI at 70°F and 0.5 Stress Ratio

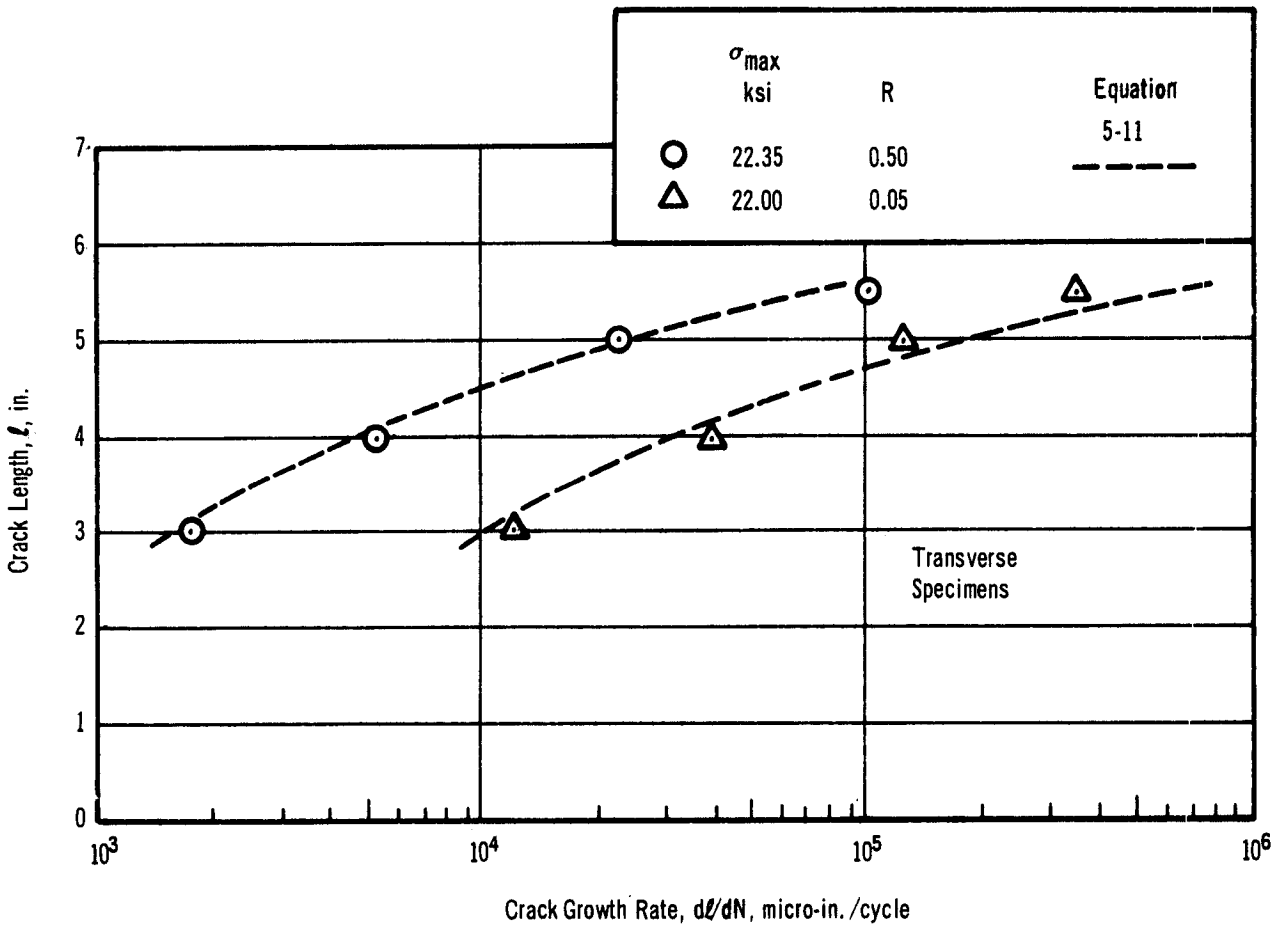

Figure 5-14. Effect of Stress Ratio on Uniaxial Crack Growth Rate for 2219-T87 at 70°F

5.2.3.4 Growth Rates at Equal Stress Intensities

Since it is established that growth rate increases with increasing crack length, it is possible to propose that at a given maximum stress the growth rate increases with increasing stress intensity. By similar reasoning, one may propose that at any given crack length the growth rate is greater the higher the stress intensity. These propositions were substantiated in this program.

A third and a fourth proposition may be advanced as follows: at equal stress intensities, the crack growth rate is greater the higher the maximum stress and at equal stress intensities the crack growth rate is greater the longer the crack. These two propositions appear reasonable at first glance. However, they are true only for special cases, as will be shown.

Figure 5-15 illustrates typical uniaxial ℓ versus N curves for 2219-T87 tested at room temperature and at a 0.50 stress tatio. The point on each curve at which the crack length and maximum stress produce a stress intensity of 56.5 ksi $(in.)^{1/2}$ is indicated. The growth rate on each curve at this stress intensity is indicated by a straight line tangent to the point. The slopes of these lines are shown in the figure as $d\ell/dN$, the crack growth rate. The measured growth rate for the test at 36.7 ksi is lower than the growth rates for the tests at 22.3 ksi and 49.3 ksi at the same stress intensity.

Figure 5-16 is a plot of maximum dynamic stress (0.50 stress ratio) versus crack growth rates calculated by means of eq. (5-11). For these calculations, the constants used in the equation were those determined experimentally in 2219-T87 tests at 70°F. First, values of ℓ were calculated for ratios of K/K_c of 0.5, 0.6, 0.7, 0.8, and 0.9, at stress levels in the range 10 to 60 ksi. Critical crack lengths at these stress levels were also calculated. The average K_c for 2219-T87 at 70°F was used in these calculations. The points were then located in the figure. Smooth dashed curves were drawn connecting points of equal K/K_c. Experimental points from five uniaxial dynamic tests are also shown in the figure. The experimental crack growth rates compare well with the curves predicted by eq. (5-11).

Figure 5-16 indicates that the crack growth rate (for equal stress intensities) increases with increasing maximum cyclic stress above about 35 ksi but decreases with increasing maximum cyclic stress below 35 ksi. This result, while substantiated by the experimental data, must be carefully interpreted because it does not mean that at stresses below 35 ksi a reduction in crack growth rate would result from an increase in stress. In fact, a reduction in crack growth rate would result from an increase in stress only if the crack were shortened, which is not physically possible in a given specimen.

Figure 5-17 is a similar plot of crack growth rate data, but incorporates the effect of crack length. Bold dashed curves are plotted for constant maximum cyclic stress levels by means of eq. (5-11) with the use of constants for Ti-5Al-2.5Sn ELI at -423°F. Thin dashed curves connect points at which the combination of stress and crack length produce equal stress intensities.

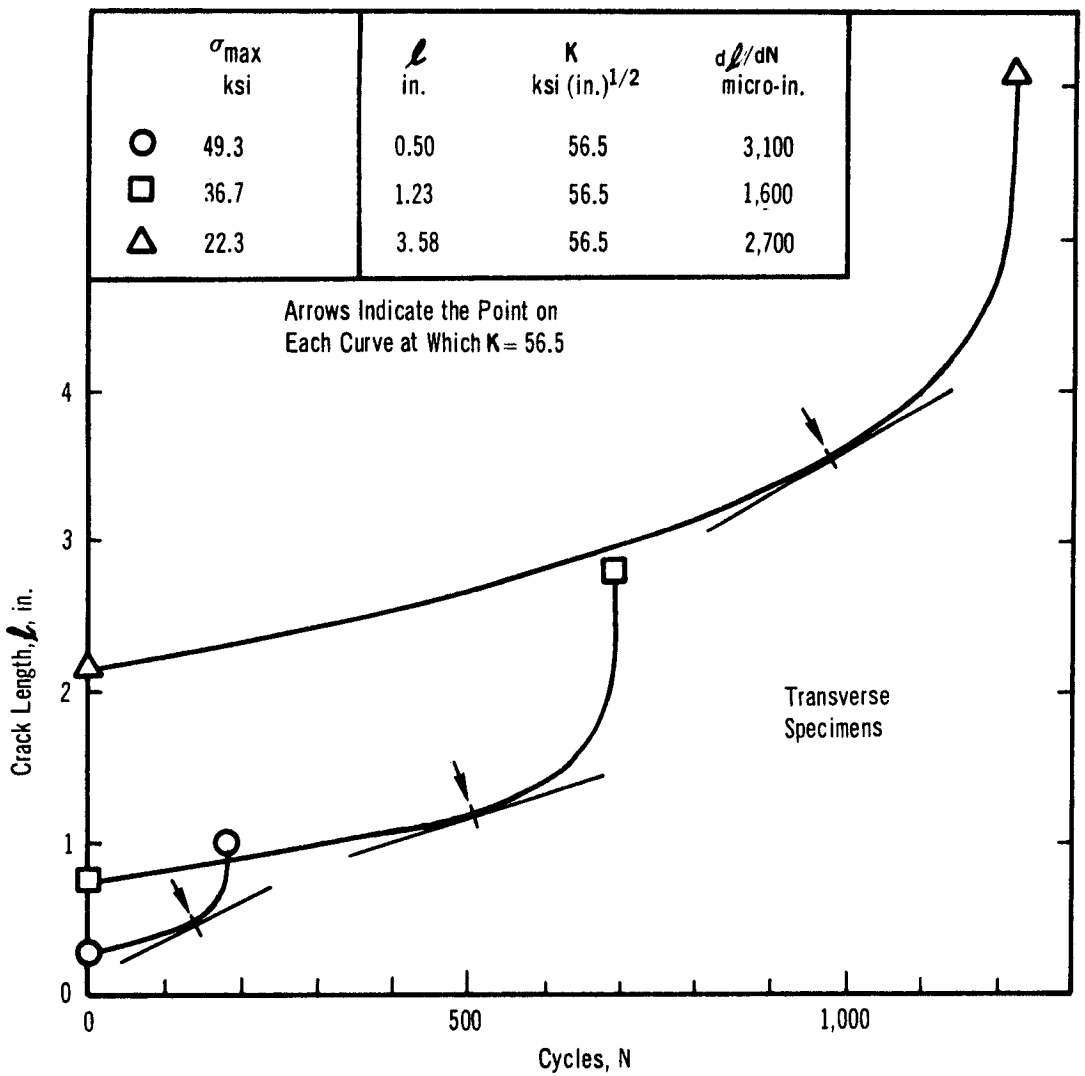

Figure 5-15. Typical Uniaxial Crack Growth Curves for 2219-T87 at 70°F and 0.5 Stress Ratio

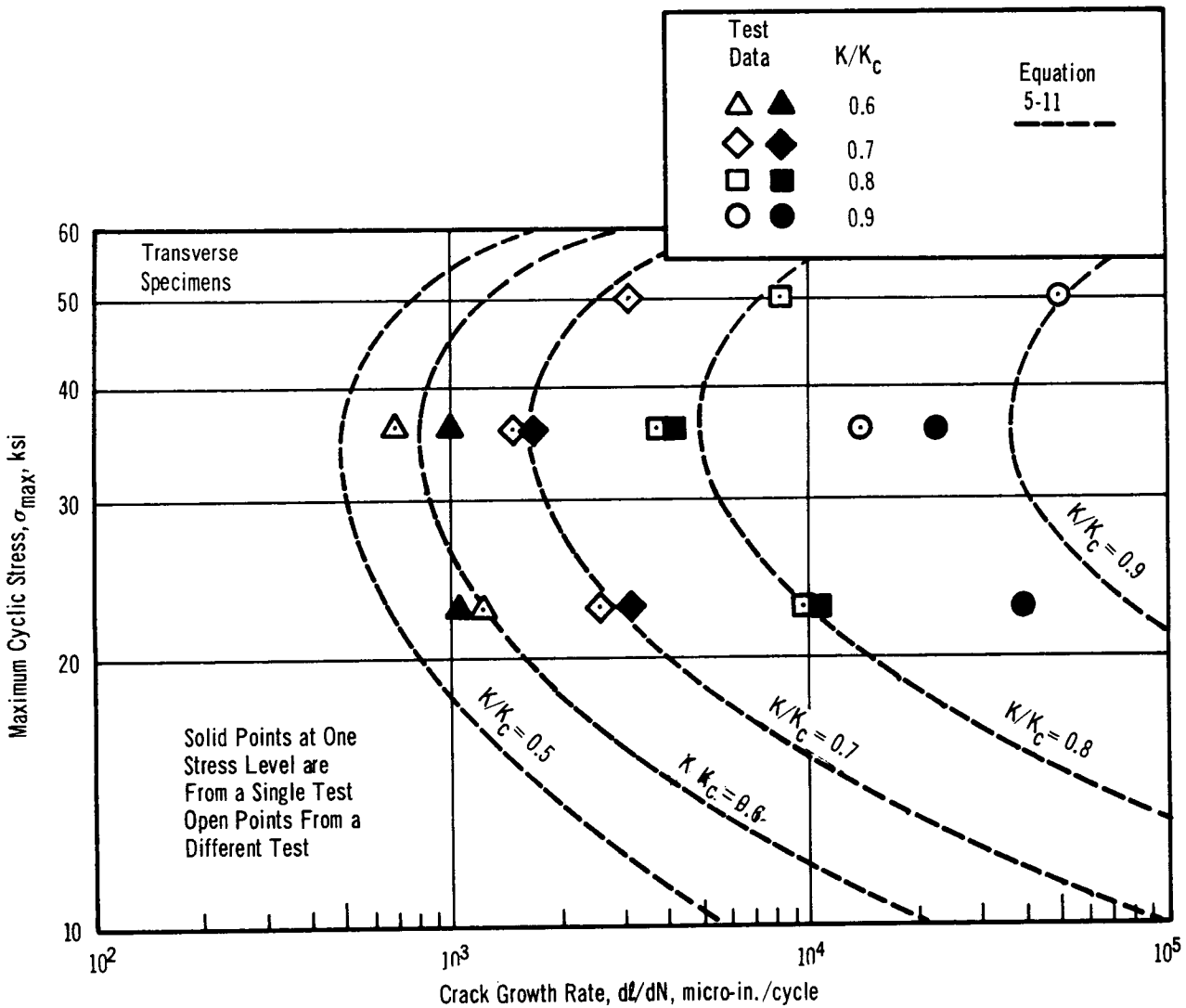

Figure 5-16. Comparison of Theoretical and Experimental Uniaxial Crack Growth Rates at Constant K/K_c Ratio for 2219-T87 at 70°F and 0.5 Stress Ratio

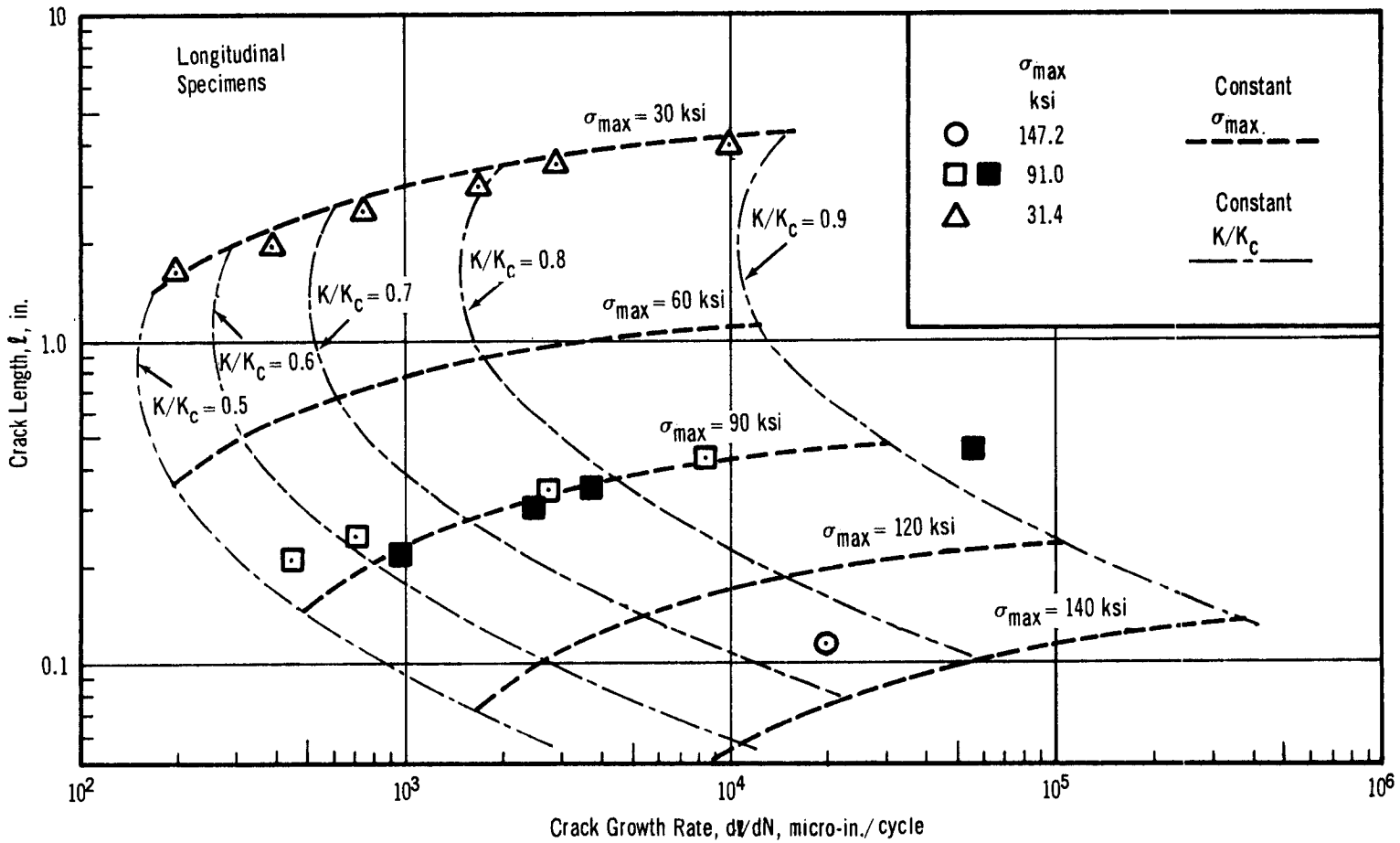

Figure 5-17. Effect of Crack Length and Maximum Cyclic Stress on Crack Growth for Ti-5Al-2.5Sn ELI at –423°F and 0.05 Stress Ratio

For valid interpretation of Figure 5-17, only the case of a dynamic (growing) crack may be considered. For example, a static crack has a growth rate of zero, a value not shown in the figure. Nor can a shrinking crack be considered, as pointed out above. With these limitations in mind, one may conclude from the figure that an increase in stress level increases the crack growth rate for any given instantaneous crack length. Also, the stress intensity can be maintained at a constant value only by reduction of the stress.

Section 6

BIAXIAL TEST RESULTS

Results and analysis of tests of cylindrical specimens are summarized in this section. Individual test results are given in Appendix D. Static tests of 10-in.-diam cylinders originally scheduled for all test temperatures were cancelled after several unsuccessful room temperature tests. Because of the excessive bulging caused by the long (5 in.) initial crack, crack growth did not proceed in a uniform axial direction.

6.1 CYCLIC TESTS

Initial crack lengths for biaxial cyclic tests were determined from uniaxial test results using a biaxial-uniaxial correlation developed by Kuhn for the Christensen-Denke equation. For most tests, calculated maximum hoop stresses corresponded with the highest and lowest maximum stresses utilized in the uniaxial cyclic tests.

Biaxial yield strengths and ultimate strengths were assumed to be 1.13 times the uniaxial strengths except for Ti-5Al-2.5Sn ELI (average of experimental data for aluminum alloys tested at Douglas). For this alloy the biaxial strengths were assumed to be 1.25 times uniaxial due to texture strengthening (ref. 10).

To aid in determining the size effect on biaxial crack propagation properties, two 4-in.-diam 2219-T87 cylinders were tested at room temperature.

6.1.1 Methods of Analysis

Equations used in analyzing biaxial test results are those presented in Section 5, modified to account for radius of curvature and bending at the crack tip.

By analyzing results of static tests performed on precracked cylinders, Anderson has developed a modification of Irwin's critical stress intensity equation (ref. 12) to account for biaxial effects, as:

$$K_c = \sigma_H \left(1 + C\frac{\ell_{cB}}{D}\right)\left(\frac{\pi \ell_{cB}}{2} + \frac{K_c^2}{2\sigma_{yB}^2}\right)^{1/2} \qquad (6\text{-}1)$$

where

K_c = critical stress intensity as calculated from uniaxial tests

σ_H = hoop stress at failure in biaxial test

C = bulge coefficient

D = cylinder diameter

ℓ_{cB} = total critical crack length (biaxial)

σ_{yB} = biaxial yield strength

A value of the bulge coefficient, C, was computed from the results of each biaxial test.

Kuhn's biaxial modification (ref. 5) of the Christensen-Denke equation is:

$$R_p = \frac{3\ell_{cB}}{\left[\frac{\sigma_{uB}}{\sigma_H\left(1 + 4.6\frac{\ell_{cB}}{r}\right)}\left(1 - \frac{\ell_{cB}}{w}\right)\right]^2 - 1} \qquad (6\text{-}2)$$

where

R_p = notch resistance factor calculated from uniaxial tests

ℓ_{cB} = total critical crack length

σ_{uB} = biaxial ultimate strength

σ_H = hoop stress at failure

r = radius of cylinder

w = length of cylinder

Eq. (6-2) was used in determining the initial crack lengths for biaxial cyclic tests. Initial crack lengths were selected as approximately one-half the critical crack length predicted by eq. (6-2).

6.1.2 Test Results

Biaxial cyclic test conditions and results are presented in Tables 6-I and 6-II. Crack growth curves of individual tests are given in Appendix D. Photographs of typical failed biaxial specimens are shown in Figures 6-1 and 6-2.

The average values of the bulge coefficient, C, shown for Ti-5Al-2.5Sn ELI differ from those reported by Anderson (ref. 12). This difference may be attributed to the fact that Anderson's values were based on K_{cn}, the critical stress intensity factor calculated using the initial crack length, ℓ_o, rather than the critical crack length, ℓ_{cB}. Another notable difference between the bulge coefficients shown in the tables and those computed by Anderson is the lack of a large temperature effect on the C values computed in this program.

While the critical crack lengths for the 4-in.-diam cylinders, as shown in Table 6-I, were shorter than those for the 10-in.-diam cylinders tested at the same stress levels, the Anderson-Irwin biaxial modification appears to account for the size effect since the C values for both sizes are the same.

Average C values were used in plotting eq. (6-1) as hoop stress versus critical crack length for the 10-in.-diam cylinders in Figures 6-3 and 6-4.

Biaxial strengthening of Ti-5Al-2.5Sn ELI due to texturing was accounted for in calculation of the C values by use of a biaxial yield strength 25% greater than uniaxial in eq. (6-1). The good agreement between the theoretical curves and experimental points of Figure 6-4 demonstrates that no modification of the fracture mechanics equation is needed when applied to highly textured material.

Crack growth curves for biaxial dynamic tests were plotted in the same manner as uniaxial curves. As shown in Table 6-III, coordinates (F, ℓ_F) of the common point of intersection of the biaxial crack growth curves varies with test conditions as did those for uniaxial test results. The value of ℓ_F remained constant at -1.0 for both materials. The value of F varied with stress ratio, material and test temperature. F values determined from 10-in.-diam cylinder tests were twice the uniaxial F value determined for the same stress schedule and test conditions. For the tests of the 4-in.-diam 2219-T87 cylinders tested at room temperature, the F values were higher than for the 10-in.-diam cylinders.

TABLE 6-I

RESULTS OF BIAXIAL CYCLIC TESTS PERFORMED ON 2219-T87 CYLINDERS

Specimen			Crack length (6)		Hoop stress			Cycles to fail	Bulge coefficient
No.	Diam (in.)	Thick (in.)	Initial ℓ_o (in.)	Critical ℓ_{cB} (in.)	Maximum σ_{max} (ksi)	Minimum σ_{min} (ksi)	At failure (ksi)	N_F	C
Test temperature, 70°F									
MB	10.18	0.062	0.24	0.52	49.33	2.50	49.10	136	5.98
PA	10.13	0.064	0.25	(1)	49.94	2.65	(1)	(1)	(1)
JB	10.14	0.062	0.80	1.95	21.44	1.00	21.13	530	4.94
AA	10.12	0.060	0.65	2.05	21.62	0.87	21.52	1533	4.32
TE	4.09	0.063	0.32	1.06	20.94	0.70	19.93	2847	6.15
TA	4.10	0.063	0.30	1.03	21.00	1.09	20.38	3257	6.26
Test temperature, -320°F									
KA	10.10	0.061	0.39	0.59	(2)	(2)	52.89	1	7.35
DA	10.16	0.062	0.25	0.78	44.14	21.80	43.60	335	7.76
CB	10.15	0.061	0.22	0.78	43.45	1.34	42.91	271	8.08
IB	10.14	0.062	(3)	(3)	(3)	(3)	(3)	(3)	(3)
NB	10.14	0.061	0.98	1.43	28.21	1.58	27.88	7	7.24
GA	10.14	0.061	0.68	1.57	26.65	0.68	24.60	145	7.83
PB	10.15	0.063	0.98	1.60	(2)	(2)	25.35	1	7.17
FA	10.12	0.060	0.99	1.45	28.25	14.05	29.10	228	6.47
Test temperature, -423°F									
EB	10.15	0.060	0.65	(4)	50.25	3.33	(4)	(4)	(4)
KB	10.14	0.062	0.14	(5)	(5)	(5)	(5)	(5)	(5)
IA	10.13	0.062	0.12	(5)	(5)	(5)	(5)	(5)	(5)
NC	10.14	0.062	0.76	1.58	25.74	1.19	25.21	133	7.12
MC	10.13	0.062	0.91	1.42	26.05	1.32	26.05	69	8.05
CA	10.15	0.061	0.96	1.60	26.06	12.99	25.86	128	6.63

(1) Specimen failed in weld after 8 cycles.

(2) Specimen failed during loading on first cycle.

(3) Specimen failed during precracking.

(4) Test discontinued after 134 cycles due to lack of liquid hydrogen.

(5) Excessive leaking during three attempts to pressurize.

(6) Parallel with rolling direction of sheet.

TABLE 6-II

RESULTS OF BIAXIAL CYCLIC TESTS PERFORMED ON Ti-5Al-2.5Sn ELI CYLINDERS

Specimen			Crack length (5)		Hoop stress			Cycles to fail	Bulge coefficient
No.	Diam (in.)	Thick (in.)	Initial ℓ_o (in.)	Critical ℓ_{cB} (in.)	Maximum σ_{max} (ksi)	Minimum σ_{min} (ksi)	At failure (ksi)	N_F	C
Test temperature, 70°F									
EM	10.04	0.020	0.29	0.85	84.36	4.63	83.89	344	7.90
GM	10.05	0.020	0.80	0.96	57.48	2.88	80.16(1)	401	7.26
AO	10.05	0.019	0.54	1.61	56.02	2.48	55.13	3674	7.04
HO	10.05	0.020	0.85	1.49	60.84	2.96	58.68	7	7.05
Test temperature, -320°F									
BO	10.08	0.019	0.49	0.51	(2)	(2)	105.43	1	9.06
AN	10.05	0.018	0.39	0.65	89.16	2.23	89.16	121	8.84
DM	10.05	0.020	0.23	0.48	112.09	56.76	107.04	59	9.82
DN	10.04	0.021	0.98	1.44	(2)	(2)	42.70	1	9.39
GO	10.05	0.021	0.98	1.33	35.22	2.01	33.61	29	15.89*
JO	10.05	0.021	0.98	1.78	37.07	19.17	34.70	1324	9.18
Test temperature, -423°F									
FM	10.05	0.021	0.20	(3)	(2)	(2)	100.73	1	(3)
EN	10.10	0.020	0.24	0.35	88.65	4.50	85.58	2	9.98
IN	10.05	0.021	0.22	0.35	88.58	45.25	88.39	66	8.73
CO	10.05	0.021	0.35	(4)	(4)	(4)	(4)	(4)	(4)
HN	10.05	0.019	0.96	1.26	30.63	1.60	30.21	132	8.75
IM	10.04	0.020	1.01	1.80	32.87	3.33	16.38	3	12.61
IO	10.06	0.020	0.96	1.18	31.06	14.56	30.58	461	9.72
KO	10.04	0.021	1.00	1.42	30.61	15.11	33.13	29	5.69

*Not used for average

(1) System pressure spike after 400 cycles.

(2) Specimen failed during loading on first cycle.

(3) Instrumentation failure.

(4) Excessive leaking during three attempts to pressurize.

(5) Perpendicular to rolling direction of sheet.

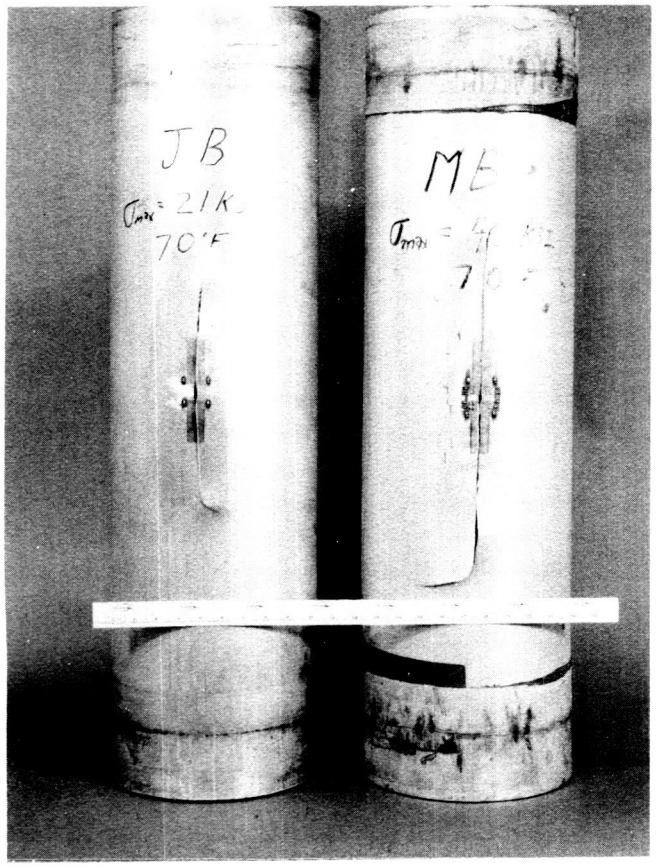

a, 2219-T87, 70°F

b, 2219-T87, −320°F

Figure 6-1. Failed 10 in. Diam Biaxial Test Specimens (1 of 3)

c, 2219-T87, −423°F

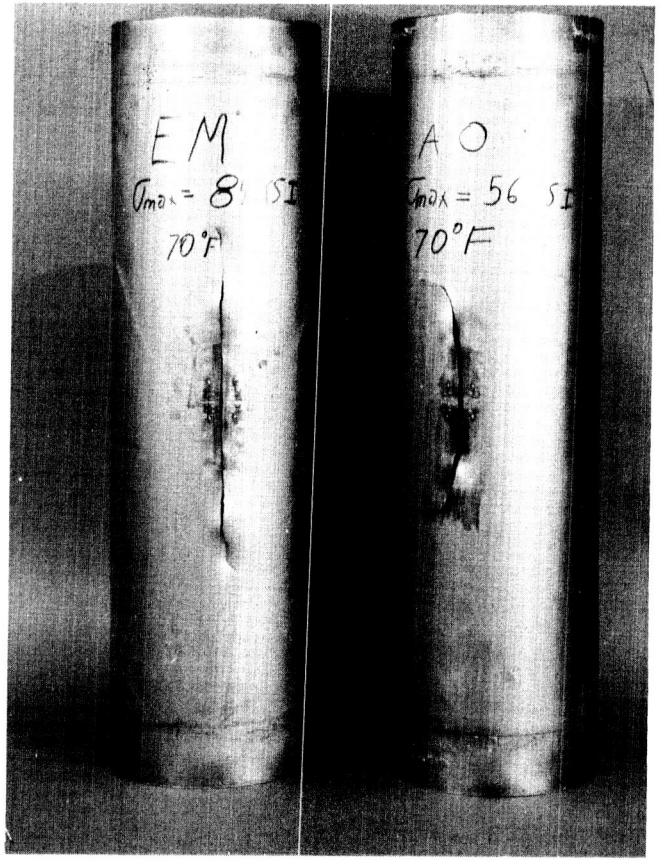

d, Ti-5Al-2.5Sn ELI, 70°F

Figure 6-1. Failed 10-in. Diam Biaxial Test Specimens (2 of 3)

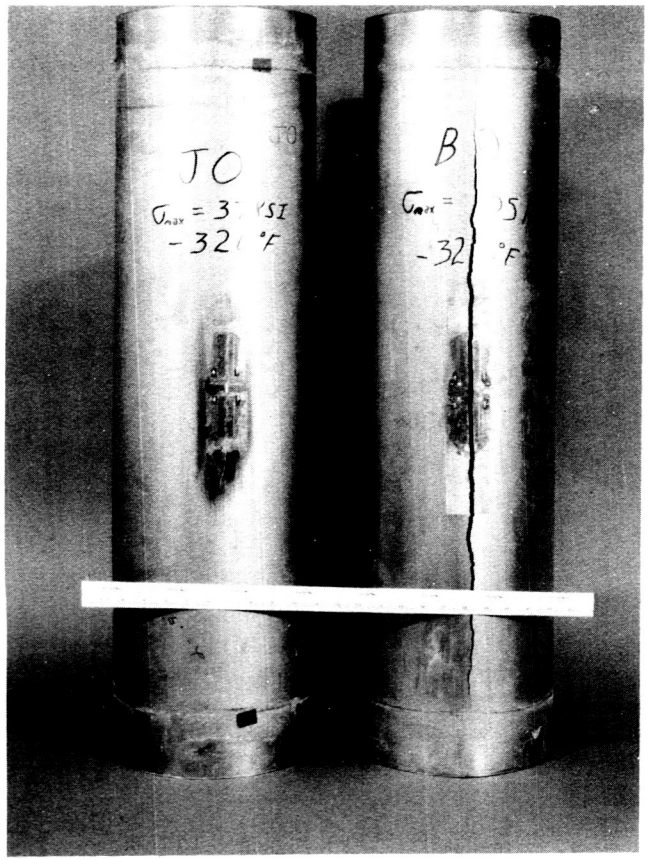

e, Ti-5Al-2.5Sn ELI, −320°F

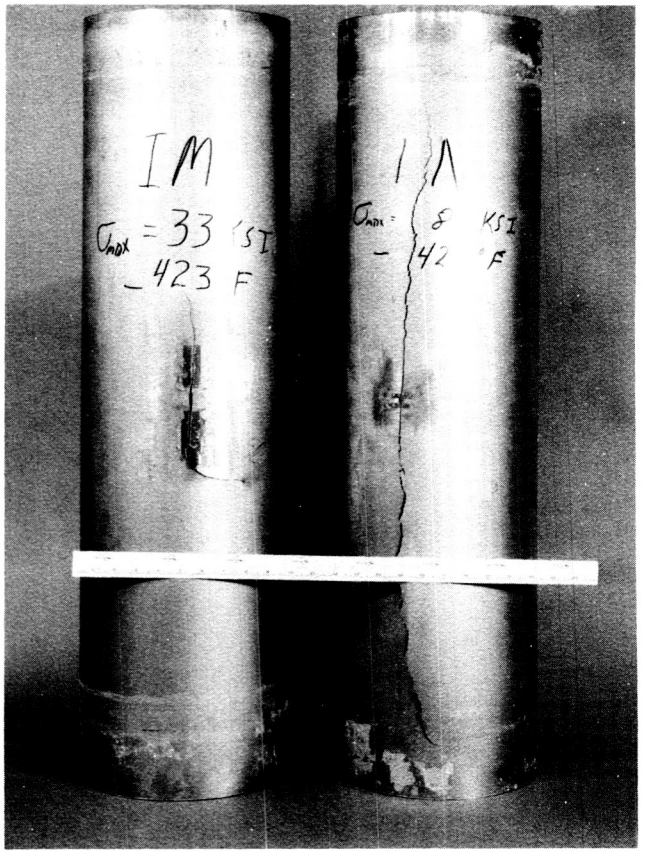

f, Ti-5Al-2.5Sn ELI, −423°F

Figure 6-1. Failed 10-in. Diam Biaxial Test Specimens (3 of 3)

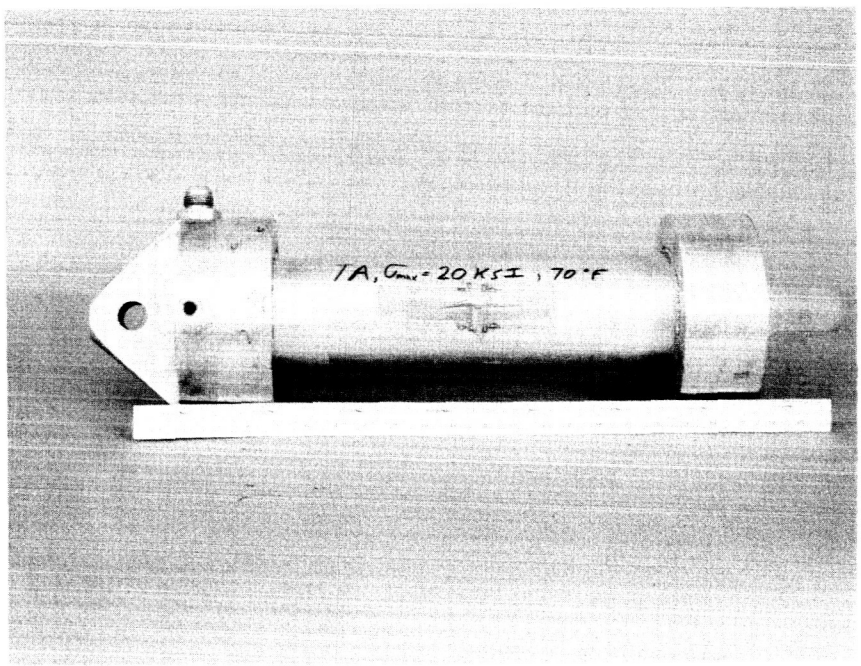

Figure 6-2. Failed 4-in. Diam Biaxial Test Specimen

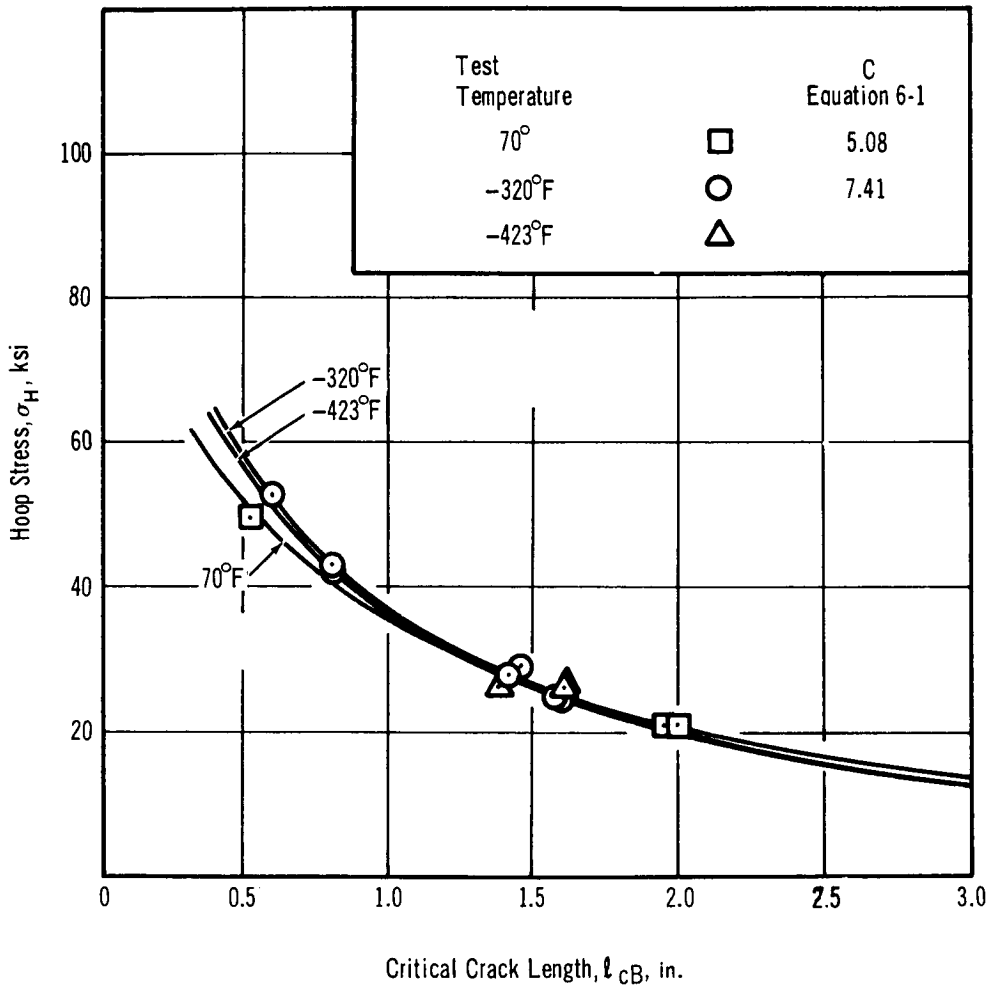

Figure 6-3. Hoop Stress at Failure vs. Critical Crack Length for 10-in. Diam 2219-T87 Cylinders. Curves Calculated from Average K_c and C.

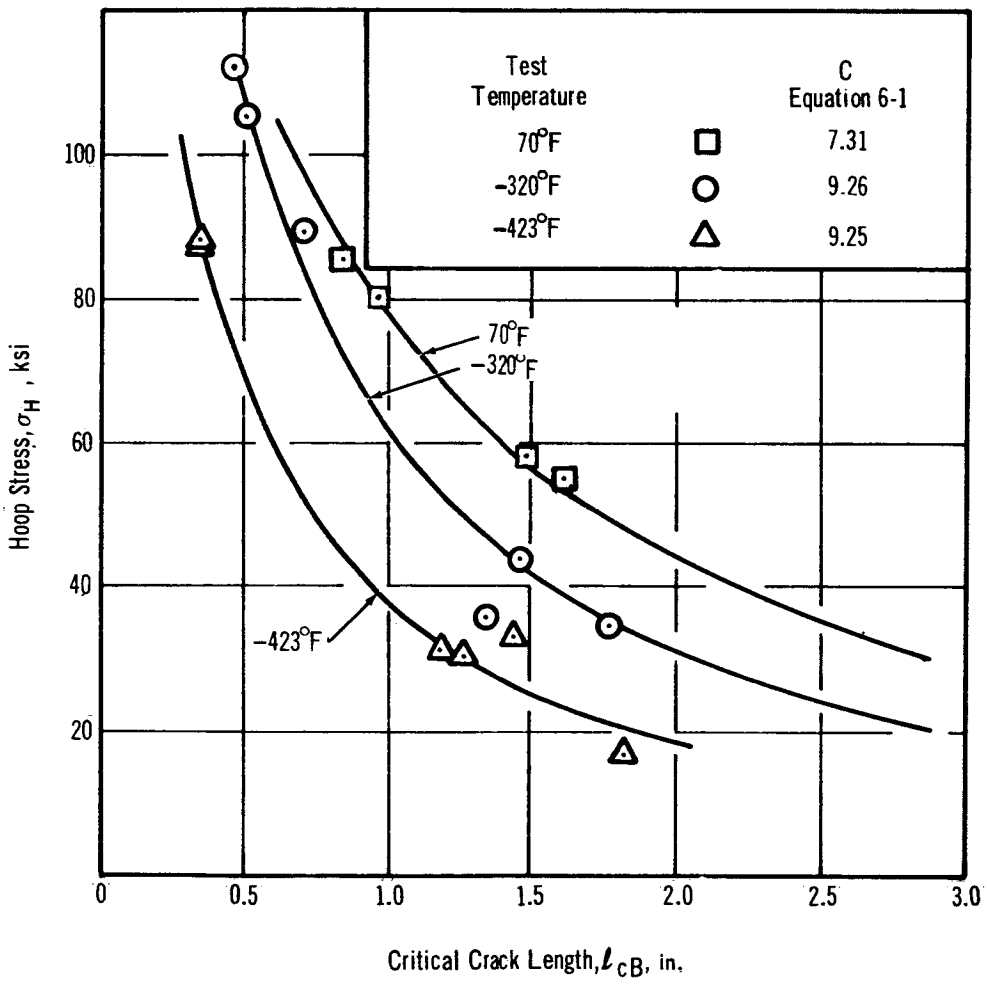

Figure 6-4. Hoop Stress at Failure versus Critical Crack Length for 10-in. Diam Ti-5Al-2.5Sn ELI. Curves Were Calculated from Average K_C and C.

TABLE 6-III

AVERAGE F VALUES DETERMINED
FROM BIAXIAL CYCLIC TESTS

Alloy	Test Temp. °F	F	
		$\frac{\sigma_{min.}}{\sigma_{max.}} = 0.05$	$\frac{\sigma_{min.}}{\sigma_{max.}} = 0.50$
4-in. diam			
2219-T87	70	22.75	(1)
10-in. diam			
2219-T87	70	13	(1)
	-320	10	16
	-423	12	21
Ti-5Al-2.5Sn ELI	70	13	(1)
	-320	24	32
	-423	28	38

(1) No data.

Section 7

DISCUSSION OF RESULTS

7.1 CORRELATION OF DATA

The concept of a common crack growth curve for a given stress schedule and the parametric techniques employed in analyzing and presenting the test data in this program have certain rigid limitations. Namely, the common growth curve concept is applicable only to fatigue cracks already in existence and does not apply to the period of crack initiation. Consequently, the approach can only be employed in dealing with fatigue crack growth after initiation. Secondly, the parametric technique used in this report may be completely unsatisfactory under some conditions not explored in this program.

Caution should be exercised in adapting the technique to types of stress scheduling other than those employed in this program. For example, constant net section stress cycling will produce growth curves of a lower degree than constant gross stress cycling. Caution should also be exercised in the use of the parametric technique at stress intensities much less than half the critical stress intensity. There are indications in some uniaxial test results that the actual growth rate of the crack at low stress intensities is much lower than predicted by the parametric equation. In spite of these limitations, the techniques are useful and aid in the task of correlating data obtained under a variety of conditions.

7.1.1 Biaxial and Uniaxial Crack Propagation

One objective of this program was to develop a means of utilizing uniaxial crack propagation data in predicting the behavior of cracks under biaxial conditions. Such a means was developed but must necessarily conform to the experimental boundaries of the program. The effects of certain variables such as stress ratio, frequency and loading profile, cylinder length-to-diameter ratio, uniaxial specimen width, stress states other than 1:0 and 1:2, and very low stress intensities were either not explored at all or were not explored sufficiently to define their influence. All comments in this section concerning correlation are made with respect to the experimental boundaries of the program.

7.1.1.1 Size Effects

Size effects in uniaxial testing were not examined. Presumably, however, specimen width influences the F value since width is known to influence critical crack length.

The effect of diameter on the critical crack length of biaxial specimens is adequately accounted for in Anderson's biaxial modification of the Irwin equation. The critical crack length for 4-in.-diam cylinders tested at 21 ksi maximum stress at 70°F was approximately half the length of the critical crack in 10-in.-diam cylinders, and approximately 1/7 the length of the critical crack in 16-in. wide uniaxial specimens. The effect of decreasing radius of curvature, therefore, is reduction of the critical crack length, a finding predicted by the Anderson modification.

The effect of diameter on the biaxial F value, F_B, was also observed in this program. For 2219-T87 at 70°F, F_B was observed to increase from 13 for 10-in.-diam cylinders to 22.75 for 4-in.-diam cylinders. Based only on the limited data available, this size effect can be described analytically as:

$$F_B = \frac{k}{r} + F_U \qquad (7\text{-}1)$$

where

F_B = biaxial F value

k = a size-effect constant

r = cylinder radius

F_U = uniaxial F value

The value of k for 2219-T87 at 70°F and a stress ratio of 0.05 is 32.5. By means of eq. (7-1), biaxial F values can be predicted from uniaxial test results. Conversely, eq. (7-1) can be solved for the constant, k, when the uniaxial and biaxial F values are known. Solution of eq. (7-1) for k, using uniaxial F values and the biaxial F values obtaining from testing the 10-in.-diam cylinders, resulted in values for k listed in Table 7-I.

7.1.1.2 Residual Cyclic Life

The combined effects of stress state and radius of curvature on residual cyclic life, N_R, are illustrated for 2219-T87 at 70°F in Figure 7-1. Solid curves represent actual test data accumulated at a maximum cyclic stress of approximately 21 ksi and a stress ratio of 0.05. The dashed portions of the curves are extrapolations to the F coordinate.

The figure indicates that for a given residual cyclic life, a longer crack can be tolerated in specimens of greater radius of curvature. This feature is brought about by the much larger critical crack lengths characteristic of larger radius of curvature. When one considers the residual cyclic life at a crack length equal to half the critical length, however, the specimen with the smallest radius of curvature has the greatest life remaining.

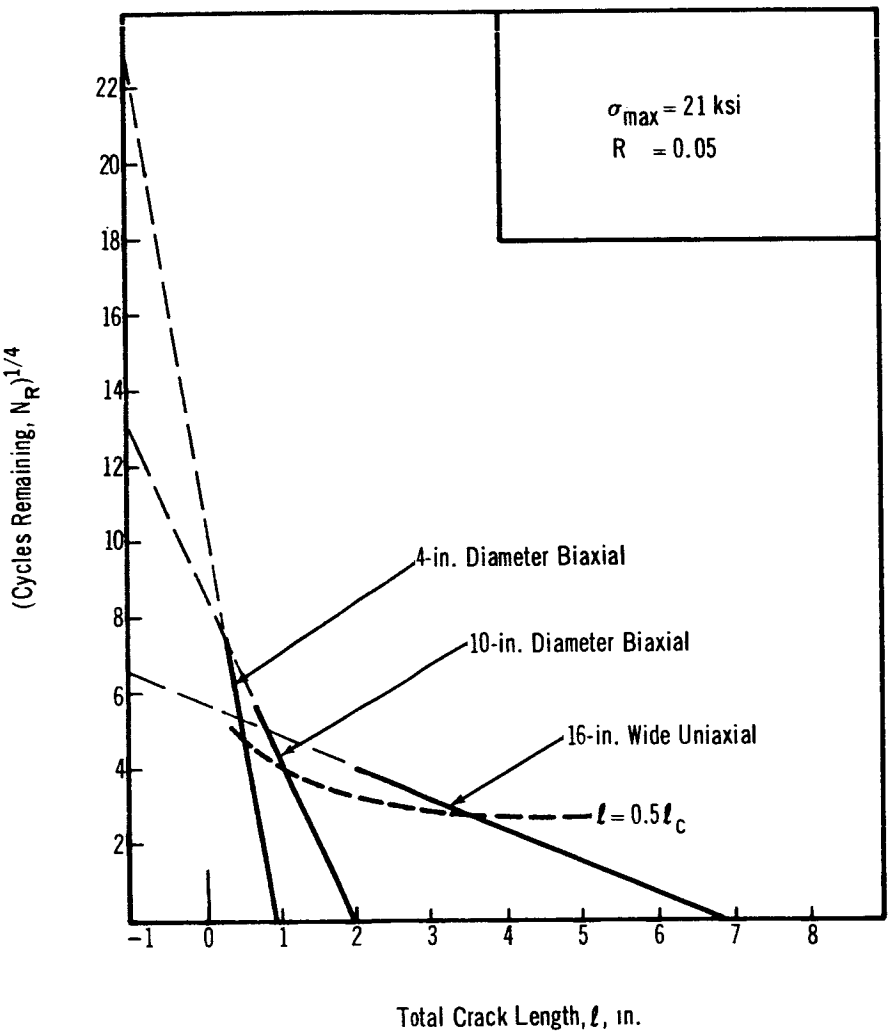

Figure 7-1. Comparison of Uniaxial and Biaxial Crack Propagation for 2219-T87 at 70°F

TABLE 7-I

VALUES OF SIZE EFFECT CONSTANT
CALCULATED FROM EQ. (7-1)

Alloy	Test Temp (°F)	Size Effect Constant, k	
		$\frac{\sigma \text{ min.}}{\sigma \text{ max.}} = 0.05$	$\frac{\sigma \text{ min.}}{\sigma \text{ max.}} \doteq 0.50$
2219-T87	70	32.5	----
	-320	25.0	40.0
	-423	30.0	52.5
Ti-5Al-2.5Sn ELI	70	32.5	----
	-320	60.0	80.0
	-423	70.0	95.0

The residual cyclic life of a cracked biaxial specimen, N_R, may be determined from uniaxial test results provided that constants in the various equations are known. These constants include the bulge coefficient, C, in the Anderson biaxial modification of the Irwin equation, and the size effect constant, k, in eq. (7-1). N_R may then be computed from

$$N_R = \left[F_B \left(\frac{\ell_{cB} - \ell}{\ell_{cB} + 1} \right) \right]^4 \qquad (7\text{-}2)$$

where

ℓ_{cB} = biaxial critical crack length calculated from the Anderson-Irwin equation, eq. (6-1)

F_B = biaxial F value calculated from eq. (7-1)

7.1.2 Fracture Mechanics and Crack Growth Rate

For the stress schedules employed in this program, the relationship between the stress intensity and the crack growth rate appears to be quite complex. Attempts to apply various published crack propagation rate equations (ref. 14) were unsatisfactory. A reasonable estimate of the crack growth rate for the tests performed in this program can be obtained by the use of eq. (5-11):

$$\frac{d\ell}{dN} = \frac{\left(\ell_c + 1\right)^4}{4F^4\left(\ell_c - \ell\right)^3}$$

Some published growth rate equations indicate that $d\ell/dN$ is some function of K (ref. 14). Eq. (5-11) can be expressed in terms of K and K_C rather than ℓ and ℓ_c, but the result is awkward. The growth rate, as given by eq. (5-11), is inversely dependent on the F value. Comparison of K_C and F for the two materials at all test temperatures reveals an inverse relationship between these two parameters; that is, in most cases, as K_C decreases as a function of temperature, F increases.

At least two material characteristics must be involved in the definition of crack propagation behavior. One characteristic is the critical stress intensity, K_C, which merely defines the end point of the test. A second characteristic may be the fatigue resistance of the material, possibly represented by F.

7.2 APPLICATION OF RESULTS

The use of large scale cryogenic tankage and the growing durations of space exposure combine to increase the probability of the damaging impact of meteoroids with the tank wall. Repeated loading of a tank penetrated by a meteoroid is likely to cause through-the-thickness crack propagation. The presence of such damage need not terminate the mission provided that intolerable leaks can be eliminated by patching or caulking and that sufficient cyclic life was designed into the vehicle.

Examples are given below to demonstrate how a designer may use the techniques and data developed in this program. The examples are simplified for clarity and do not attempt to account for variations in materials from heat to heat, stress corrosion, sustained load effects, and other influences.

7.2.1 Design for Safe Cyclic Life

The use of crack propagation data in the design of a propellant tank is illustrated in the following example.

A liquid hydrogen tank, 20-ft in diameter, is to be designed for a system intended for a deep space mission. Ti-5Al-2.5Sn ELI and 2219-T87 were selected as candidate materials for this application. It is known that the tank must be pressurized a maximum of 50 times between 5% and 100% of the maximum operating pressure. During the mission, the vehicle is expected to be impacted at least once by a meteoroid causing a damaged area 0.2-in. maximum dimension. It is necessary to determine which material should be used and the maximum allowable operating stress in the cylindrical portion of the tank. The criterion for material selection is to be minimum weight for safe cyclic life. A safety factor of two on the number of cycles will be used.

The following materials properties for -423° F are assumed to be available:

	2219-T87	Ti-5Al-2.5Sn
Biaxial yield strength, σ_{yB}, ksi	83.4	241.6
Critical stress intensity, K_c, ksi $(in.)^{1/2}$	93.9	90.9
Bulge coefficient, C	7.3	9.2
Uniaxial F-value, F_U	6.0	14.0
Size effect constant, k	30.0	70.0

First calculate the biaxial F-value, F_B from eq. (7-1), as:

$$F_B = \frac{k}{r} + F_U \qquad (7\text{-}1)$$

For 2219-T87:

$$F_B = \frac{30.0}{120} + 6$$

$$= 6.25$$

For Ti-5Al-2.5Sn ELI:

$$F_B = \frac{70.0}{120} + 14$$

$$= 14.58$$

Second, calculate the critical biaxial crack length, ℓ_{cB}, which would occur after cycling 100 times (safety factor times actual number of cycles) starting with a crack length, ℓ, equal to the maximum meteoroid damage area dimension, 0.2 in., as:

$$\ell_{cB} = \frac{N_R^{1/4} + F_B \ell}{F_B - N_R^{1/4}} \qquad (7\text{-}3)$$

For 2219-T87:

$$\ell_{cB} = \frac{(100)^{1/4} + 6.25 \times 0.2}{6.25 - (100)^{1/4}}$$

$$= 1.43 \text{ in.}$$

For Ti-5Al-2.5Sn ELI:

$$\ell_{cB} = \frac{(100)^{1/4} + 14.58 \times 0.2}{14.58 - (100)^{1/4}}$$

$$= 0.53 \text{ in.}$$

The foregoing calculations are presented graphically in Figure 7-2.

Finally, calculate the maximum cyclic hoop stress, σ_H, characteristic of the biaxial critical crack lengths from:

$$\sigma_H = K_c \Big/ \left(1 + C \frac{\ell_{cB}}{D}\right) \left[\frac{\Pi \ell_{cB}}{2} + \frac{K_c^2}{2 \times \sigma_{yB}^2}\right]^{1/2} \qquad (7\text{-}4)$$

For 2219-T87:

$$\sigma_H = 93,900 \Big/ \left(1 + 7.3 \frac{1.43}{240}\right) \left[\frac{3.14 \times 1.43}{2} + \frac{(93.9)^2}{2(83.4)^2}\right]^{1/2}$$

$$= 53.2 \text{ ksi}$$

For Ti-5Al-2.5Sn ELI:

$$\sigma_H = 90,900 \Big/ \left(1 + 9.2 \frac{0.53}{240}\right) \left[\frac{3.14 \times 0.53}{2} + \frac{(90.9)^2}{2(241.6)^2}\right]^{1/2}$$

$$= 93.7 \text{ ksi}$$

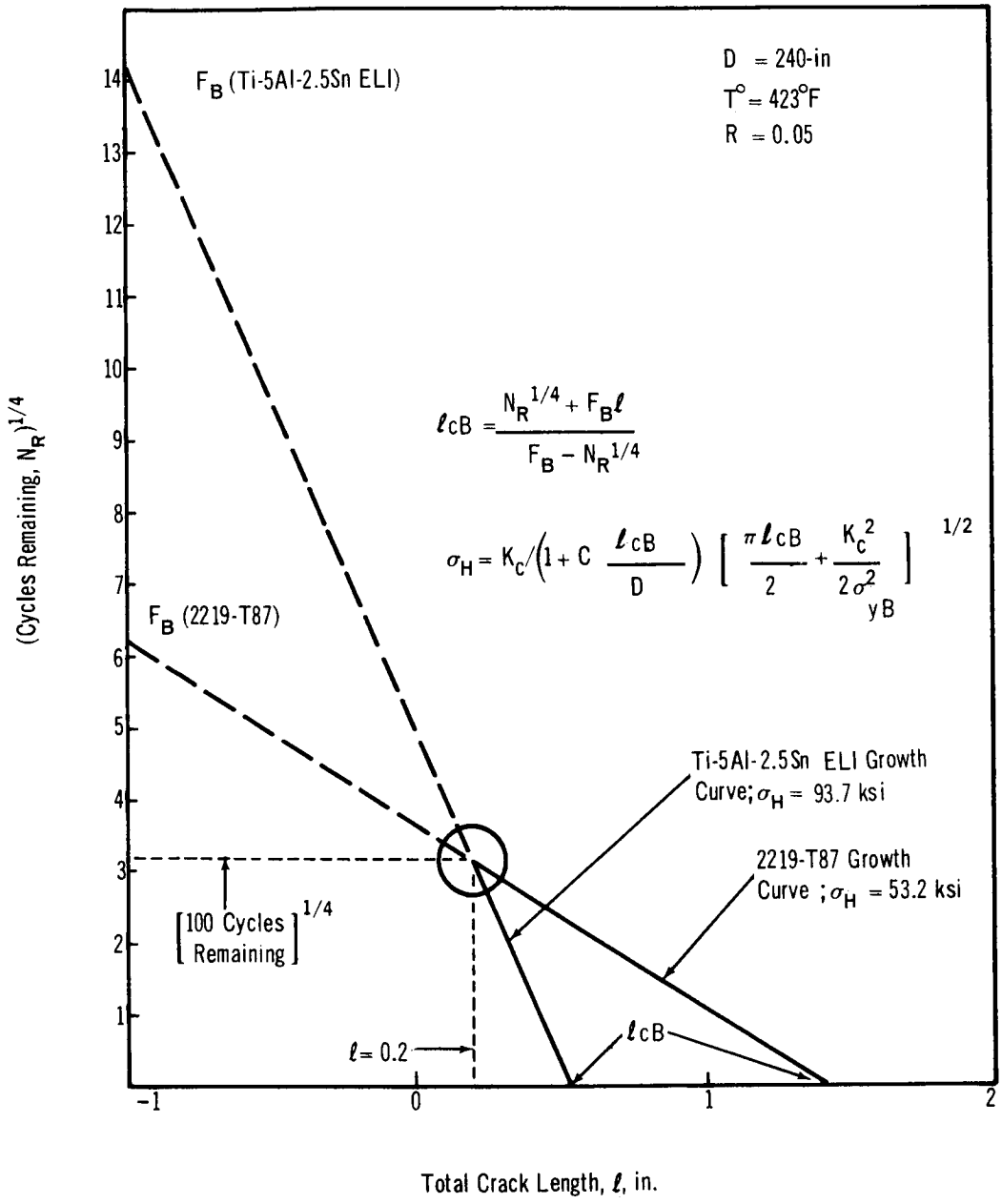

Figure 7-2. Large Liquid Hydrogen Tank Design Calculations

Since the maximum cyclic hoop stress for the Ti-5Al-2.5Sn ELI tank is approximately 76% higher than for the 2219-T87 tank, the titanium tank would represent the least tank weight. The best design for safe cyclic life and minimum weight for the example stated is a Ti-5Al-2.5Sn ELI tank operating at a maximum hoop stress of 93.7 ksi.

7.2.2 Mission Decisions Based on Cyclic Flaw Growth Data

For the case in which a crack is discovered in the tank wall during a mission, a further example will be given. The tank and mission conditions will be the same as before; that is, the 20-ft-diam liquid hydrogen tank fabricated from Ti-5Al-2.5Sn ELI is found to have been damaged by meteoroid impact and a crack 0.3 in. long exists in the tank wall. Successful completion of the mission requires that the tank be fully pressurized (to 93.7 ksi hoop stress) ten more times.

To determine the cyclic life remaining for the tank, the following calculations can be made:

First, calculate the biaxial F-value, F_B as:

$$F_B = \frac{k}{r} + F_U \qquad (7\text{-}1)$$

$$= 14.58 \text{ (for Ti-5Al-2.5Sn ELI)}$$

Second, calculate the critical biaxial crack length for a hoop stress of 93.7 ksi, as:

$$\sigma_H = K_c \Big/ \left\{ \left(1 + C \frac{\ell_{cB}}{D} \right) \left[\frac{\Pi \ell_{cB}}{2} + \frac{K_c^2}{2 \times \sigma_{yB}^2} \right]^{1/2} \right\} \qquad (7\text{-}4)$$

$$\ell_{cB} = 0.53 \text{ in. (by series of approximations)}$$

Finally, calculate the life remaining, N_R, for the tank by:

$$N_R = \left[\frac{F_B(\ell_{cB} - \ell)}{\ell_{cB} + 1} \right]^4$$

$$= \left[\frac{14.58\ (0.53 - 0.3)}{0.53 + 1} \right]^4$$

$$= (2.29)^4$$

$$= 27.5 \text{ cycles}$$

The life remaining for the damaged tank in the example exceeds mission requirements, therefore successful completion of the mission, theoretically, is indicated. If the life remaining for the tank had been less than that required, it would be possible to calculate the reduction in pressure necessary to prolong the tank's cyclic life.

7.2.3 Crack Propagation Testing

The parametric relationship developed in this program can be employed to reduce the number of tests required in studies of fatigue crack propagation behavior. Figure 7-3 is an example of how crack growth curves for a wide range of stresses can be predicted from constants established in a few tests.

For a single test, the critical stress intensity, K_c, and the F value can be determined. Of course, duplicate or triplicate testing improves confidence in the data.

To construct a master crack growth diagram, such as Figure 7-3, critical crack lengths for maximum cyclic stresses of interest should be calculated from K_c, by:

$$\ell_c = \frac{2w}{\Pi} \left[\arctan \left(\frac{K_c^2}{w\sigma^2_{max.}} \right) \right] - \frac{K_c^2}{\Pi\sigma_y^2} \qquad (7\text{-}5)$$

On a plot of $N_R^{1/4}$ versus ℓ, straight lines can then be drawn from the point having the coordinates (F, - 1) to the critical crack lengths. Each straight line is a predicted growth curve for a given maximum cyclic stress.

In Figure 7-3, the technique is illustrated for 2219-T87 at -423° F at 2 stress ratios, 0.05 and 0.50.

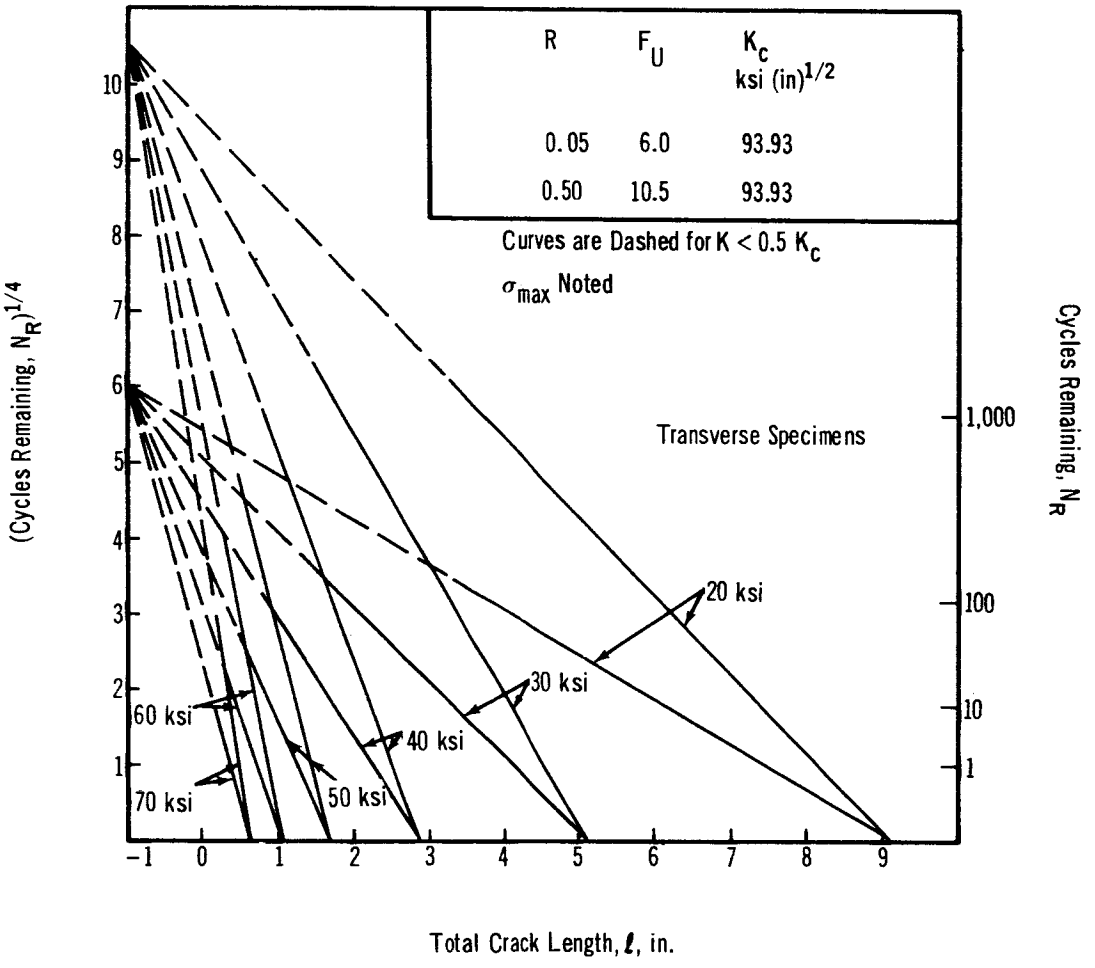

Figure 7-3. Constructed Uniaxial Crack Growth Curves for 2219-T87 at –423°F

Section 8
CONCLUSIONS

(1) Plane stress crack propagation data can be employed in the design of propellant tanks in which it is assumed through-the-thickness cracks will exist (possibly caused by meteoroid penetration). Further, uniaxial plane stress crack propagation data can be employed to predict biaxial plane stress crack propagation behavior. A parametric equation was developed in this program for these purposes.

(2) The Anderson biaxial modification of the Irwin stress intensity equation adequately accounts for bulging and radius of curvature in relating stress to critical crack length.

(3) The parametric equation developed in this program and the concept of common crack growth curves are tools which can reduce the number of tests required in studies of crack propagation behavior.

(4) Plane stress crack growth rate is not dependent solely upon stress intensity. At least two of the three parameters, stress, stress intensity, and crack length, are necessary to define crack growth rate.

Appendix A

CHEMICAL COMPOSITION AND POLE FIGURE ANALYSIS OF TEST MATERIALS

The results of chemical analyses of each sheet of 2219-T37 and Ti-5Al-2.5Sn ELI used in the test program are presented as average values in Tables A-I and A-II.

A typical pole figure for the Ti-5Al-2.5Sn ELI sheet is presented in Figure A-1. The figure indicates that the poles for the basal (0001) planes coincide and that these planes lie parallel with the plane of the sheet. Such preferred orientation in sheet products of some titanium alloys has been shown to enhance biaxial strength (ref. 10).

TABLE A-I

CHEMICAL COMPOSITION OF 2219 ALUMINUM ALLOY

Material	2219 Aluminum Alloy
Temper	T37
Specification	MIL-A-8920
Thickness	0.060 in.
Supplier	ALCOA
Heat No.	732-292

Element	Weight (%)				
	Specification		Douglas		
	Max.	Min.	Max.	Avg.	Min.
Copper	6.8	5.8	6.8	6.22	5.8
Magnesium	0.02	-	0.03	0.02	0.01
Silicon	0.20	-	0.17	0.13	0.07
Iron	0.30	-	0.37	0.22	0.17
Titanium	0.10	0.02	0.08	0.07	0.05
Manganese	0.40	0.20	0.33	0.27	0.22
Zinc	0.10	-	0.07	0.05	0.04
Vanadium	0.15	0.05	-	-	-
Zirconium	0.25	0.10	-	-	-
Others					
Each	0.05	-	-	-	-
Total	0.15	-	-	-	-
Aluminum	Bal.				

TABLE A-II

CHEMICAL COMPOSITION OF Ti-5Al-2.5Sn (ELI)

Material	Ti-5Al-2.5Sn ELI
Temper	Annealed
Specification	TMCA internal
Thickness	0.020 in.
Supplier	TMCA
Heat No.	D-5907

Element	Weight (%)			
	TMCA	Douglas		
		Max.	Avg.	Min.
Aluminum	5.2	-	-	-
Tin	2.5	-	-	-
Iron	0.16	0.19	0.15	0.14
Manganese	0.002	-	-	-
Carbon	0.025	0.020	0.015	0.011
Nitrogen	0.014	0.015	0.011	0.007
Hydrogen	0.009-0.013	-	-	-
Oxygen	0.07	-	-	-

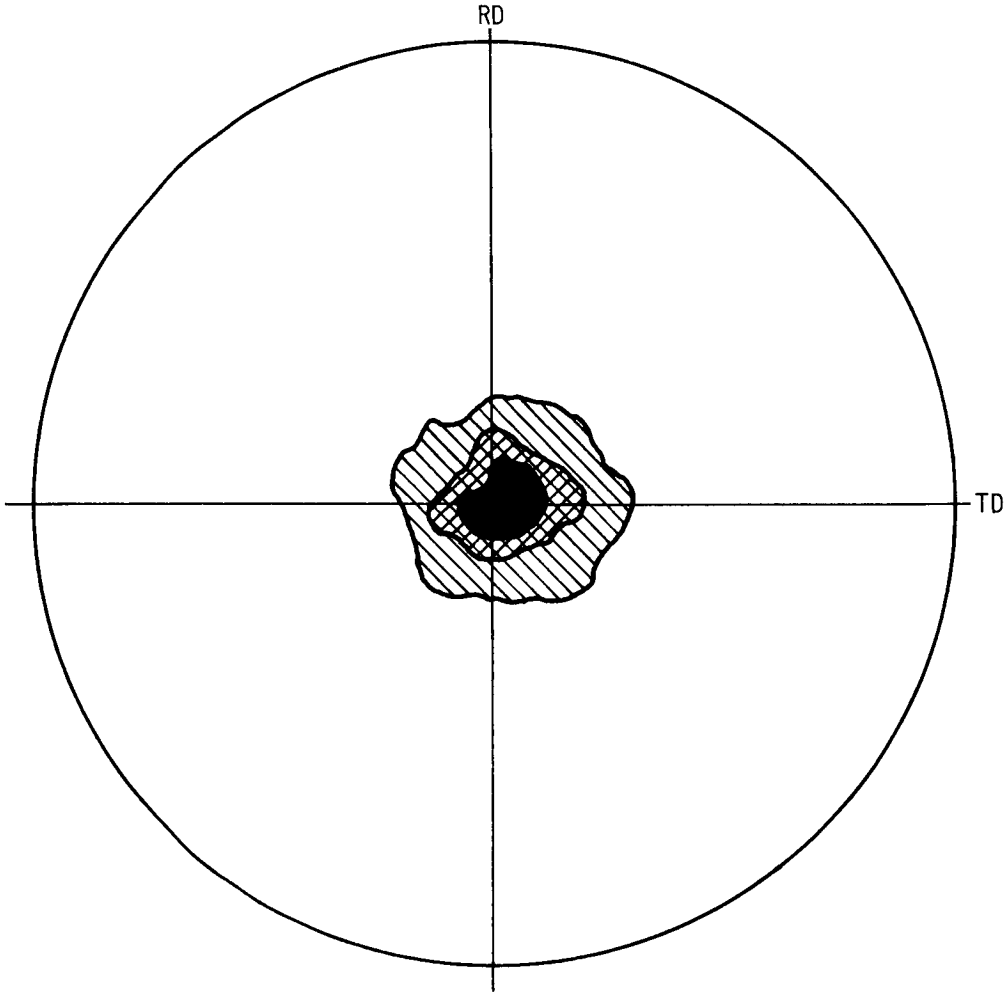

Figure A-1. Typical Basal (0001) Plane Pole Figure for Ti-5Al-2.5Sn ELI

Appendix B

MECHANICAL PROPERTIES

Average property values utilized for all computations in this report are shown in Tables B-I and B-II. The results of mechanical property tests performed on 2219-T87 and Ti-5Al-2.5Sn ELI at 70°, -320° and -423°F are presented in Tables B-III through B-VIII.

TABLE B-I

AVERAGE PROPERTIES OF 2219-T87
0.060-IN. SHEET

Temperature		70°F		-320°F	-423°F
Direction		L	T	T	T
Uniaxial yield	ksi	58.2	57.7	71.3	73.8
Uniaxial ultimate	ksi	69.7	70.0	88.4	100.6
Elongation in 2 in.	%	9.8	10.0	9.5	-
Elastic modulus	psi x 10^{-6}	9.8	9.8	11.4	13.4
Elastic Poisson's ratio		0.292	0.314	0.319	-
K_c	ksi $(in)^{1/2}$	-	80.65	97.29	93.93
R_p	in.	-	5.79	5.05	3.66
Biaxial yield (1)	ksi	-	65.2	80.6	83.4
Biaxial ultimate (1)	ksi	-	79.1	99.9	113.7
Bulge coefficient	C	-	5.08	7.41	7.27
Uniaxial F value					
R = 0.05		-	6.5	5	6
R = 0.50		-	10.5	8	10.5
Biaxial F value					
R = 0.05		-	13	10	12
R = 0.50		-	-	16	21
Size effect constant	k				
R = 0.05		-	32.5	25	30
R = 0.50		-	-	40	52.5

(1) Calculated from uniaxial.

L = Longitudinal.

T = Transverse.

TABLE B-II

AVERAGE PROPERTIES OF Ti-5Al-2.5Sn ELI
0.020-IN. SHEET

Temperature	70°F		-320°F	-423°F
Direction	L	T	L	L
Uniaxial yield ksi	109.3	107.4	171.2	193.3
Uniaxial ultimate ksi	118.3	115.1	189.5	205.7
Elongation in 2 in. %	15.6	16.6	12.0	(2).
Elastic modulus psi x 10^{-6}	15.6	16.0	18.9	20.6
Elastic Poisson's ratio	0.416	0.414	0.364	-
Plastic Poisson's ratio	0.700	0.784	-	-
K_c ksi $(in)^{1/2}$	234.92	-	159.83	90.91
R_p in.	49.57	-	2.70	0.60
Biaxial yield (1) ksi	136.6	-	214.0	241.6
Biaxial ultimate (1) ksi	147.9	-	236.9	257.1
Bulge coefficient C	7.31	-	9.26	9.25
Uniaxial F value				
R = 0.05	6.5	-	12	16
R = 0.50	13	-	14	19
Biaxial F value				
R = 0.05	13	-	24	28
R = 0.50	-	-	32	38
Size effect constant k				
R = 0.05	32.5	-	60	70
R = 0.50	-	-	80	95

(1) Calculated from uniaxial.

(2) Broke outside gauge marks.

L = Longitudinal.

T = Transverse.

TABLE B-III

RESULTS OF MECHANICAL PROPERTY TESTS PERFORMED ON 2219-T87 0.060-IN. SHEET AT ROOM TEMPERATURE

Sheet No.	Direction	Thickness (in.)	0.2% Yield strength (ksi)	Ultimate strength (ksi)	Elongation in 2 in. (%)	Elastic modulus psi x 10^{-6}	Elastic Poisson's Ratio
A	L	0.0615	58.2	69.7	10	9.6	-
		0.0610	58.3	69.5	9	9.8	-
	T	0.0602	60.0	71.1	8	10.0	-
		0.0604	58.8	70.6	10	9.8	-
B	L	0.0614	59.1	70.4	10	9.2	-
		0.0610	58.9	70.1	9	9.7	-
	T	0.0610	58.2	70.1	8	10.4	-
		0.0605	58.8	70.7	9	9.6	-
C	L	0.0614	58.8	70.1	11	9.7	-
		0.0610	59.1	70.4	10	9.7	-
	T	0.0610	58.2	70.3	9	9.6	-
		0.0610	58.2	70.2	10	9.9	-
D	L	0.0620	58.6	69.9	10	9.6	-
		0.0615	58.7	70.1	9	9.5	-
	T	0.0612	58.1	70.5	8	9.9	-
		0.0615	58.0	70.3	10	9.7	-
E	L	0.0600	58.3	69.6	9	9.7	-
		0.0595	58.8	70.1	10	10.1	-
	T	0.0595	58.5	70.3	9	9.8	-
		0.0595	58.7	70.3	10	9.9	-
F	L	0.0605	58.8	70,1	9	9.9	-
		0.0602	58.7	70.0	10	9.7	-
	T	0.0600	58.4	70.1	9	9.7	-
		0.0600	58.4	70.2	10	9.7	-
G	L	0.0610	58.7	69.9	10	9.6	-
		0.0605	59.1	70.1	10	9.9	-
	T	0.0606	58.2	70.1	11	9.9	-
		0.0605	58.2	70.3	10	10.0	-
H	L	0.0615	58.4	69.7	10	9.8	-
		0.0615	58.4	69.7	10	9.8	-
	T	0.0615	57.6	70.1	10	9.4	-
		0.0610	58.1	70.4	11	9.7	-
I	L	0.0620	57.9	69.6	10	10.0	-
		0.0620	58.2	69.7	10	9.8	-
	T	0.0620	57.2	69.6	10	9.9	-
		0.0620	57.1	69.6	11	9.6	-
J	L	0.0620	57.6	69.7	10	9.9	-
		0.0620	58.3	69.8	10	9.9	-
	T	0.0620	57.2	69.8	10	9.6	-
		0.0618	57.1	69.9	11	9.8	-
K	L	0.0620	57.1	68.8	-	9.6	0.295
		0.0615	58.4	69.7	10	9.7	-
	T	0.0620	56.4	69.3	-	9.9	0.299
		0.0615	57.2	69.7	11	10.2	-
L	L	0.0620	56.7	68.5	-	9.8	0.292
		0.0615	58.3	69.5	9	9.8	-
	T	0.0625	55.8	68.6	-	10.3	0.329
		0.0615	57.6	70.0	12	9.8	-
M	L	0.0630	56.3	68.6	-	9.8	0.266
		0.0620	58.2	69.6	9	9.8	-
	T	0.0620	56.7	69.2	-	10.0	0.321
		0.0615	-	70.3	10	-	-
N	L	0.0625	56.8	68.9	-	9.8	0.319
		0.0620	58.2	69.6	10	9.6	-
	T	0.0620	56.3	69.3	-	9.9	0.305
		0.0615	57.4	70.0	11	9.5	-
O	L	0.0630	57.1	69.3	-	10.1	0.284
		0.0615	59.2	71.2	10	9.9	-
	T	0.0630	56.3	69.8	-	10.0	0.289
		0.0620	57.6	70.6	11	9.7	-
P	L	0.0645	57.2	69.0	-	9.7	0.296
		0.0634	59.2	70.6	10	9.8	-
	T	0.0640	56.9	69.7	-	9.7	0.342
		0.0632	57.7	70.3	10	10.0	-

L = Longitudinal

T = Transverse

TABLE B-IV

RESULTS OF MECHANICAL PROPERTY TESTS PERFORMED
ON 2219-T87 0.060-IN. SHEET AT -320°F

Sheet No.	Direction	Thickness (in.)	0.2% Yield strength (ksi)	Ultimate strength (ksi)	Elongation in 2 in. (%)	Elastic modulus psi x 10^{-6}	Elastic Poisson's Ratio
F	T	0.0600	71.4	88.4	10	11.5	0.321
G	T	0.0605	71.3	88.4	9	11.2	0.317

TABLE B-V

RESULTS OF MECHANICAL PROPERTY TESTS PERFORMED
ON 2219-T87 0.060-IN. SHEET AT -423°F

Sheet No.	Direction	Thickness (in.)	0.2% Yield strength (ksi)	Ultimate strength (ksi)	Elongation in 2 in. (%)	Elastic modulus psi x 10^{-6}	Elastic Poisson's Ratio
N	T	0.0620	73.3	99.7	-	12.0	0.341
P	T	0.0635	74.4	101.6	-	14.0	0.526

TABLE B-VI

RESULTS OF MECHANICAL PROPERTY TESTS PERFORMED ON Ti-5Al-2.5Sn ELI 0.020-IN. SHEET AT ROOM TEMPERATURE

Sheet No.	Direction	Thickness (in.)	0.2% Yield strength (ksi)	Ultimate strength (ksi)	Elongation in 2 in. (%)	Elastic modulus psi x 10^{-6}	Elastic Poisson's Ratio	Plastic Poisson's Ratio
A	L	0.0192	110.0	120.4	20 (1)	16.3	-	-
		0.0195	117.1	122.0	26 (1)	15.6	-	-
	T	0.0190	113.7	121.3	16	17.5	-	-
		0.0200	104.0	114.4	-	15.3	0.416	0.698
B	L	0.0210	108.1	119.6	20 (1)	15.8	-	-
		0.0210	114.6	120.4	22 (1)	15.2	-	-
	T	0.0208	113.5	119.2	15	17.0	-	-
		0.0220	103.5	112.4	-	14.8	0.421	0.825
C	L	0.0230	115.0	126.4	20 (1)	16.4	-	-
		0.0230	113.1	120.0	20 (1)	15.2	-	-
	T	0.0220	114.8	121.7	16	17.2	-	-
		0.0235	103.0	112.7	-	14.7	0.428	0.720
D	L	0.0210	113.1	124.2	20 (1)	15.6	-	-
		0.0210	-	121.2	20 (1)	16.0	-	-
	T	0.0210	111.4	117.1	17	17.0	-	-
		0.0210	101.9	111.1	-	14.5	0.417	0.858
E	L	0.0220	111.4	123.6	20 (1)	15.8	-	-
		0.0220	113.6	120.0	22 (1)	15.4	-	-
	T	0.0215	111.6	118.5	17	17.0	-	-
		0.0210	104.3	113.3	-	15.3	0.363	0.782
F	L	0.0220	108.9	120.4	20 (1)	16.3	-	-
		0.0220	111.4	116.4	20 (1)	15.5	-	-
	T	0.0210	110.5	115.1	17	17.3	-	-
		0.0200	103.5	112.0	-	15.0	0.439	0.708
G	L	0.0200	115.6	130.0	20 (1)	16.7	-	-
		0.0200	120.0	129.2	20 (1)	16.9	-	-
	T	0.0200	119.0	128.6	16	18.2	-	-
		0.0195	110.8	121.6	-	16.2	0.366	0.579
H	L	0.0205	110.4	122.0	20 (1)	16.6	-	-
		0.0210	111.9	119.2	20 (1)	15.3	-	-
	T	0.0210	110.5	115.9	18	16.6	-	-
		0.0205	103.3	112.1	-	16.1	0.439	0.984
I	L	0.0220	109.3	119.6	18 (1)	16.3	-	-
		0.0220	113.3	117.0	20 (1)	15.4	-	-
	T	0.0200	109.5	113.5	18	17.1	-	-
		0.0200	100.3	108.9	-	14.8	0.457	0.896
J	L	0.0210	111.2	122.3	18 (1)	16.0	-	-
		0.0208	110.8	119.2	20 (1)	16.2	-	-
	T	0.0210	108.6	112.5	18	16.6	-	-
		0.0210	101.0	108.9	-	14.8	0.426	0.981
K	L	0.0220	107.1	118.2	18 (1)	15.9	-	-
		0.0220	108.9	117.4	20 (1)	16.6	-	-
	T	0.0204	112.9	118.4	16	16.8	-	-
		0.0200	103.2	112.2	-	15.5	0.421	0.645
L	L	0.0184	114.8	126.9	18 (1)	17.2	-	-
		0.0185	112.2	119.6	20 (1)	16.6	-	-
	T	0.0188	110.2	116.7	18	17.0	-	-
		0.0185	100.5	110.7	-	15.1	0.439	0.775
Q	L	0.0200	96.5	107.0	-	14.1	0.427	0.662
		0.0175	107.5	113.4	16	15.5	-	-
	T	0.0170	102.4	110.8	-	15.5	0.430	0.939
R	L	0.0190	97.2	107.7	-	14.1	0.424	0.620
		0.0160	110.9	119.3	17	15.6	-	-
	T	0.0160	104.4	110.6	15	16.3	-	-
		0.0160	105.5	114.3	-	15.7	0.413	0.836

L = Longitudinal.

T = Transverse.

(1) % Elongation in 1 in.

TABLE B-VI (Cont'd)

Sheet No.	Direction	Thickness (in.)	0.2% Yield strength (ksi)	Ultimate strength (ksi)	Elongation in 2 in. (%)	Elastic modulus psi x 10^{-6}	Elastic Poisson's Ratio	Plastic Poisson's Ratio
S	L	0.0190	100.7	111.0	-	14.9	0.425	0.658
		0.0165	111.6	117.6	16	16.2	-	-
	T	0.0165	107.9	113.4	16	16.3	-	-
		0.0170	100.0	109.4	-	14.6	0.388	0.654
T	L	0.0200	100.0	108.9	-	14.3	0.422	0.650
		0.0178	110.0	116.7	17	16.1	-	-
	T	0.0170	107.0	112.6	18	16.6	-	-
		0.0175	100.9	110.9	-	14.9	0.425	0.845
U	L	0.0210	103.0	114.5	-	15.1	0.408	0.765
		0.0200	113.2	119.9	14	15.8	-	-
	T	0.0190	113.7	118.1	15	16.8	-	-
		0.0200	106.6	115.9	-	15.2	0.408	0.653
V	L	0.0230	104.7	115.9	-	14.9	0.409	0.758
		0.0220	113.5	120.4	16	16.2	-	-
	T	0.0212	113.2	119.6	15	17.6	-	-
		0.0220	105.5	116.4	-	15.7	0.401	0.861
X	L	0.0230	100.4	110.6	-	14.7	0.430	0.790
		0.0215	109.8	116.7	15	16.1	-	-
	T	0.0215	118.8	115.7	17	17.0	-	-
		0.0220	104.8	114.3	-	15.3	0.418	0.810
Z	L	0.0205	100.0	111.2	-	14.2	0.418	0.722
		0.0195	110.0	117.8	17	16.0	-	-
	T	0.0180	113.5	117.7	16	17.0	-	-
		0.0190	102.8	111.6	-	15.1	0.412	0.893
AI	L	0.0210	104.3	115.2	-	14.6	0.421	0.671
		0.0202	112.1	119.9	17	15.5	-	-
	T	0.0190	113.8	119.5	18	16.7	-	-
		0.0200	105.2	114.0	-	15.1	0.409	0.635
BI	L	0.0200	103.4	114.2	-	14.7	0.391	0.663
		0.0190	110.5	119.5	15	15.8	-	-
	T	0.0184	112.7	118.9	18	16.7	-	-
		0.0190	106.9	117.3	-	15.7	0.382	0.616
CI	L	0.0210	103.5	115.0	-	14.7	0.428	0.709
		0.0200	110.0	119.7	14	15.5	-	-
	T	0.0200	101.4	111.7	-	14.8	0.406	0.803
DI	L	0.0200	105.7	116.4	-	15.2	0.391	0.734
		0.0190	113.2	121.6	13	16.0	-	-
	T	0.0184	110.9	117.7	16	15.9	-	-
		0.0190	105.2	115.3	-	16.0	0.415	0.831

L = Longitudinal.

T = Transverse.

(1) % Elongation in 1 in.

TABLE B-VII

RESULTS OF MECHANICAL PROPERTY TESTS PERFORMED
ON Ti-5Al-2.5Sn ELI 0.020-IN. SHEET at -320° F

Sheet No.	Direction	Thickness (in.)	0.2% Yield strength (ksi)	Ultimate strength (ksi)	Elongation in 2 in. (%)	Elastic modulus psi x 10^{-6}	Elastic Poisson's Ratio
S	L	0.0165	- (1)	193.3	16	20.4	0.346
T	L	0.0180	- (1)	188.3	11	18.5	0.350
X	L	0.0220	175.3	190.9	12	18.7	0.387
Z	L	0.0200	167.6	186.0	10	18.5	0.374
BI	L	0.0195	170.6	189.1	14	18.3	0.365

(1) Stress-strain curve erratic near yield.

TABLE B-VIII

RESULTS OF MECHANICAL PROPERTY TESTS PERFORMED ON Ti-5Al-2.5Sn ELI 0.020-IN. SHEET AT -423° F

Sheet No.	Direction	Thickness (in.)	0.2% Yield strength (ksi)	Ultimate strength (ksi)	Elongation in 2 in. (%)	Elastic modulus psi x 10^{-6}	Elastic Poisson's Ratio
R	L	0.0170	192.6	197.7	(1)	19.8	0.326
U	L	0.0205	- (2)	206.3	(1)	20.4	-
V	L	0.0220	- (2)	213.6	(1)	21.1	-
AI	L	0.0210	- (2)	204.8	(1)	19.3	0.342
CI	L	0.0200	194.0	206.0	(1)	22.5	0.316

(1) Broke outside gauge marks.

(2) Stress-strain curve erratic near yield

Appendix C

UNIAXIAL CRACK GROWTH CURVES

All uniaxial cyclic test results are presented in this appendix, Figures C-1 through C-12. Included are crack growth curves for 2219-T87 and Ti-5Al-2.5Sn ELI at 70, -320, and -423° F. The curves are plotted as explained in Section 5.2.1.2 as the fourth root of cycles remaining to failure, $N_R^{1/4}$, versus crack length, ℓ. Tests of one material performed at a given temperature and stress ratio are plotted in a single figure.

Several data points from each test are plotted in the figures. A dashed straight line is drawn through the test points and represents the common growth curve for a particular stress schedule. The coordinates of the common point of intersection were selected by optimizing the location of a straight edge intersecting the abscissa at ℓ_c and passing through most of the data points. The value of ℓ_c used for each dashed straight line is that calculated by eq. (5-1), using the average K_c and the nominal maximum stress for the test in question.

For some curves, the experimental and theoretical ℓ_c values are not equal. This difference is due to the fact that the theoretical curves (dashed straight lines) are based on an unchanging maximum cyclic stress. In some tests, fracture occurred on the final cycle at a stress lower than the maximum cyclic stress experienced throughout the test. The experimental critical crack length corresponds with the actual stress at fracture then, whereas the theoretical critical crack length corresponds with the maximum cyclic stress.

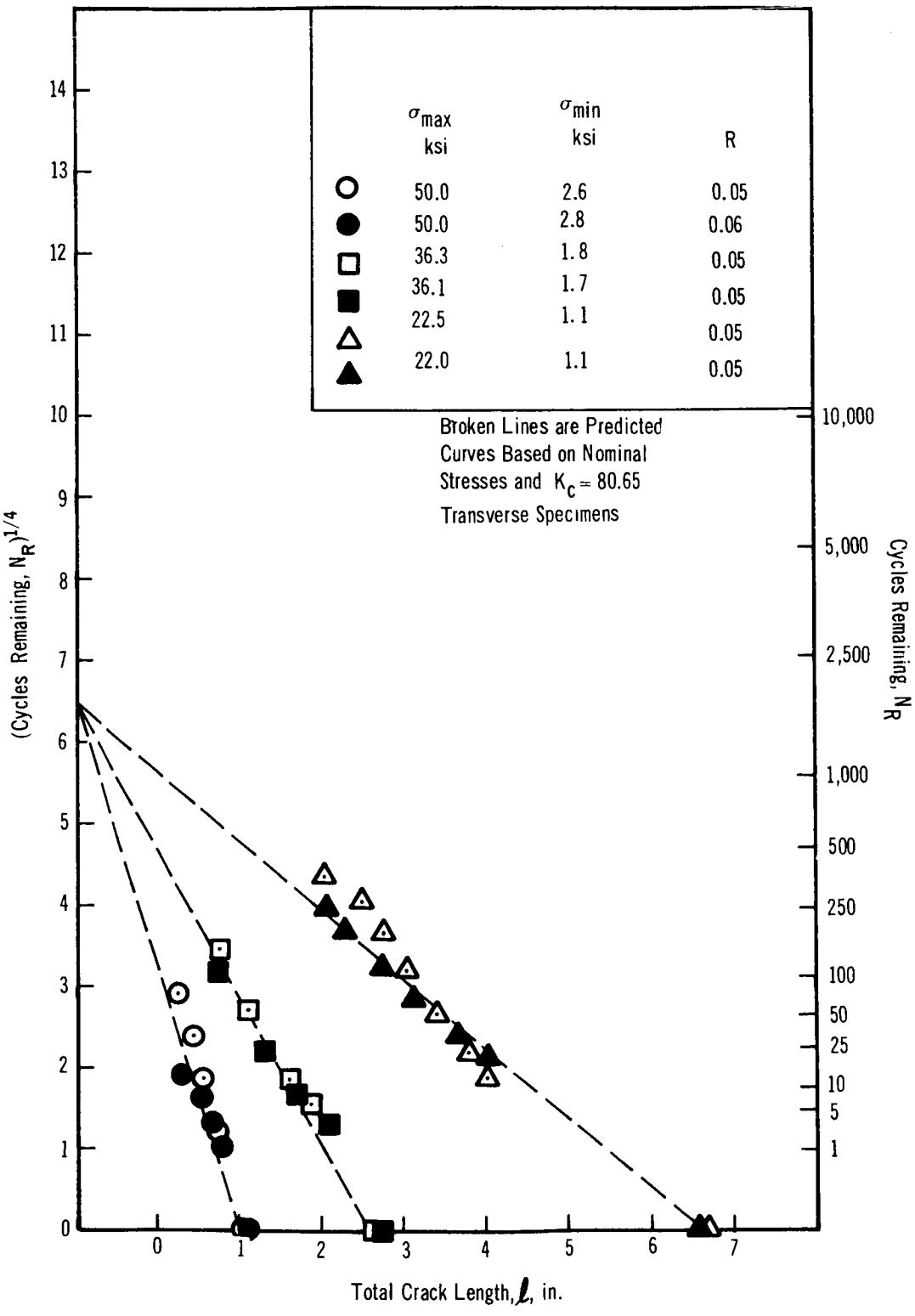

Figure C-1. Uniaxial Cyclic Test Results for 2219-T87 at 70°F and 0.05 Stress Ratio

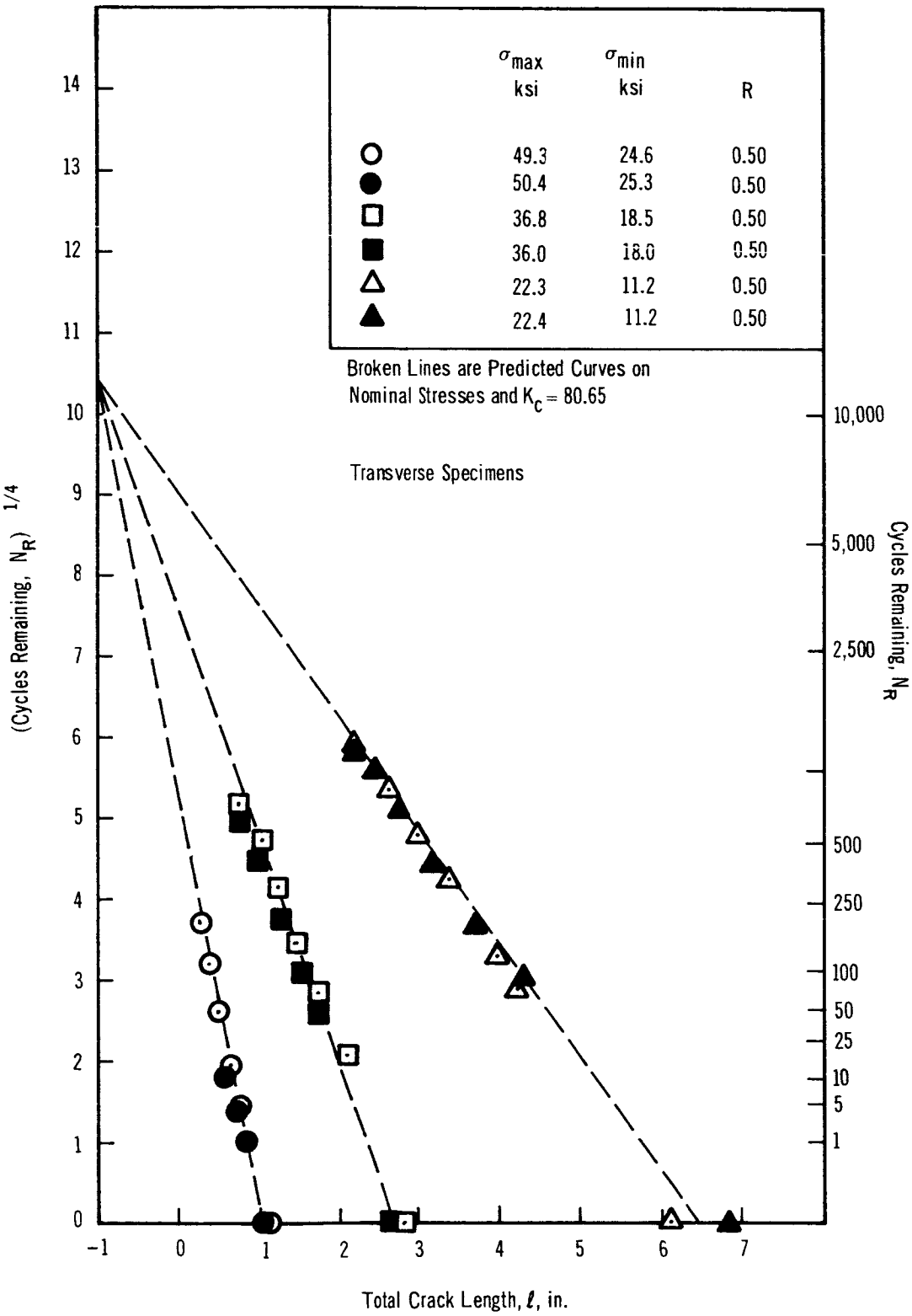

Figure C-2. Uniaxial Cyclic Test Results for 2219-T87 at 70°F and 0.50 Stress Ratio

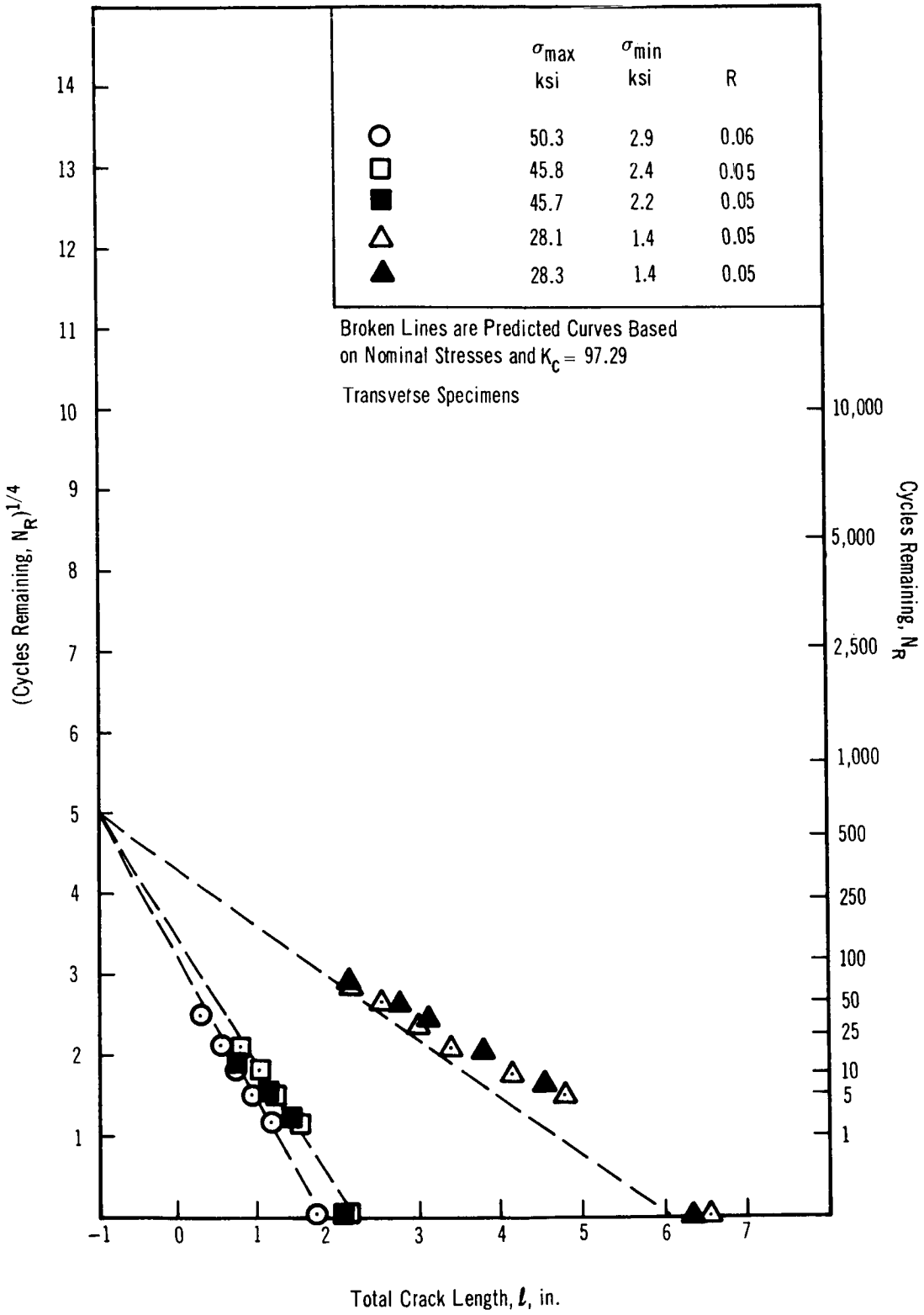

Figure C-3. Uniaxial Cyclic Test Results for 2219-T87 at –320°F and 0.05 Stress Ratio

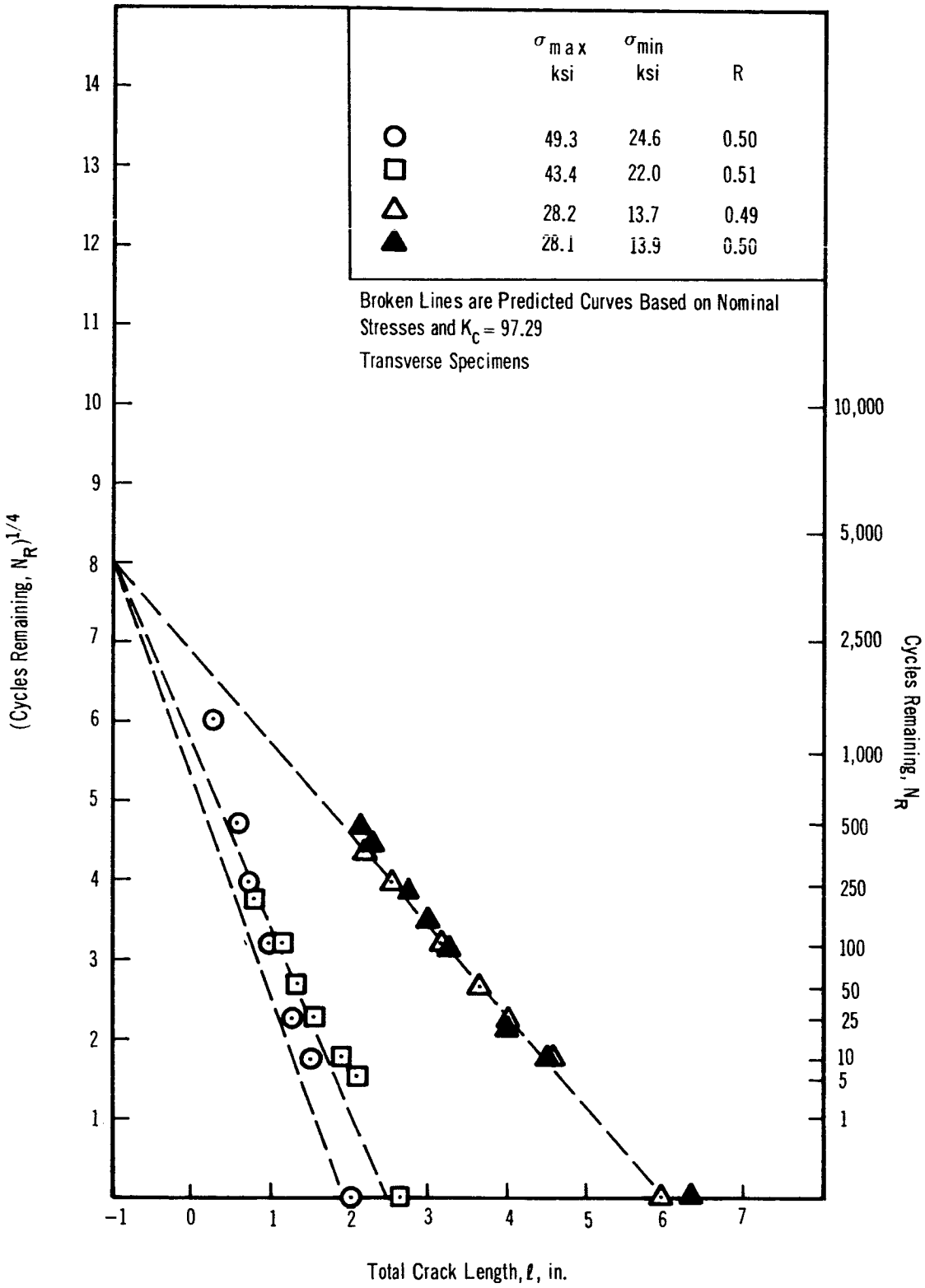

Figure C-4. Uniaxial Cyclic Test Results for 2219-T87 at –320°F and 0.50 Stress Ratio

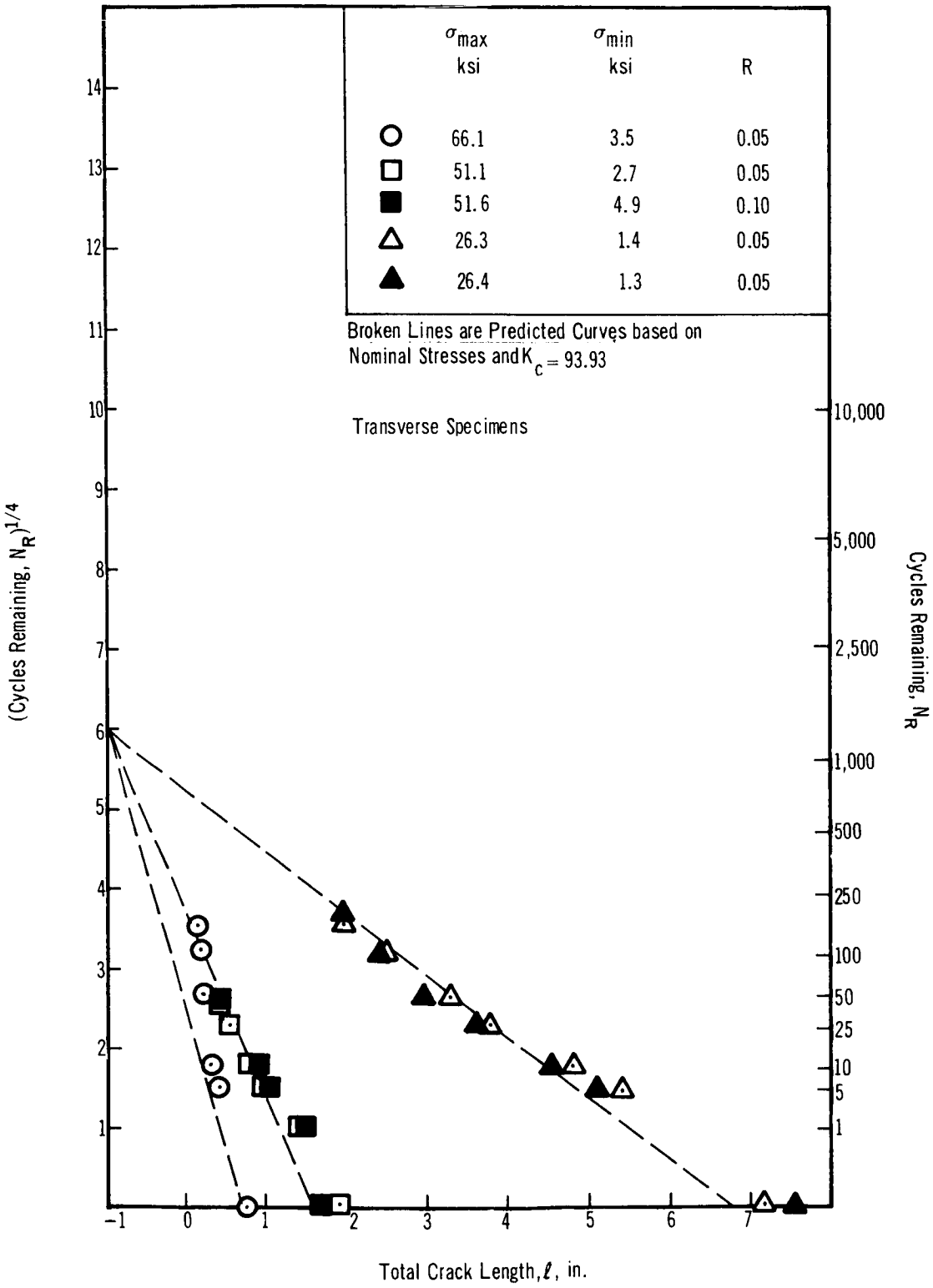

Figure C-5. Uniaxial Cyclic Test Results for 2219-T87 at –423°F and 0.05 Stress Ratio

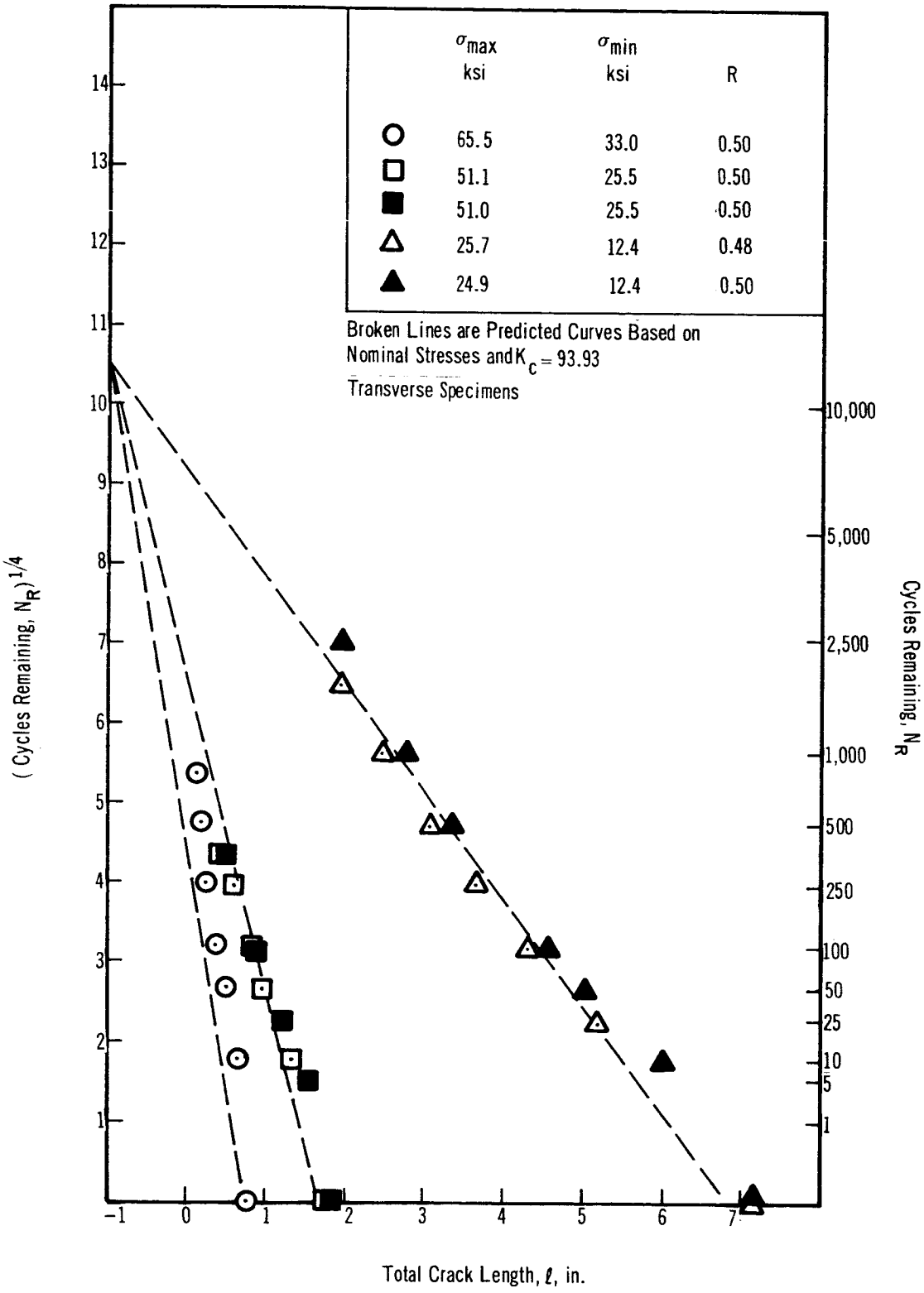

Figure C-6. Uniaxial Cyclic Test Results for 2219-T87 at –423°F and 0.50 Stress Ratio

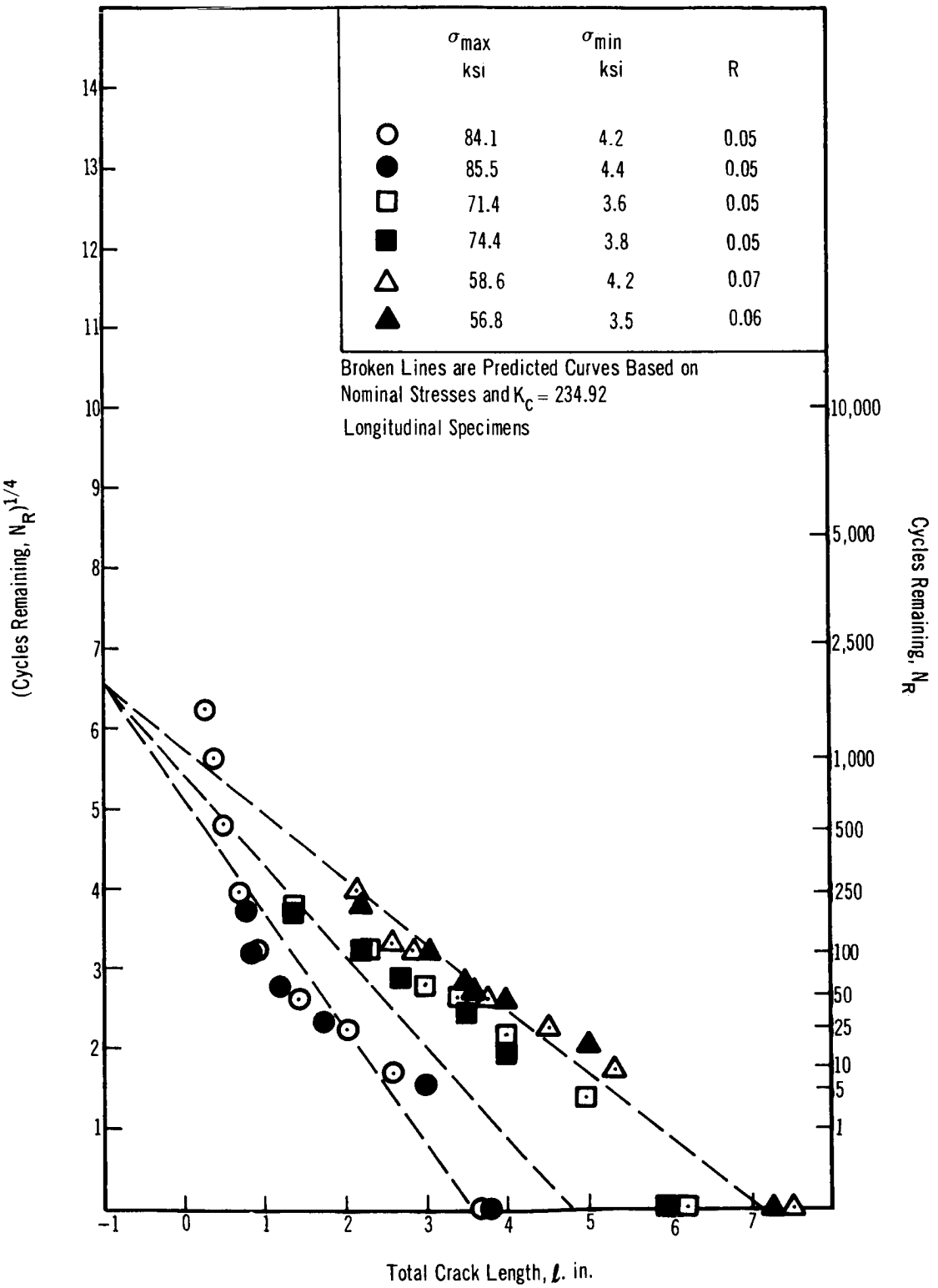

Figure C-7. Uniaxial Cyclic Test Results for Ti-5Al-2.5Sn ELI at 70°F and 0.05 Stress Ratio

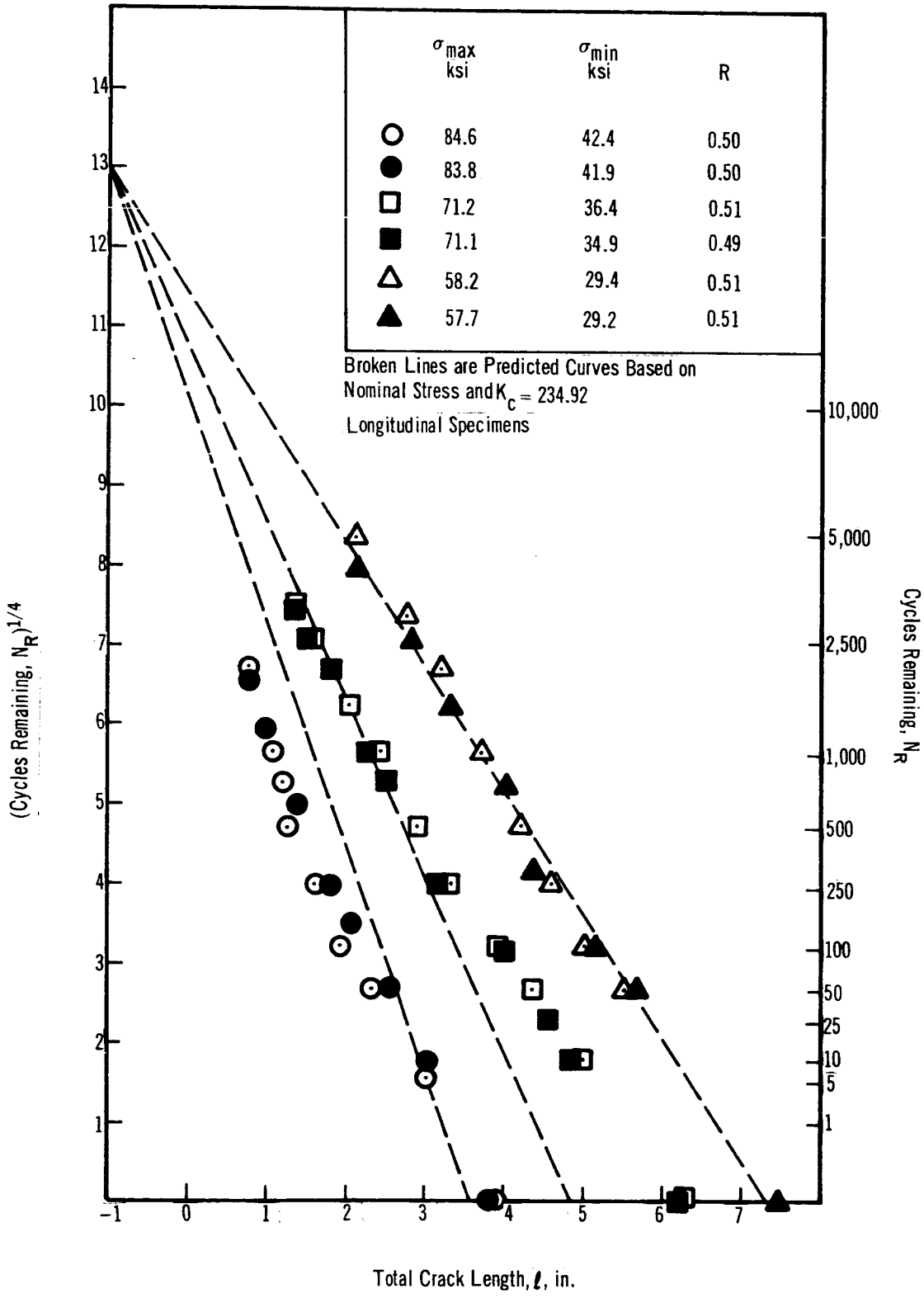

Figure C-8. Uniaxial Cyclic Test Results for Ti-5Al-2.5Sn E-LI at 70°F and 0.50 Stress Ratio

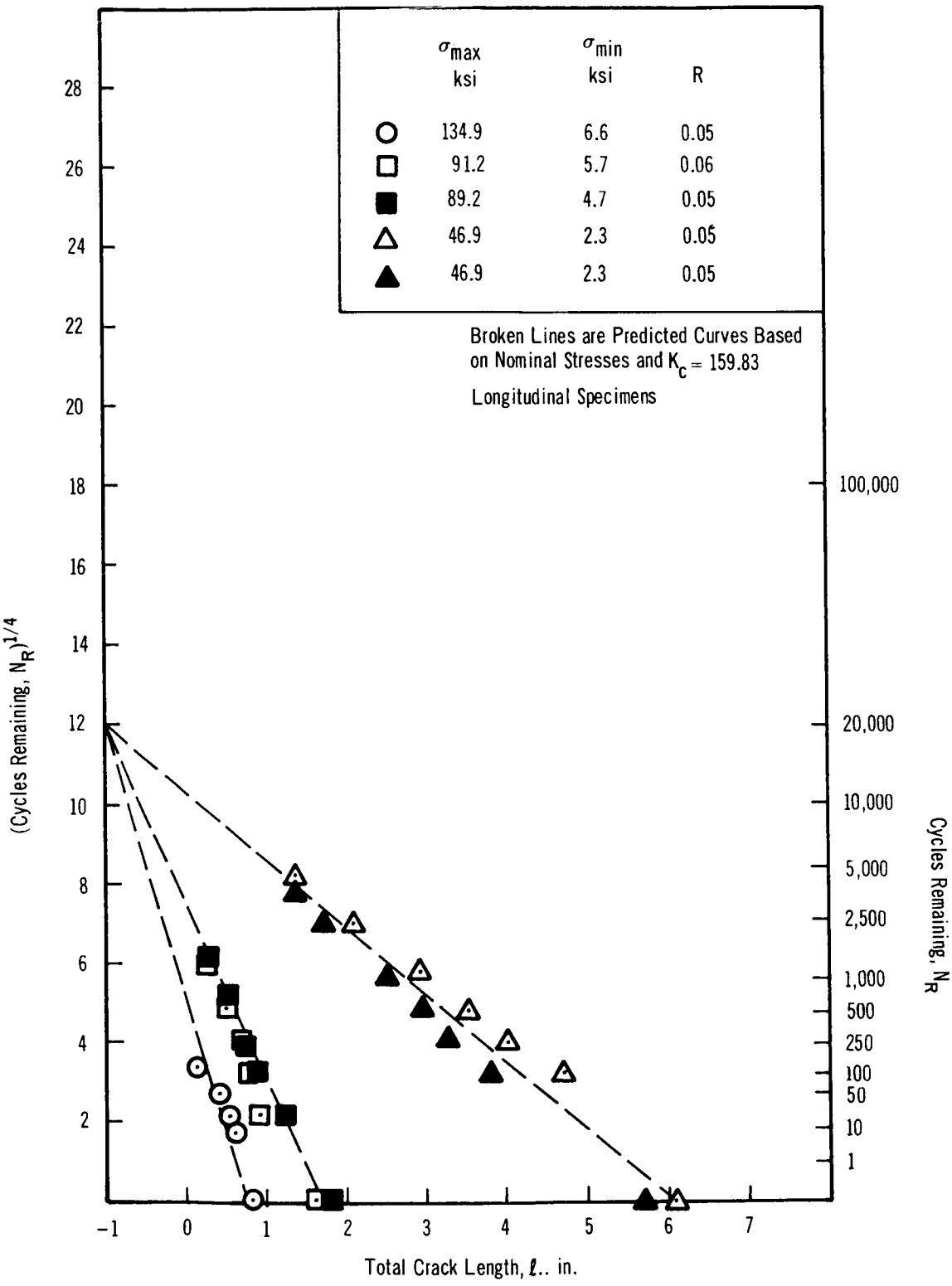

Figure C-9. Uniaxial Cyclic Test Results for Ti-5Al-2.5Sn ELI at −320°F and 0.05 Stress Ratio

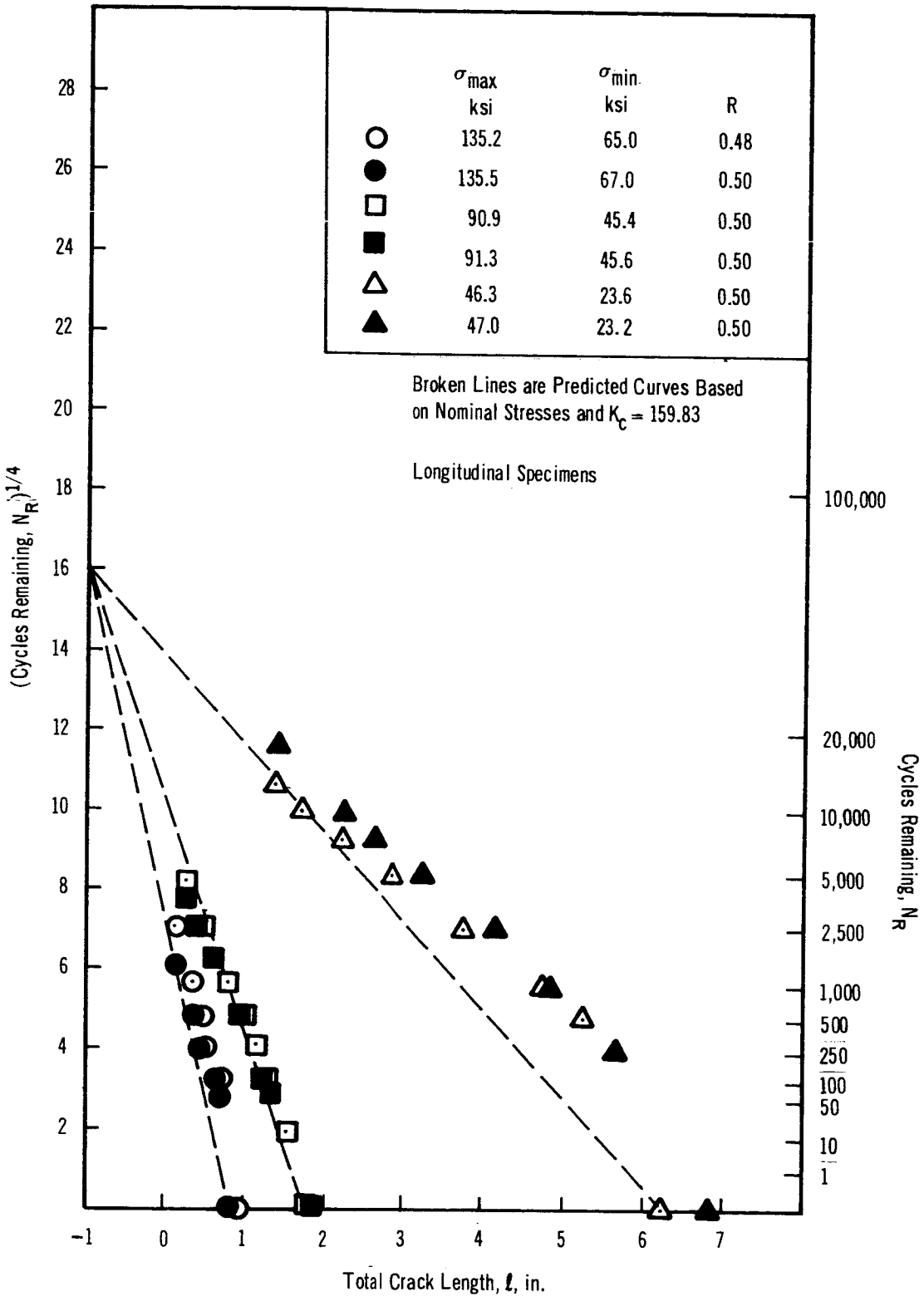

Figure C-10. Uniaxial Cyclic Test Results for Ti-5Al-2.5Sn ELI at −320°F and 0.50 Stress Ratio

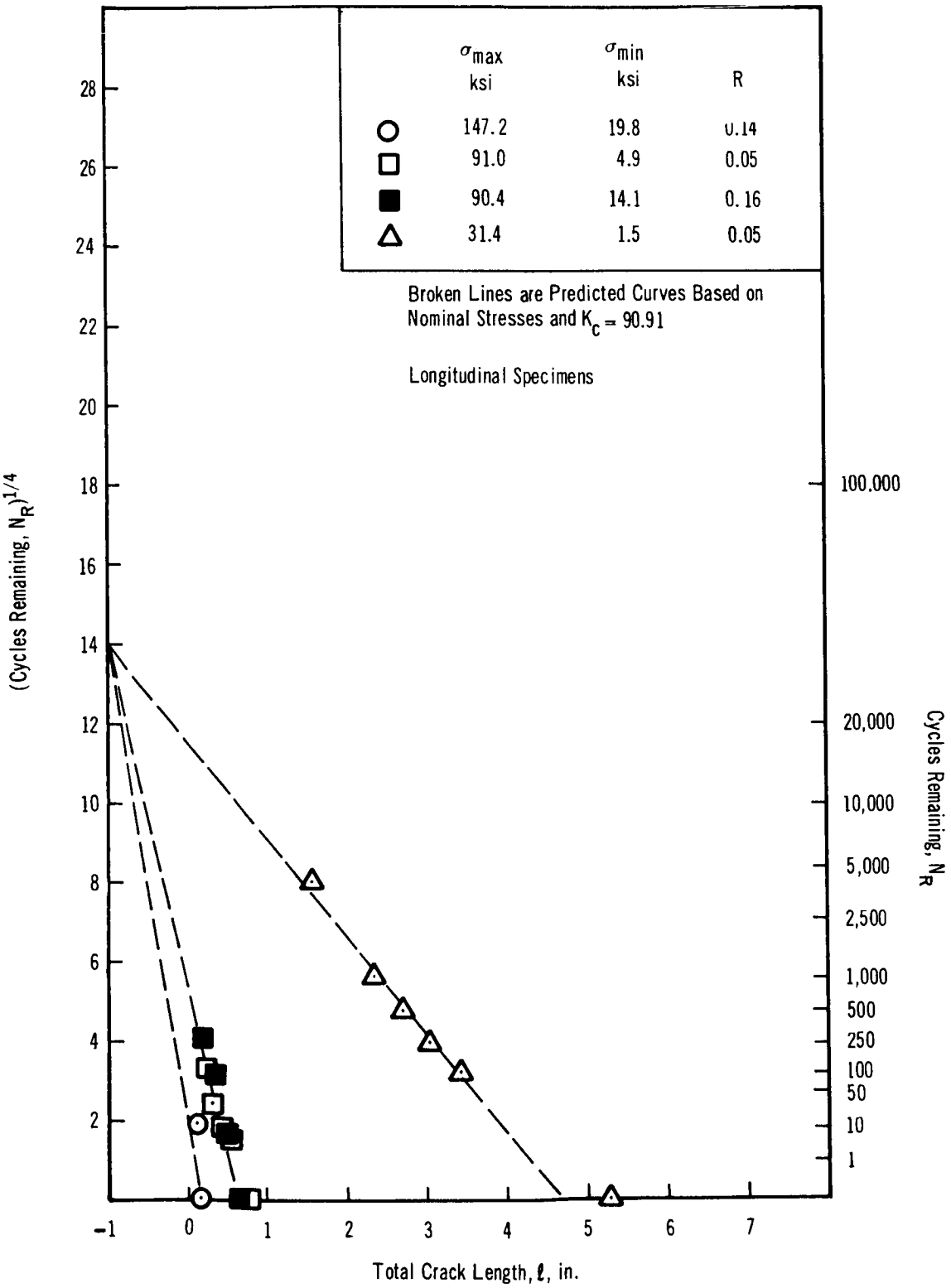

Figure C-11. Uniaxial Cyclic Test Results for Ti-5Al-2.5Sn ELI at –423°F and 0.05 Stress Ratio

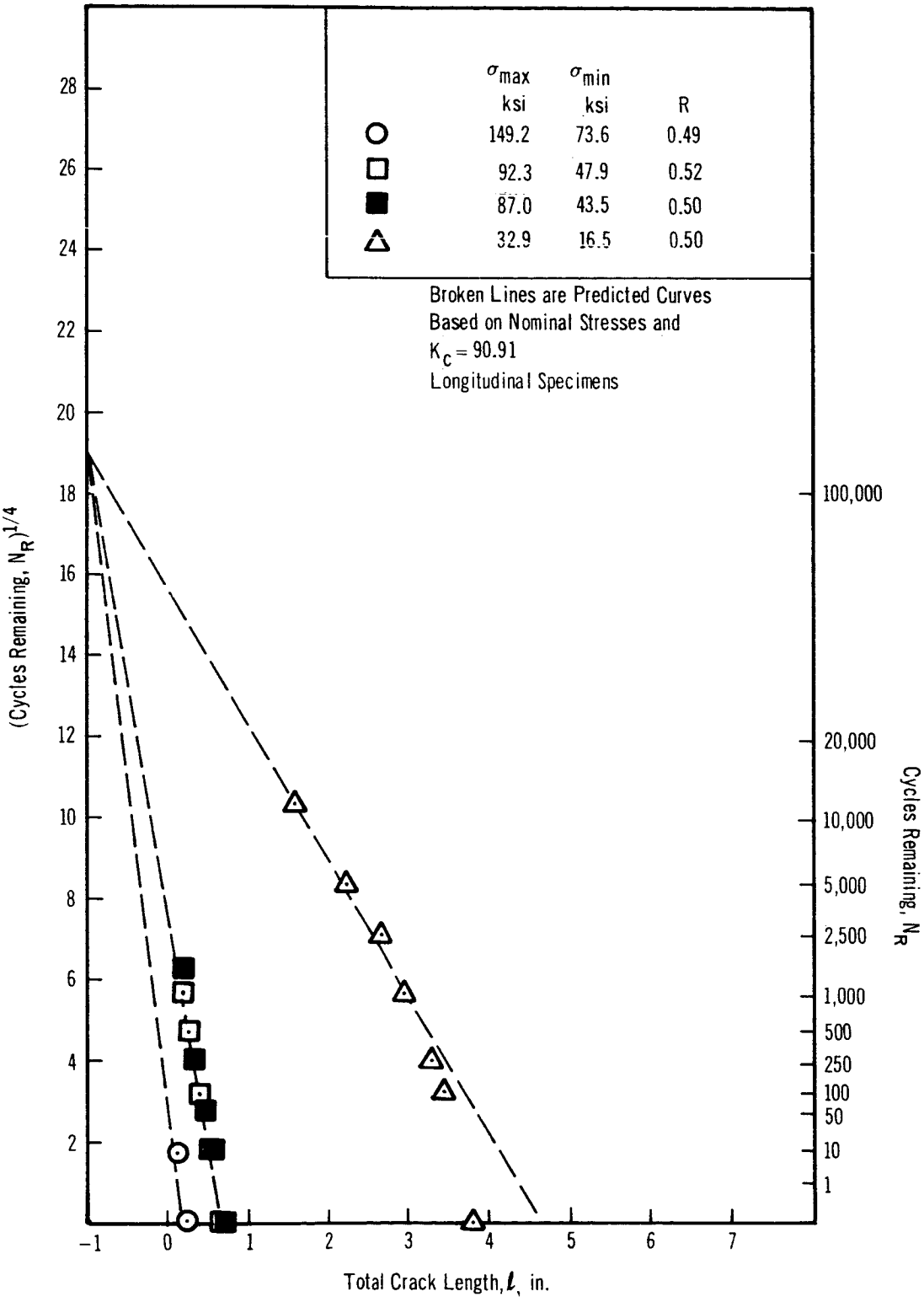

Figure C-12. Uniaxial Cyclic Test Results for Ti-5Al-2.5Sn ELI at −423°F and 0.50 Stress Ratio

Appendix D

BIAXIAL CRACK GROWTH CURVES

All biaxial cyclic test results are presented in this appendix. The data plots are similar to those presented in Appendix C for uniaxial test results and as explained in Section 5.2.1.2.

The curves are plotted as the fourth root of cycles remaining, $N_R^{1/4}$, versus crack length, ℓ. For clarity, the scales used for the biaxial plots are expanded. The expanded scales do not permit extrapolating the theoretical curves to the point of common intersection. However, the F coordinate is given in each figure. Figures D-1 through D-11 are presented in this Appendix.

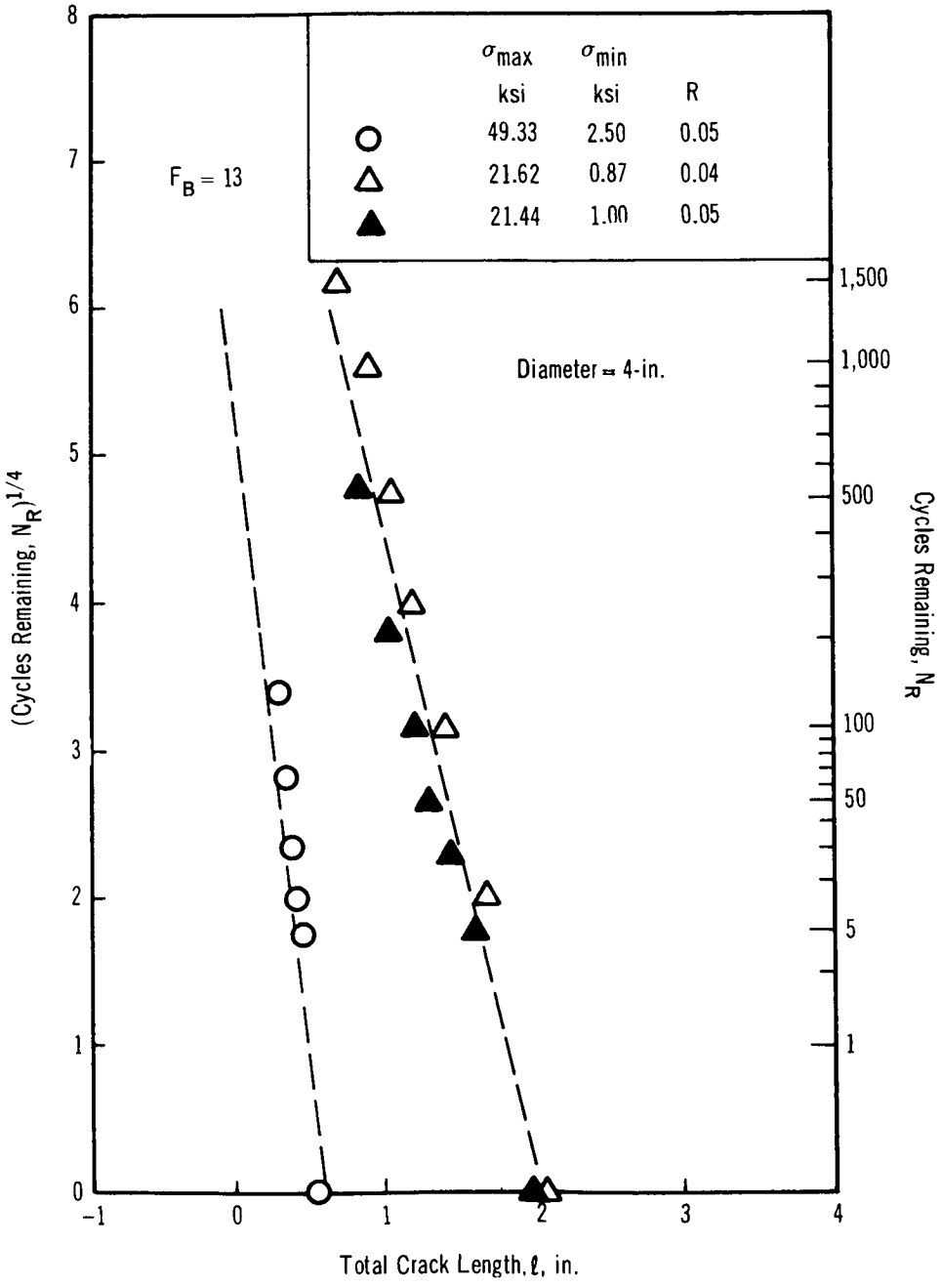

Figure D-1. Biaxial Cyclic Test Results for 10-in. Diam Cylinders of 2219-T87 at 70°F and 0.05 Stress Ratio

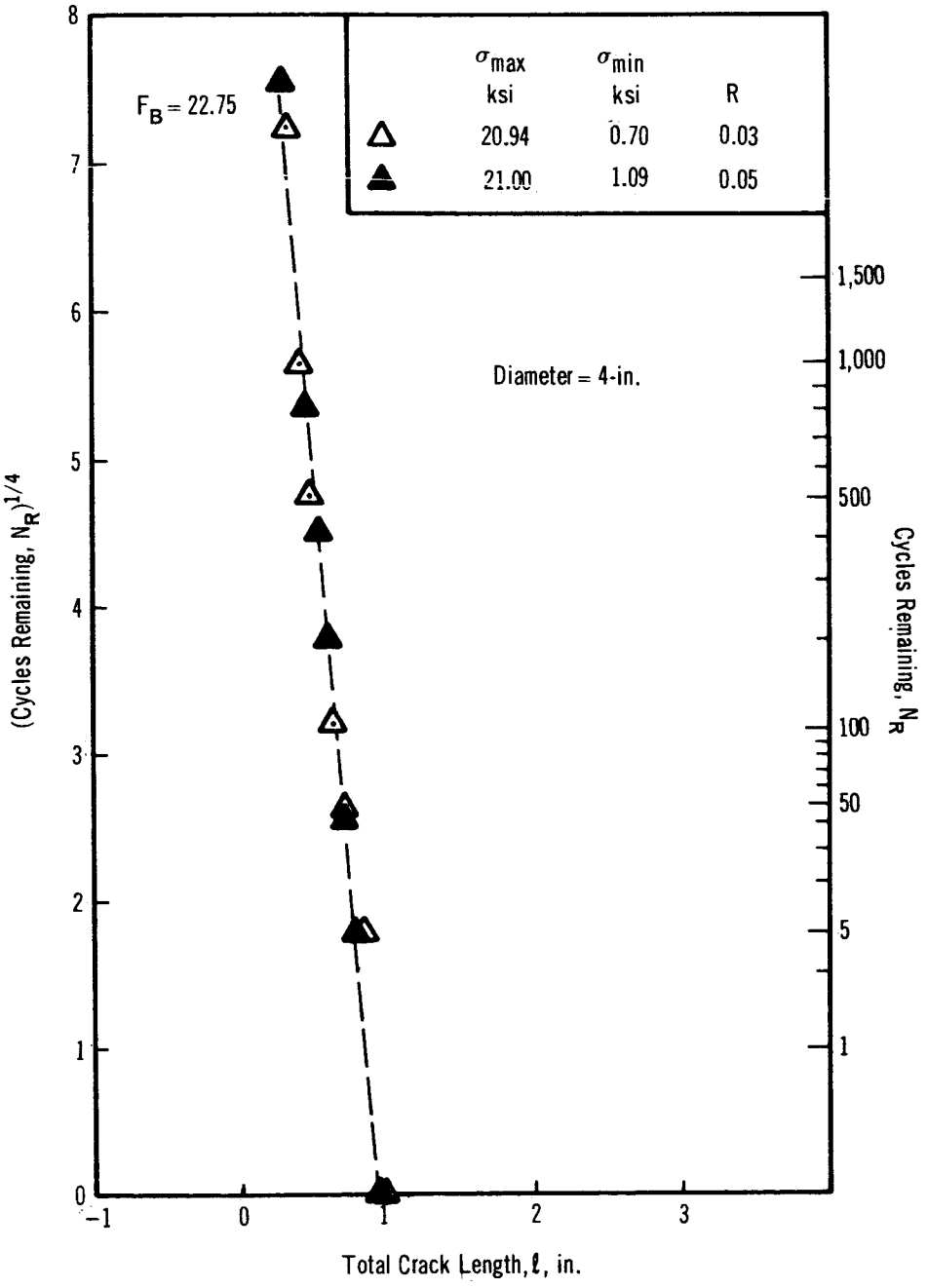

Figure D-2. Biaxial Cyclic Test Results for 4-in. Diam Cylinders of 2219-T87 at 70°F and 0.05 Stress Ratio

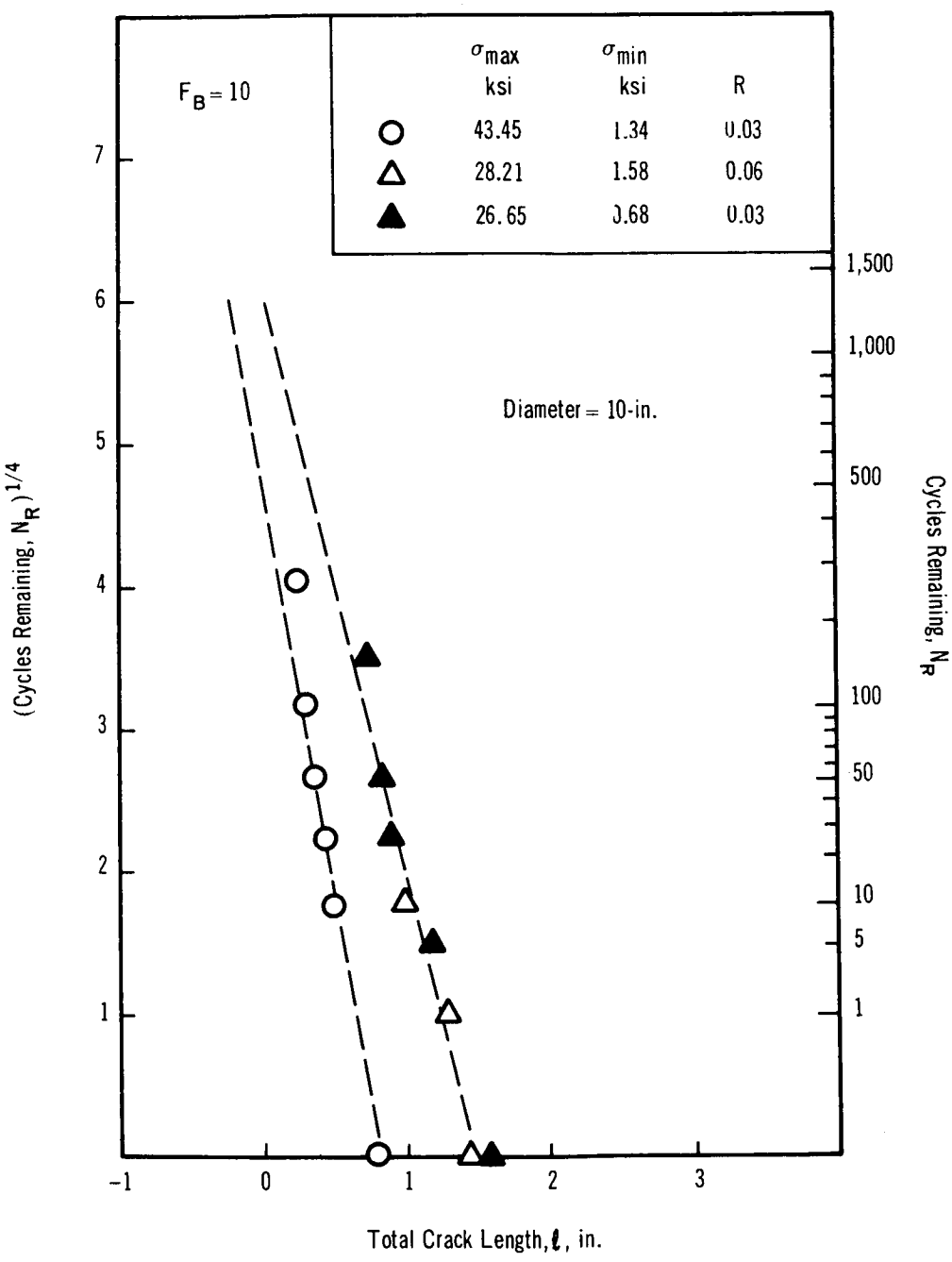

Figure D-3. Biaxial Cyclic Test Results for 2219-T87 at −320°F and 0.05 Stress Ratio

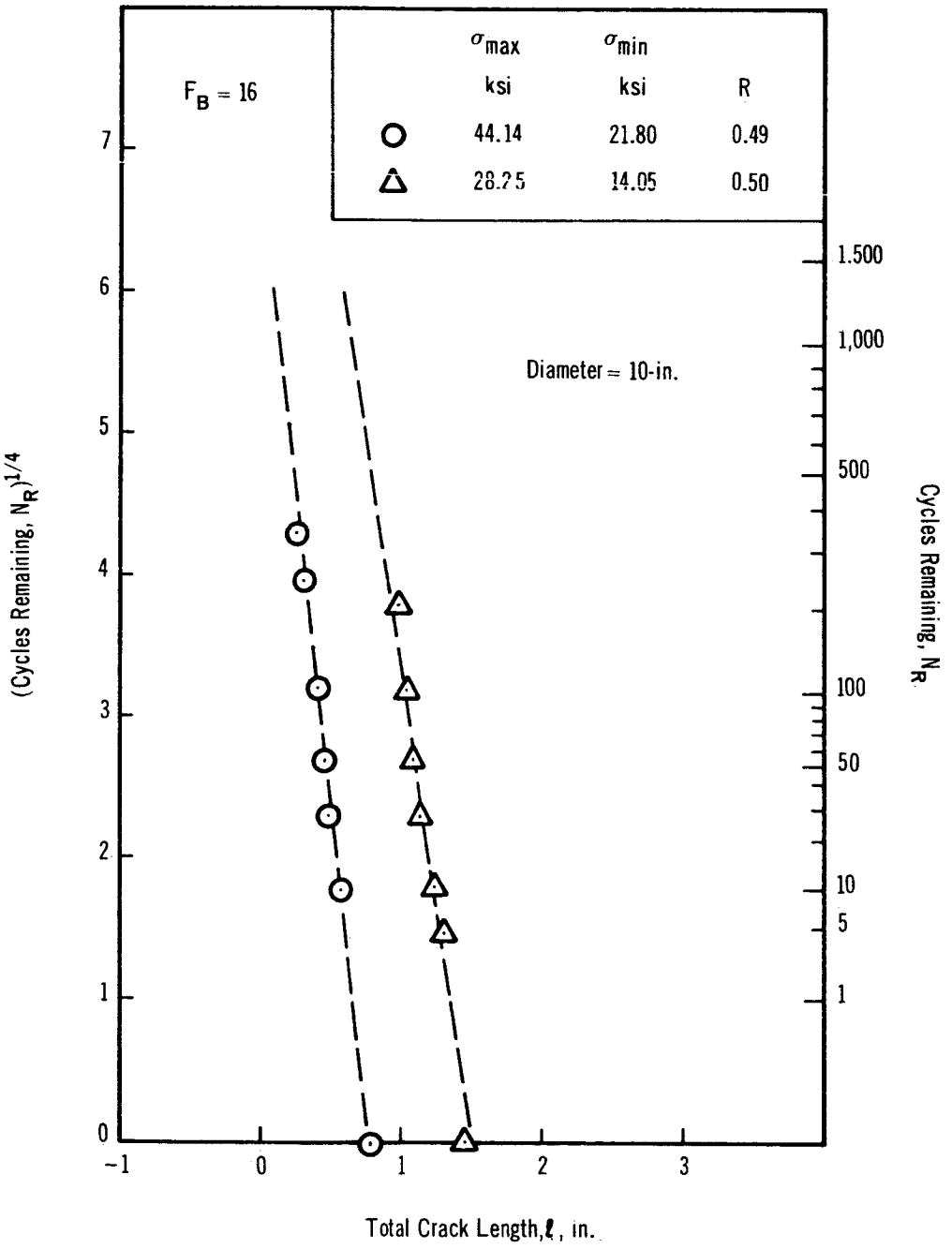

Figure D-4. Biaxial Cyclic Test Results for 2219-T87 at –320°F and 0.50 Stress Ratio

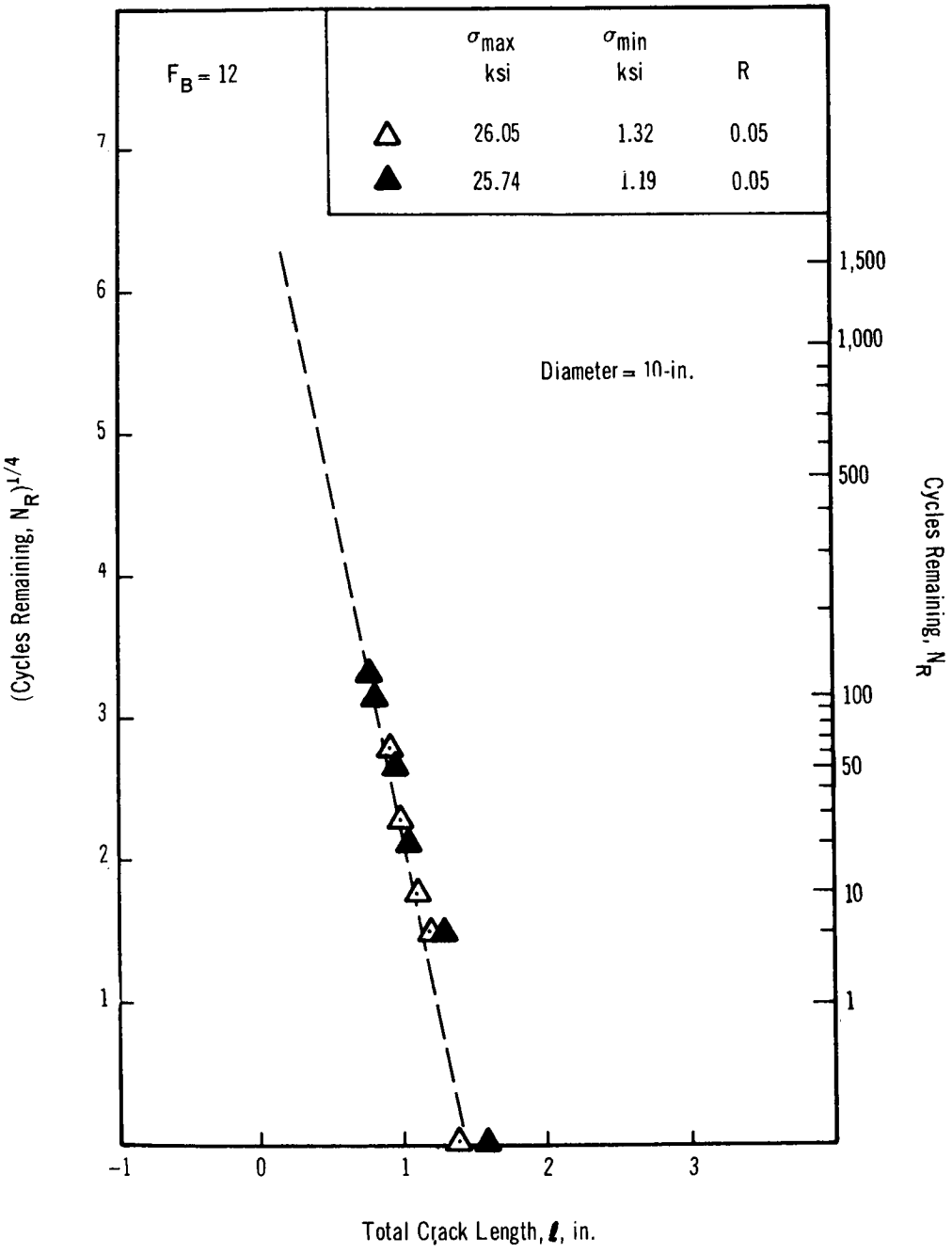

Figure D-5. Biaxial Cyclic Test Results for 2219-T87 at −423°F and 0.05 Stress Ratio

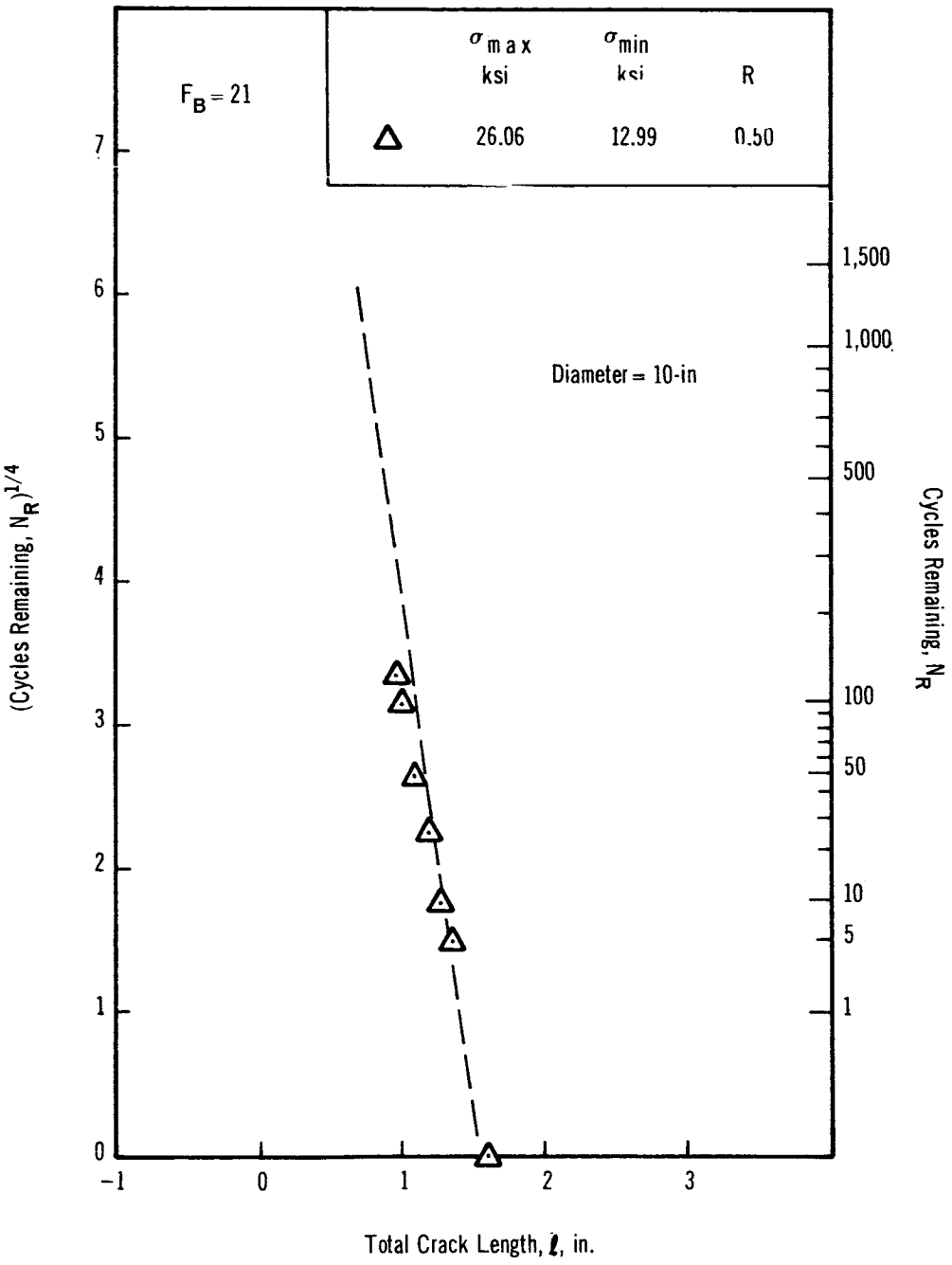

Figure D-6. Biaxial Cyclic Test Results for 2219-T87 at −423°F and 0.50 Stress Ratio

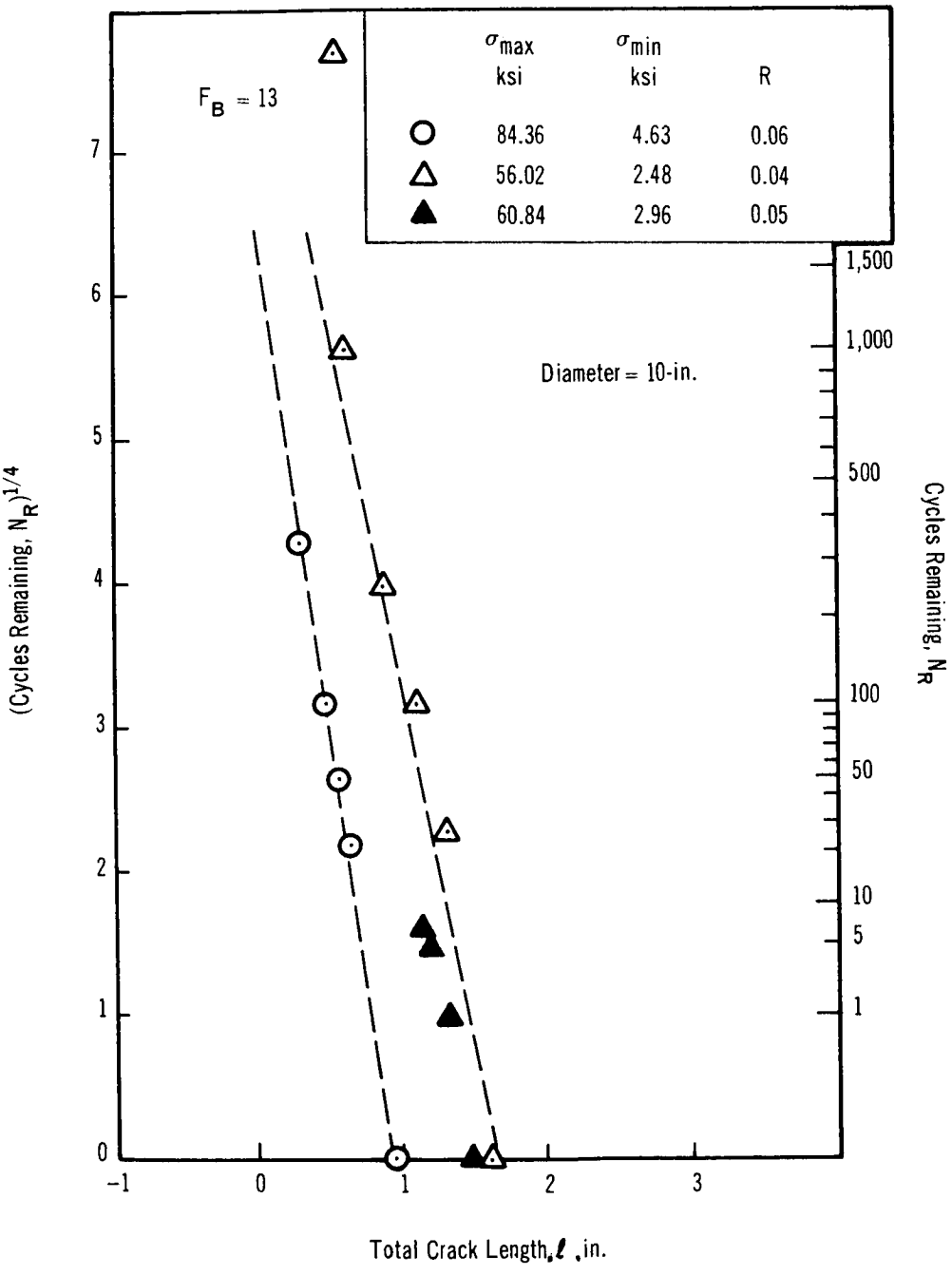

Figure D-7. Biaxial Cyclic Test Results for Ti-5Al-2.5Sn ELI at 70°F and 0.05 Stress Ratio

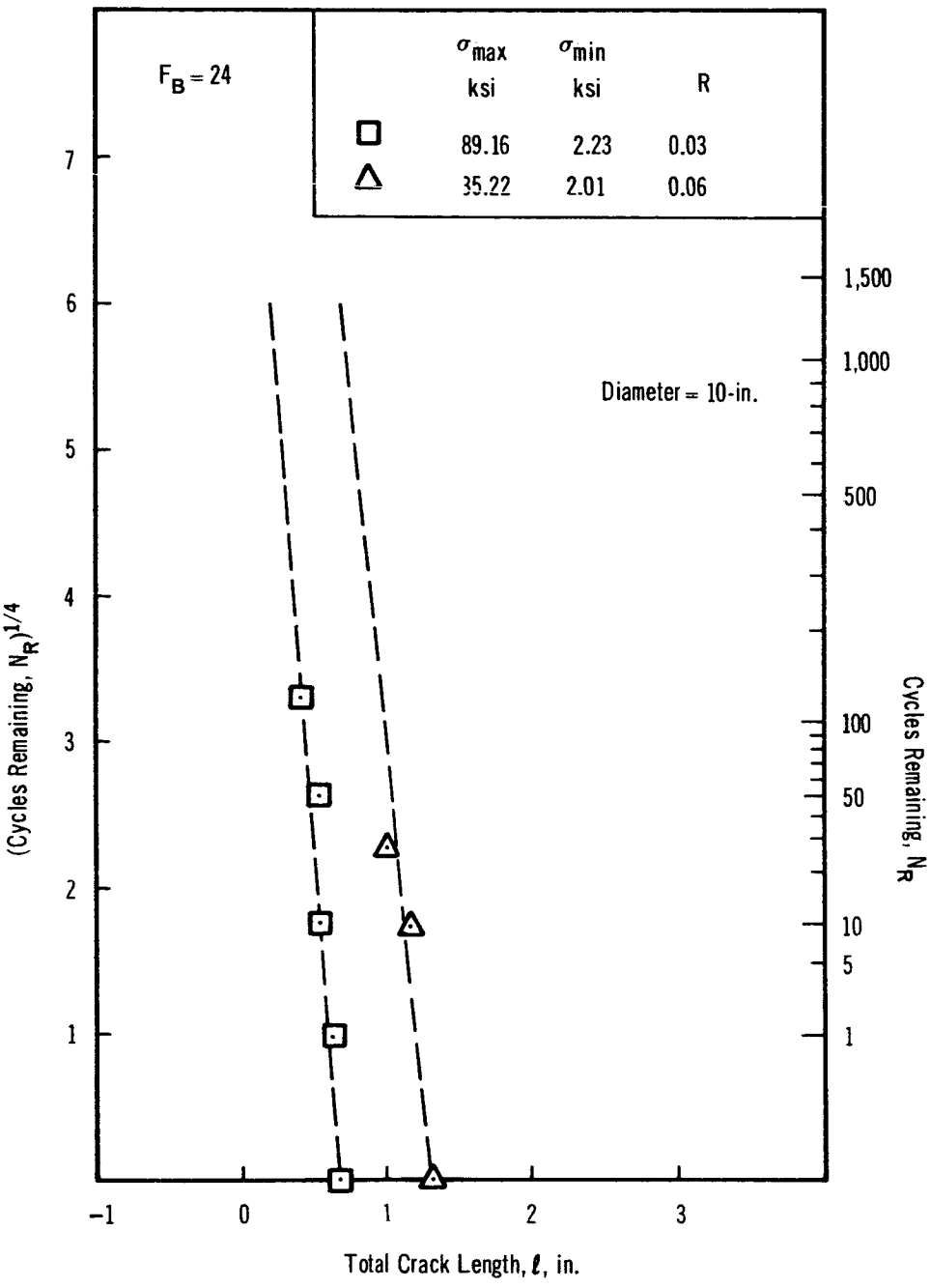

Figure D-8. Biaxial Cyclic Test Results for Ti-5Al-2.5Sn ELI at −320°F and 0.05 Stress Ratio

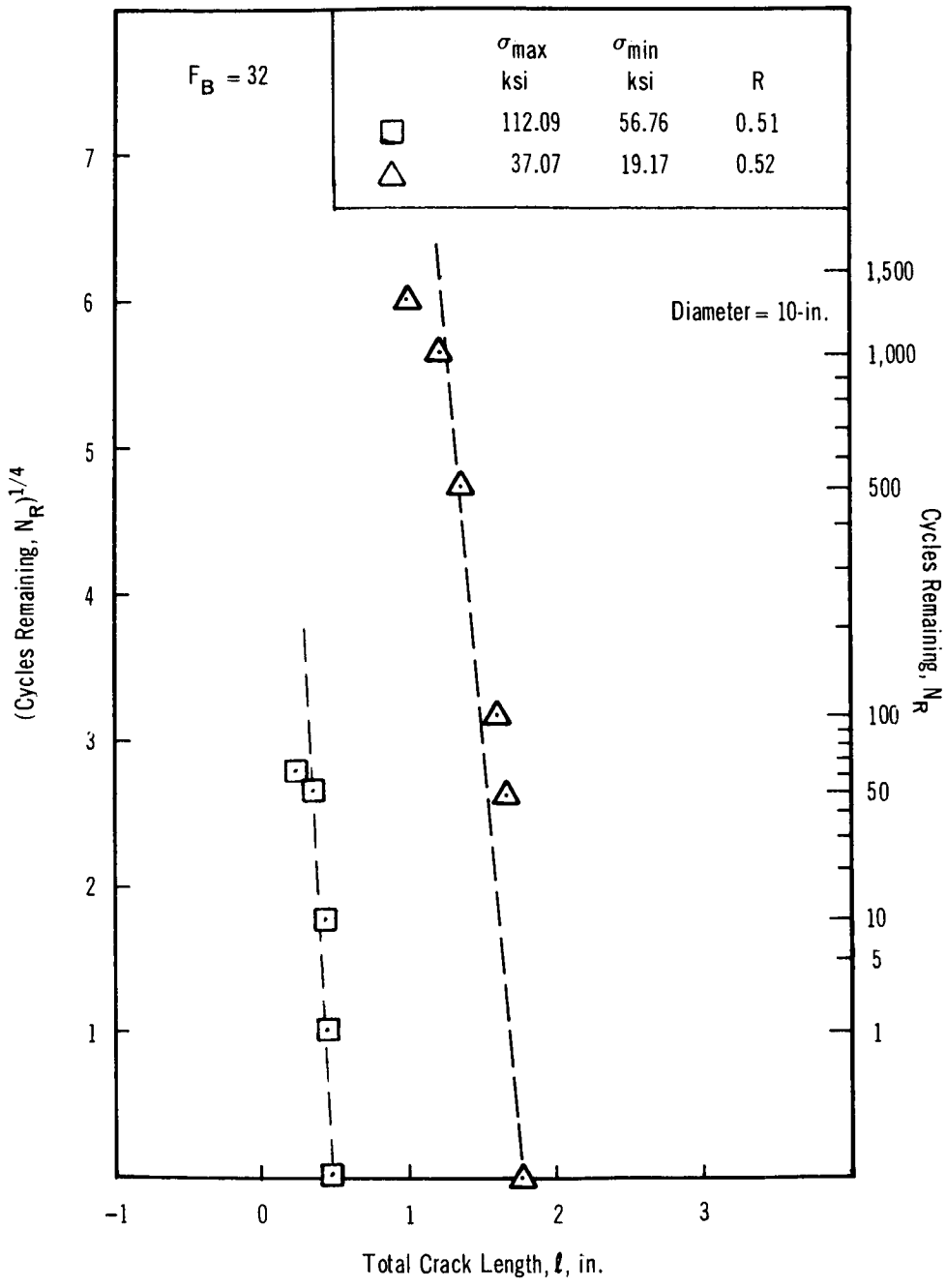

Figure D-9. Biaxial Cyclic Test Results for Ti-5Al-2.5Sn ELI at −320°F and 0.50 Stress Ratio

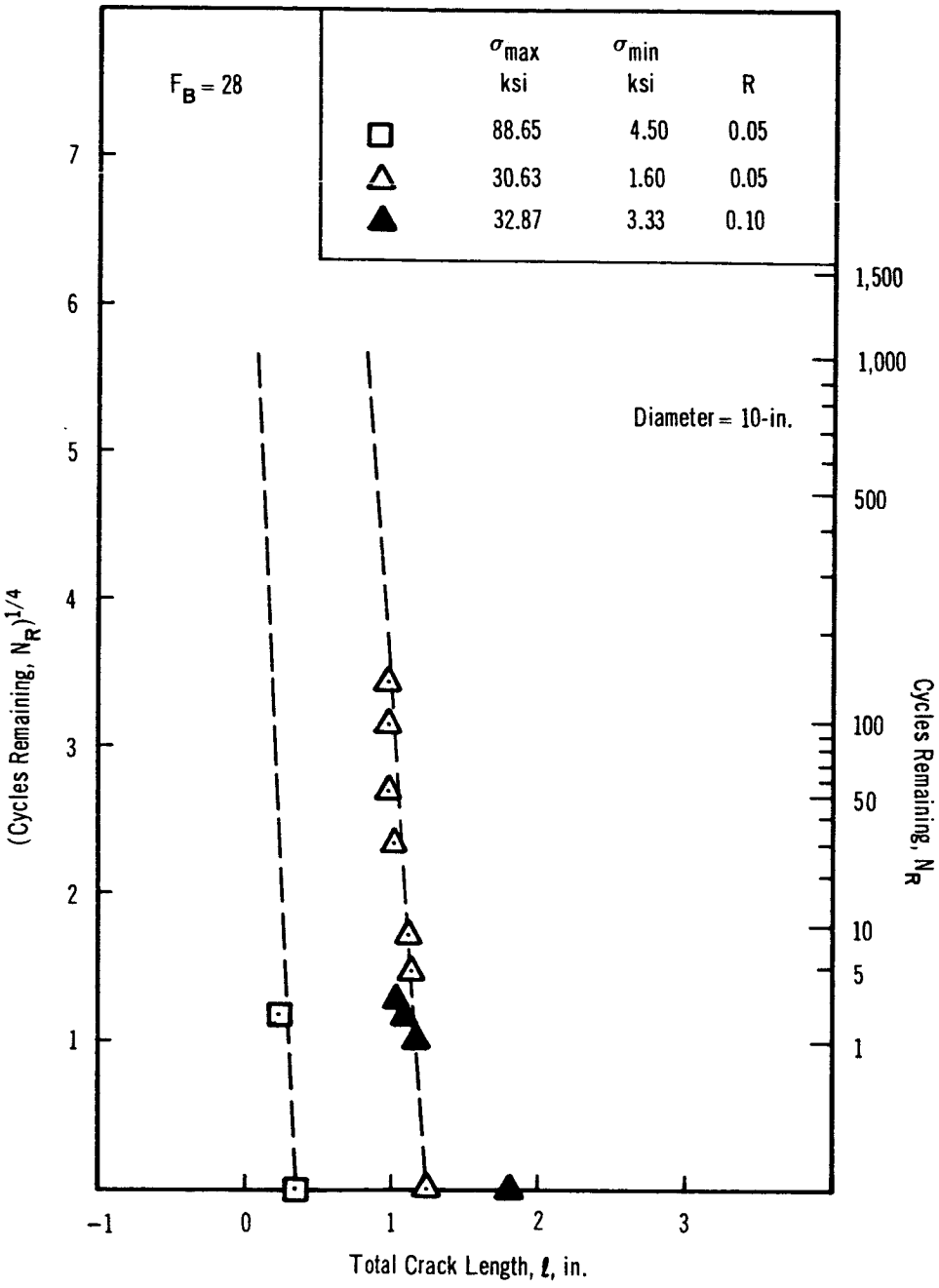

Figure D-10. Biaxial Cyclic Test Results for Ti-5Al-2.5Sn ELI at −423°F and 0.05 Stress Ratio

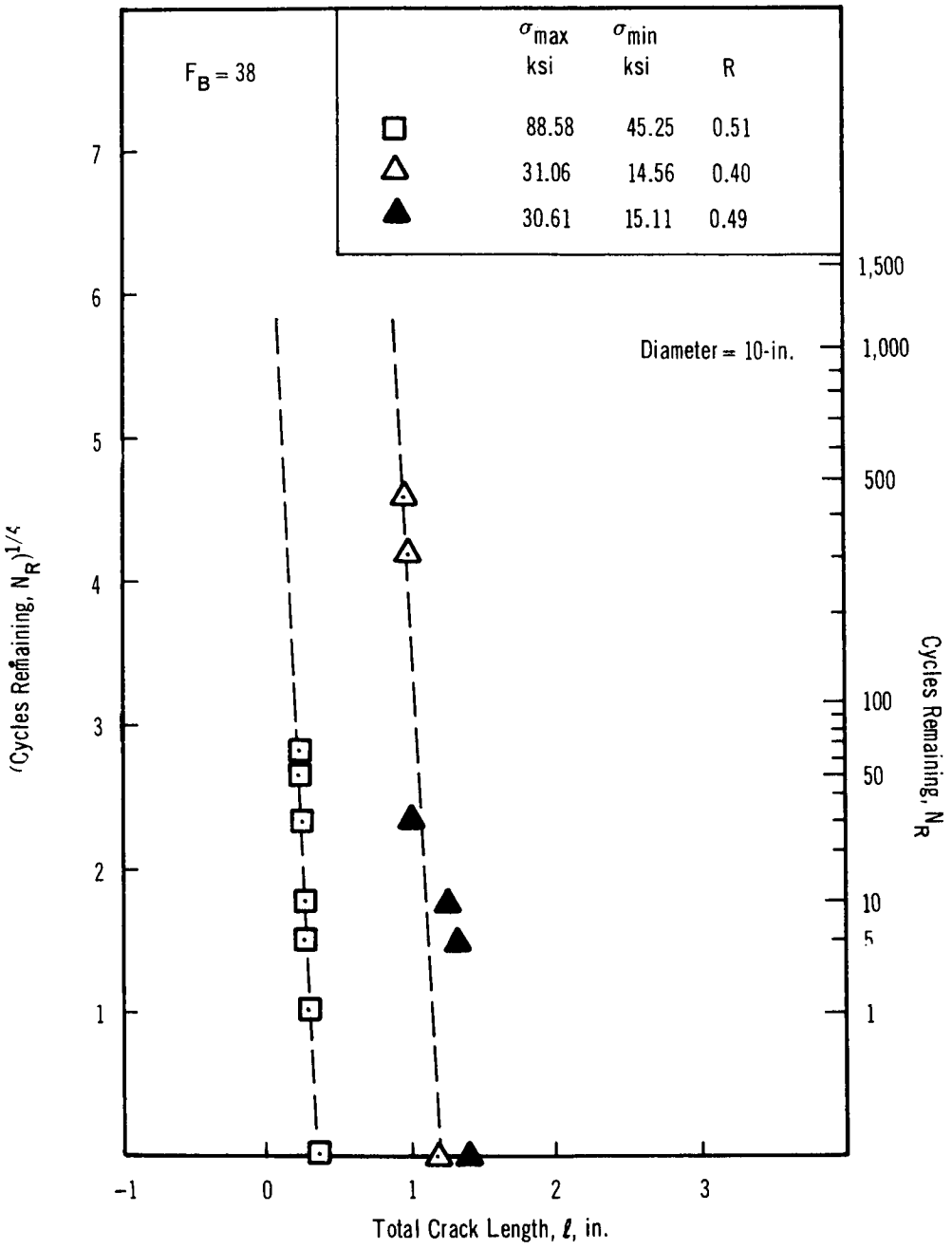

Figure D-11. Biaxial Cyclic Test Results for Ti-5Al-2Sn ELI at −423°F and 0.50 Stress Ratio

REFERENCES

1. McEvily, Jr., A. J.; and Illg, W.: The Rate of Fatigue-Crack Propagation in Two Aluminum Alloys. NACA TN-4394, September 1958.

2. Martin, D. E.; and Sinclair, G. M.: Crack Propagation Under Repeated Loading. Proceedings of the Third U. S. National Congress of Applied Mechanics, June 1958, p 595.

3. Hunt, R. T.: Crack Propagation Prediction and Crack-Stopper Techniques for Stiffened and Unstiffened Flat Sheet in a Supersonic Transport Environment. ASD-TDR-63-773, August 1963.

4. Tiffany, C. F.; Lorenz, P. M.; and Hall, L. R.: Investigation of Plane-Strain Flaw Growth in Thick-Walled Tanks. NASA CR-54837, February 1966.

5. Kuhn, P.: The Prediction of Notch and Crack Strength Under Static and Fatigue Loading. Paper No. 843C, SAE-ASME Air Transport and Space Meeting, New York, N. Y., April 27-30, 1964.

6. Christensen, R. H.; and Denke, P. H.: Crack Strength and Crack Propagation Characteristics of High Strength Metals. ASD TR-61-207, January 1962.

7. Broek, D.; and Schijve, J.: The Effect of Sheet Thickness on the Fatigue Crack Propagation in 2024-T3 Alclad Sheet Material. NLR-TR M. 2129, National Aero- and Astronautical Research Institute, Amsterdam, April 1963.

8. Grosskreutz, J. C.; and Shaw, G. G.: Mechanisms of Fatigue in 1100-0 and 2024-T4 Aluminum. AFML-TR-65-127, July 1965.

9. Fager, J. A.: Development of Titanium Alloy for Lightweight LH_2 Tankage. Journal of Spacecraft and Rockets, May-June, 1965.

10. Babel, H. W.; Eitman, D. A.; and McIver, R. W.: The Biaxial Strengthening of Textured Titanium. ASME Preprint 66-MET-6, Metals Engineering Conference, April 18-22, 1966.

11. Srawley, J. E.; and Brown, Jr., W. F.: Fracture Toughness Testing. NASA TN D-2599, January 1965.

12. Anderson, R. B.: Fracture Mechanics of Through-Cracked Cylindrical Pressure Vessels. NASA TM X-52079, February 1965.

13. Irwin, G. R.: Fracture Testing of High-Strength Materials Under Conditions Appropriate for Stress Analysis. Naval Research Laboratory Report 5486, July 1960.

14. Paris, P.; and Erdogan, F.: A Critical Analysis of Crack Propagation Laws. Journal of Basic Engineering, ASME, December 1963.

15. Krafft, J. M.: On Prediction of Fatigue Crack Propagation Rate from Fracture Toughness and Plastic Flow Properties. Trans. ASM, Vol. 58, 1965, pp 691-699.

16. Liu, H. W.: Size Effects on Fatigue Crack Propagation. Office of Aerospace Research, ARL 64-68, April 1964.

17. Weibull, W.: A Theory of Fatigue Crack Propagation in Sheet Specimens. International Conference on Mechanisms of Fatigue in Crystalline Solids, November 1962.